The printing of this thesis was financially supported by:

Amgen B.V.

INstruchemie B.V.

Macrogen Europe

Pfizer B.V.

Colofon

ISBN: 978-94-6295-001-6

Cover design:	Remko van Vught
Printed by:	Proefschriftmaken.nl || Uitgeverij BOXPress
Published by:	Uitgeverij BOXPress, 's-Hertogenbosch

The research presented in this thesis was performed at the Membrane Biochemistry and Biophysics group of the Utrecht University. This work was funded by the Focus & Massa project of the Utrecht University, The Netherlands.

Functionalized nanobodies for cancer therapy

Gefunctionaliseerde nanobodies als kankertherapie
(met een samenvatting in het Nederlands)

Proefschrift

ter verkrijging van de graad van doctor aan de Universiteit Utrecht op gezag van de rector magnificus, prof.dr. G.J. van der Zwaan, ingevolge het besluit van het college voor promoties in het openbaar te verdedigen op woensdag 26 november 2014 des middags te 2.30 uur

door

Remko Wilhelmus Maria van Vught

geboren op 28 februari 1986
te Tilburg

Promotoren: Prof.dr. J.A. Killian
Prof.dr. R.J. Pieters

Copromotor: Dr. E.J. Breukink

Voor mijn ouders

Table of contents

Chapter 1

General introduction

Cancer treatment

Cancer is the collective term for diseases associated with uncontrolled cell division. In 2012, cancer was estimated to be diagnosed in 14.1 million people worldwide and the cause of 8.2 million deaths[1]. The development of cancer has been attributed to genetic (5 - 10 %) and environmental factors (90 – 95 %)[2]. Environmental factors can be subdivided into the environment and lifestyle, of which the latter is the main cause of cancer-related deaths and includes smoking, diet and infections. The development of cancer requires 4-6 mutations to transform normal cells into cancer cells[3]. In this process, mechanisms regulating proliferation are lost and cells become self-sufficient in proliferative signals.

The line of cancer treatment depends on the disease state, aggressiveness and the timing of its discovery. Where surgical interference is often applied for solid tumors, radio- and chemotherapy is used for smaller tumors or metastases and also to treat residuals after surgery. To distinguish cancer cells from healthy cells, most chemotherapeutic drugs target rapidly growing cells by acting on DNA replication or mitosis. Unfortunately, these cytotoxic drugs also target cell types with natural rapid cell division including cells in the digestive tract, bone marrow, and hair follicles, and thus give rise to (severe) side effects.

Targeted therapies

A new class of anti-cancer drugs, the targeted therapies, aims to minimize these side effects by acting on one specific molecule. Targeted therapies can be divided into two groups: small molecule inhibitors (mainly tyrosine-kinase inhibitors) and monoclonal antibodies (mAbs)[4]. As tyrosine kinases are involved in signal transduction, theses small molecules prevent activation of the receptor and subsequently inhibit proliferation[5]. In contrast, mAbs are restricted to bind molecular targets on the outside of the cell and act on multiple levels: 1) blocking receptor activation by either binding the receptor at the ligand-receptor interface or by binding the ligand itself, 2) activating antibody dependent cell-mediated cytotoxicity, 3) inducing complement dependent cytotoxicity[6]. Their high specificity and safety profile led to the development of mAbs for various cancer indications[7]. A new generation of mAbs are the antibody drug conjugates (ADCs), which deliver very potent drugs to target cells and thereby limit side effects[8].

These conventional IgG antibodies are 150 kDa and bear two heavy and light chains (Fig. 1). As a consequence of their size (and recycling via the neonatal Fc receptor) mAbs have a long half-life and therapeutic effect[9]. In contrast, however, the tumor penetration of mAbs is hampered by the size[10]. This led to the development of antibody fragments, which are smaller without affecting the specificity. One promising set of antibody fragments are derived from heavy-chain antibodies in camelids (Fig. 1). These antibody fragments are only 15 kDa and known as nanobodies or VHH (Variable domains derived from the Heavy chain of Heavy chain only antibodies). Next to their small size, nanobodies possess unique features when compared

with other antibody (fragments)[11,12] which are summarized in table 1.

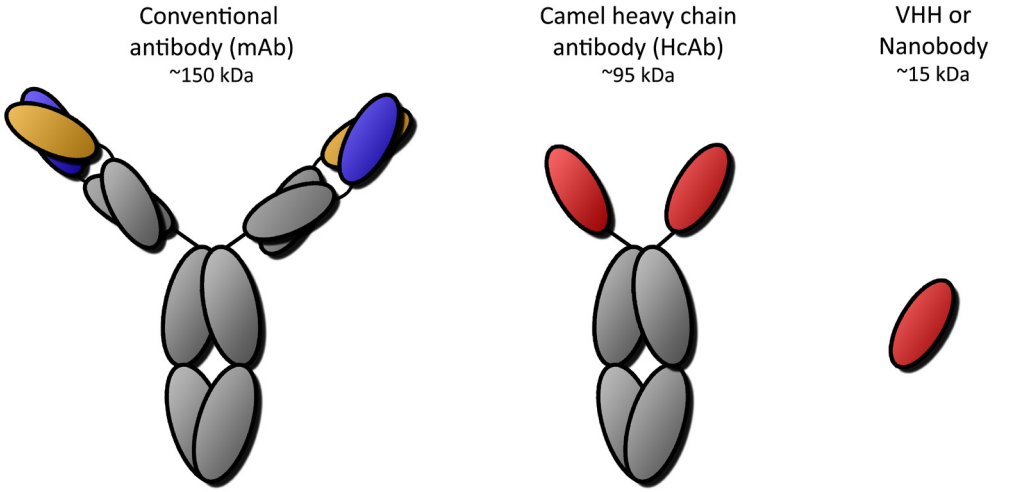

Figure 1. Schematic representation of a conventional antibody (mAb), camel heavy chain antibody (HcAb) and Variable domains derived from the Heavy chain of Heavy chain only antibodies (VHH/Nanobody). The heavy (VH) and light (VL) variable domain were depicted in blue and yellow, whereas the VH domain of heavy-chain antibodies of camelids was depicted in red.

Table 1. Overview of the unique features of nanobodies compared with other antibody (fragments).

Feature	Molecular basis
High stability in a wide range of temperatures and pH's	Efficient refolding and to a lesser extent increased thermodynamic stability
High solubility	Increased hydrophilicity
Recognition of hidden epitopes	Extended CDR3 loop
Straightforward expression in pro- and eukaryotes	Efficient folding of the single domain
Rapid tissue penetration (and clearance)	Small size

While mAbs have a long half-life, nanobodies and other antibody fragment are rapidly cleared from the circulation by the kidneys due to their smaller size (and lacking of the Fc domain). This makes nanobodies advantageous for rapid and temporal inhibition of for instance scorpion venom[13]. For treatment regimes where longer half-life is required e.g. for cancer, strategies have been developed to prolong the circulation in blood. One of these is the fusion of multiple nanobodies, where one nanobody binds albumin and thus exploits the half-life of albumin[14]. In another approach nanobodies were conjugated to PEG or effector domains, thereby increasing the size above cut-off level for glomerular filtration[15,16]. For therapeutic applications, the conjugation to delivery platforms such as liposomes can be employed[17]. This not only

enables longer circulation but also the efficient delivery of drugs next to receptor inhibition by nanobodies[18].

In the last decade, the therapeutic applications of nanobodies raised against various targets were demonstrated[12]. Currently, 7 nanobody-based medicines are in clinical trials for various diseases including rheumatoid arthritis, RSV infection, thrombosis and bone disorder[19].

Scope of this thesis

This thesis focuses on the therapeutic applications of nanobodies for cancer treatment. Towards this end, two methods were developed for the site-specific functionalization of nanobodies which enable conjugation of (small) biomolecules including toxic drugs. In addition, two nanobody-based medicines were evaluated as anti-cancer therapy. The potential of nanobodies for cancer treatment was exemplified for the epidermal growth factor receptor (EGFR). The role of EGFR has been well established and it is associated with a number of cancers. This methodology however can be applied for all surface proteins which provide selective tumor targeting and thus offers numerous applications.

In **chapter 2**, a detailed overview is given of the current approaches for site-selective modification of proteins. Based on this, their applications towards therapeutic proteins are discussed. **Chapter 3** reviews the therapeutic applications of nanobodies. First the origin of nanobodies is described, followed by an overview of established therapeutic applications.

The development of intein-based functionalized nanobodies is described in **Chapter 4**. Several substrates were evaluated for C-terminal modification of nanobodies, after which the selected substrate was validated in binding studies. Subsequent decoration on liposomes demonstrates the potential of this approach. In **Chapter 5**, the decoration of liposomes was employed for photodynamic therapy. A previously established photosensitizer was encapsulated in targeted liposomes, optimized and characterized. The dark toxicity as well as efficacy after activation by light was evaluated *in vitro*. In **Chapter 6**, the incorporation of unnatural amino acids in nanobodies was evaluated. Nanobodies were labeled with biomolecules, decorated on liposomes and multimerized through biotin-streptavidin conjugates. **Chapter 7** explores the potential of nanobody-based immunotoxins. First, selection for EGFRvIII specific nanobodies and characterization were employed. Subsequently, nanobodies were genetically fused to PE38 and evaluated on multiple cell lines. The results of this thesis are discussed in **Chapter 8**.

References

1. IARC., I. A. for R. on C. W. H. O. GLOBOCAN 2012: Estimated Cancer Incidence, Mortality and Prevalence Worldwide in 2012. *GLOBOCAN* (2012). at <http://globocan.iarc.fr/Pages/fact_sheets_cancer.aspx?>
2. Anand, P. *et al.* Cancer is a preventable disease that requires major lifestyle changes. *Pharm. Res.* **25,** 2097–116 (2008).
3. Hahn, W. C. & Weinberg, R. A. Modelling the molecular circuitry of cancer. *Nat. Rev. Cancer* **2,** 331–41 (2002).
4. Gerber, D. E. Targeted therapies: a new generation of cancer treatments. *Am. Fam. Physician* **77,** 311–9 (2008).
5. Arora, A. & Scholar, E. M. Role of tyrosine kinase inhibitors in cancer therapy. *J. Pharmacol. Exp. Ther.* **315,** 971–9 (2005).
6. Weiner, G. J. Monoclonal antibody mechanisms of action in cancer. *Immunol. Res.* **39,** 271–8 (2007).
7. Scott, A. M., Wolchok, J. D. & Old, L. J. Antibody therapy of cancer. *Nat. Rev. Cancer* **12,** 278–87 (2012).
8. Adair, J. R., Howard, P. W., Hartley, J. A., Williams, D. G. & Chester, K. A. Antibody-drug conjugates - a perfect synergy. *Expert Opin. Biol. Ther.* **12,** 1191–206 (2012).
9. Ghetie, V. & Ward, E. S. Transcytosis and catabolism of antibody. *Immunol. Res.* **25,** 97–113 (2002).
10. Yokota, T., Milenic, D. E., Whitlow, M. & Schlom, J. Rapid tumor penetration of a single-chain Fv and comparison with other immunoglobulin forms. *Cancer Res.* **52,** 3402–3408 (1992).
11. Harmsen, M. M. & De Haard, H. J. Properties, production, and applications of camelid single-domain antibody fragments. *Appl. Microbiol. Biotechnol.* **77,** 13–22 (2007).
12. Muyldermans, S. Nanobodies: natural single-domain antibodies. *Annu. Rev. Biochem.* **82,** 775–97 (2013).
13. Hmila, I. *et al.* A bispecific nanobody to provide full protection against lethal scorpion envenoming. *FASEB J.* **24,** 3479–89 (2010).
14. Tijink, B. M. *et al.* Improved tumor targeting of anti-epidermal growth factor receptor Nanobodies through albumin binding: taking advantage of modular Nanobody technology. *Mol. Cancer Ther.* **7,** 2288–97 (2008).
15. Vugmeyster, Y. *et al.* Pharmacokinetic, biodistribution, and biophysical profiles of TNF nanobodies conjugated to linear or branched poly(ethylene glycol). *Bioconjug. Chem.* **23,** 1452–62 (2012).
16. Behdani, M. *et al.* Development of VEGFR2-specific Nanobody Pseudomonas exotoxin A conjugated to provide efficient inhibition of tumor cell growth. *N. Biotechnol.* **30,** 205–9 (2013).
17. Oliveira, S. *et al.* Downregulation of EGFR by a novel multivalent nanobody-liposome platform. *J. Control. Release* **145,** 165–75 (2010).
18. Van der Meel, R. *et al.* Inhibition of tumor growth by targeted anti-EGFR/IGF-1R nanobullets depends on efficient blocking of cell survival pathways. *Mol. Pharm.* **10,** 3717–27 (2013).
19. Ablynx. Ablynx's product portfolio. *Retrieved 20-05-2014* http://http://www.ablynx.com/research–development/
20. Mullard, A. Maturing antibody-drug conjugate pipeline hits 30. *Nat. Rev. Drug Discov.* **12,** 329–32 (2013).
21. Van Vught, R., Pieters, R. J. & Breukink, E. Site-specific functionalization of proteins and their applications to therapeutic antibodies. *Comput. Struct. Biotechnol. J.* **9,** e201402001 (2014).

Chapter 2

Site-specific functionalization of proteins and their applications to therapeutic antibodies

Remko van Vught, Roland Pieters, Eefjan Breukink

Van Vught, R., Pieters, R. J. & Breukink, E. *CSBJ* **9,** e201402001 (2014)

Abstract

Protein modifications are often required to study structure and function relationships. Instead of the random labeling of lysine residues, methods have been developed to (sequence) specific label proteins. Next to chemical modifications, tools to integrate new chemical groups for bioorthogonal reactions have been applied. Alternatively, proteins can also be selectively modified by enzymes. Herein we review the methods available for site-specific modification of proteins and their applications for therapeutic antibodies.

Introduction

Proteins are the working horses of a living cell. Within and around cells they perform a magnificently diverse set of functions. Besides providing structure and stability, proteins are involved in cell signaling, catalyzing reactions, storage and transport, and are therefore extensively studied. Over the years, tools have become available for researchers to reveal structure and function relationships, as well as localization and their interactions with other proteins.

A relatively new tool is based on novel and specific chemistry. By modifying existing amino acids or introducing unnatural amino acids, proteins can be manipulated at the single amino acid level. Several methods involving the site-specific modification of proteins have been reported in the last decade. This allows the spatial and temporal control of proteins *in vivo*, as well as single molecule tracking. Modifications are introduced during protein translation, as post translational modification or chemically, after protein isolation.

Besides their usefulness for *in vitro/vivo* research, site-specific modifications are also interesting for therapeutic applications. Pharmaceutical companies have been refocusing their pipeline towards biological medicines (mainly monoclonal antibodies) because of the high specificity and safety. The 'naked' monoclonal antibodies have shown to be very effective in blocking receptors. A next generation of biological medicines are the antibody drug conjugates (ADCs), which efficiently deliver the payload to the target limiting the off target effects. Interestingly, site-specific modifications have also been applied to improve the properties of these therapeutic proteins. Here, we review the tools for site-specific modification of proteins, followed by their applications in the development of therapeutic antibodies.

Chemical modifications of proteins

The oldest and most straightforward method for labeling proteins is via the primary amino groups on lysine residues and at the N-terminus. In general, multiple accessible lysines and thus reactive amines are present on the protein surface, resulting in efficient labeling but inevitably leading to heterogeneous mixtures. Whether this method is applicable depends on the properties of the protein and the application. In the case of monoclonal antibodies, random labeling with fluorescent molecules hardly affects the antigen binding since many primary amines are present and only a small fraction may be important for this interaction. Smaller proteins such as antibody fragments are more likely to suffer from random conjugation due to a reduced number of lysines and the lack of an Fc region. There have been attempts to make this modification more specific by using preferential N-terminal labeling[1] or kinetically controlled lysine labeling[2]. Generally those methods suffer from low yields or require complex steps including the recycling of the original protein. Besides labeling the amino groups, similar obstacles exist for conjugation via carboxyl groups[3] and will therefore not be discussed in detail.

More selective is the labeling of proteins via sulfhydryl groups (also known as thiols).

In proteins, most of the thiols are present in covalently linked pairs as disulfide bonds. The introduction of a cysteine by site-directed mutagenesis can be used for selective conjugation. Coupling reactions of maleimide groups with thiols have a high specificity over amines due to the lower pKa of the SH group (>1000 fold selectivity at pH 7.0)[4]. Therefore, cysteines are most commonly used for the site-selective modifications of proteins, though in some situations it is not feasible. One major drawback of introducing an extra cysteine is protein misfolding due to non-native disulfide bridge formation. In addition, thiol maleimide adducts have been reported to have limited stability *in vivo*[5]. Reactive thiols in albumin, free cysteine or glutathione can exchange with the existing thiol maleimide complex. Interestingly, hydrolysis of the succinimide ring prevented this exchange reaction[5]. Whether other alkylation reactions (with iodo/bromoacetamide analogs) also suffer from limited stability *in vivo* needs to be determined. Alternatively, an elegant double alkylation method by reducing disulfide bridges on the protein surface and subsequent conjugation with a PEG monosulfone-enone reagent was stable in human serum for over 30 hours and did not affect the protein stability (scheme 1)[6].

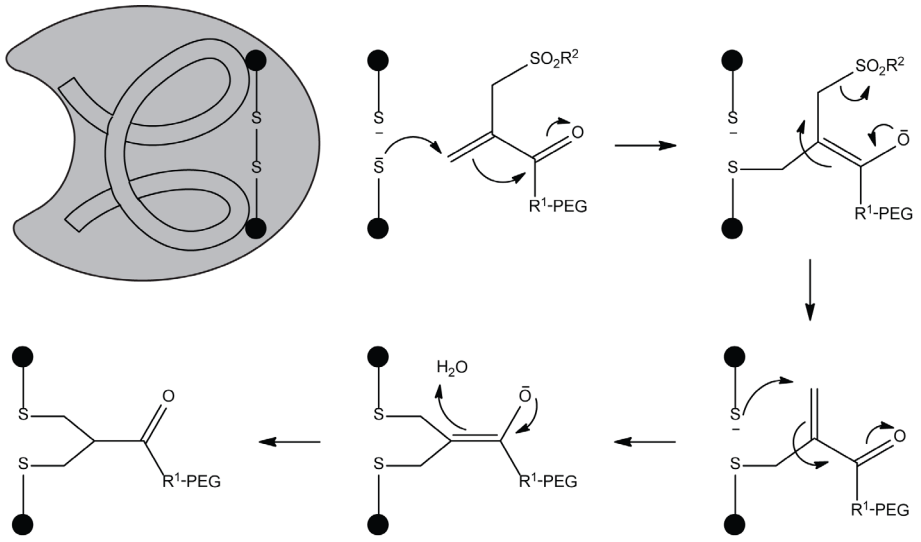

Scheme 1. Double alkylation of proteins by PEG monosulfone-enone.

Next to direct protein modification via alkylation, a reduced cysteine can be first converted to dehydroalanine. Subsequent nucleophilic addition by thiol modified biomolecules label the target protein via a thioether bond. This method is a straightforward route to natural occuring cysteine modifications including phospho[7], farnesyl[8] and N-acetylhexosamine cysteine[9], and to structural mimics of post-translational modifications, but generates epimeric products due to loss of the stereocenter in the first step. Recently, several strategies for the conversion of

cysteine to dehydroalanine have been evaluated[10].

Over the years, several site-specific chemical modifications methods have been reported for the N-terminal amino acids. N-terminal serine and threonine residues can selectively be oxidized by sodium periodate to form an aldehyde[11], followed by oxime ligation[12]. Besides oxime ligation, the oxidized serine was recently also used for the one step N-terminal dual protein functionalization using strain promoted alkyne–nitrone cycloaddition[13].
Proteins with N-terminal cysteines have been successfully used for reactions with thioesters[14] and applied for fusion proteins through native chemical ligation[15], which will be described in more detail later on.

More elegant methods are independent of the N-terminal amino acid. These approaches exploit the unique chemical properties of the N-terminus including the low pKa of the α-amino group of the N-terminus (8.9) compared with the pKa of the lysine ε-amino group (10.5). Kinetically controlled lysine labeling is performed in small steps, using multiple additions of the label and allowing the most reactive amino group to be preferentially labeled[2].

Other methods are based on the introduction of unique reactive groups. The diazotransfer reagent imidazole-1-sulfonyl azide was shown to specifically convert the N-terminal amino group into an azide group[16]. The N-terminus can also be converted into a ketone or aldehyde group by a transamination reaction[17]. Peptide library screening identified residues with high yields (A, G, D, E, N,), other amino acids were either not/less reactive or were prone to side reactions[18]. In more recent work the transamination reaction was demonstrated for labeling of a monoclonal antibody[19]. Alternatively, N-terminal modification based on ketenes was applied to introduce an alkyne in peptides and proteins[20]. This reaction is highly specific for most N-terminal amino acids but yields range from 9 to 94%.

Although these methods are generally straightforward for peptides, applications for proteins predominantly depend on the solvent accessibility of the N-terminus. Moreover, small modifications limit the usefulness of reactions with low yields due to difficulties in separating the modified from the unmodified proteins.

Metabolic modifications

Metabolic labeling of proteins involves the replacement of one or more canonical amino acids by non-canonical analogs. The first observations by Munier and Cohem showed the incorporation of phenylalanine and methionine analogs in bacterial proteins (red scheme in figure 1)[21]. Since then, many analogs have been synthesized and tested in auxotrophic bacterial hosts for incorporation at the expense of canonical amino acids[22]. The strict biological machinery accepts only minor modifications such as alkenes[23], alkynes[24] and azides[24] as amino acid side chains. The latter being of particular interest due to their compatibility with the Staudinger ligation and (copper-free) click chemistry[25].

The occurrence of multiple phenylalanine or methionine residues in proteins results in protein mixtures upon conjugation. Recently though, only one out of five azidohomoalanines of native CalB was shown to be surface accessible and reactive for functionalization[26].Instead of designing amino acid analogs to be accepted by the biological machinery, advances have been made to manipulate the biosynthetic apparatus itself. Mutations in phenylalanyl-tRNA synthetase (PheRS) caused either an increase or decrease of the binding pocket size, and thus a change in the specificity towards phenylalanine analogs (blue scheme in figure 1)[27]. The unnatural amino acid *p*-chlorophenylalanine could be incorporated into *Photinus pyralis* luciferase by expression of the mutant PheRS (A294G) in *E. coli*, replacing all phenylalanines[28]. More recently, the same has been demonstrated for non-canonical analogs using mutations in LeuRS[29], PheRS[30] and ValRS[31].

Both previous methods relied on the global replacement of canonical amino acid in proteins. The first site-specific modification of a single amino acid (based on editing the biological machinery) has been reported by Schultz[32] and Chamberlin[33] (yellow scheme in figure 1). Non-canonical amino acids were incorporated upon suppression of the amber nonsense codon (TAG) by chemically acylated suppressor transfer RNA. In theory, also the two other stop codons could be targeted. However, the least used codon (TAG/amber codon) was selected to minimize the effect of translation read through on other proteins by suppression of the stop codon. This approach was first limited to *in vitro* production of proteins, or *in vivo* by microinjection into oocytes[34]. Later on, next to the gene of interest also the synthetase/tRNA pair was expressed *in vivo*. Efforts by Schultz and coworkers have improved this approach by applying selection schemes to reduce the interaction with the biological machinery[35,36]. These include the selection with toxic genes bearing several amber codons to reduce the incorporation of canonical amino acids, as well as GFP expression in the presence of the unnatural amino acid to screen for the highest incorporation. In another example the whole biological machinery for the synthesis and incorporation of the 21st amino acid was introduced in *E. coli*[37]. Moreover, the methodology has also been transferred to yeast and to mammalian cell lines by stable transfection.

Next to the suppression of non-sense codons, frame shift suppression has been used for the site-specific introduction of non-canonical amino acids[38]. This allows for not the triplet-base codon but codons containing 4 or 5 bases to be recognized. The usage of frameshift codons is complicated by competition by the endogenous triplet recognizing tRNA, resulting in a -1 frameshift and a premature termination. Alternatively, the frameshift suppressor tRNA could also recognize endogenous codons (3+1), causing a +1 frameshift and a premature termination as well. The selection of four-base codons based on genetic occurrence frequency allowed the incorporation of multiple unnatural amino acids *in vivo*[39]. Efforts over the years have allowed over 70 novel amino acids to be genetically incorporated via this approach, including photocrosslinkers, photocaged groups and fluorescent labels[37].

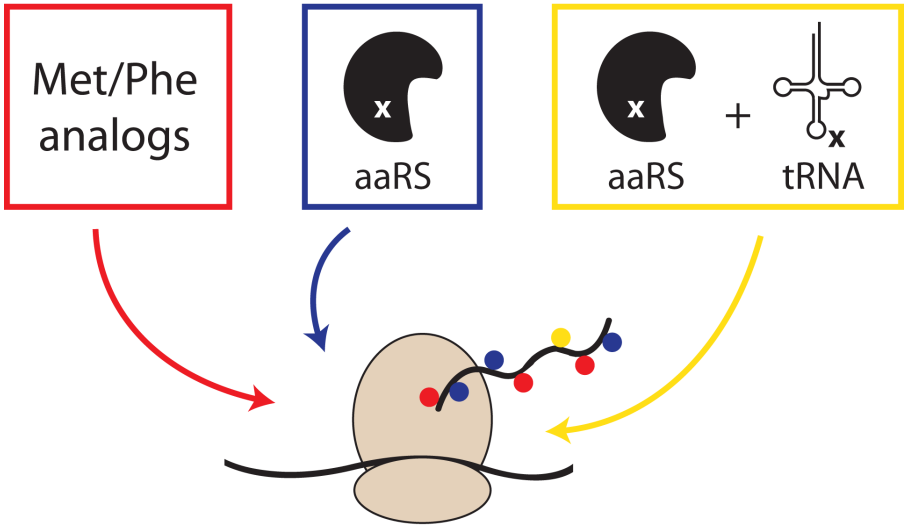

Figure 1. Metabolic labeling of proteins. The global replacement of natural amino acids by non-canonical analogs (red). Increased specificity for unnatural amino acids by manipulating the biosynthetic machinery (blue). Site-specific incorporation of unnatural amino acids by an orthogonal aminoacyl-tRNA synthetase/tRNA pair (yellow).

Post translational modifications

After translation, almost all proteins require post-translational modifications (PTMs) before becoming mature. The oxidation of cysteines is a common PTM and is important for protein folding and stability. Other PTMs increase the functional diversity of proteins by the modification of amino acids including phosphorylation, glycosylation, ubiquitination, nitrosylation, methylation, acetylation and proline cis-trans isomerization[40]. Site-specific enzymatic PTMs are of particular interest since they can be used to manipulate and/or study proteins.

Membrane associated modifications

Lipid modifications change the subcellular localization of proteins and can affect protein function[41]. Farnesyl- and N-myristoyltransferases recognize a consensus motif (CAAX and GXXXS/T) on proteins and subsequently conjugate farnesyl and myristoyl groups, respectively[42,43]. Azide functionalized analogs of those groups have been used to label and study proteins[44,45]. Although these transferases are sequence specific, the subcellular localization limits the applications for other proteins.

Another more random modification is introduced by transglutaminases (TGs), which cross-link proteins with isopeptide bonds between Lys and Gln residues[46]. TGs are involved in cell adhesion, stabilization of the extracellular matrix, apoptosis and wound healing. Importantly, multilayered epithelium, stabilized by these cross-links, protects the organism from the environment. The random crosslinking activity limits the possible applications of TGs. Cell surface

proteins bearing a Q-tag (PNPQLPF, PKPQQFM, GQQQLG, and the recently identified RLQQP[47]) have been successfully labeled with biotin and fluorescein, though background labeling was observed[48].

Formylglycine generating enzyme

In another approach the native formylglycine generating enzyme (FGE) is used to introduce formylglycine in both prokaryotes[49] and eukaryotes[50]. The aldehyde tagged protein can be readily functionalized with aminooxy- or hydrazide-functionalized biomolecules[50]. A drawback is the hydration of formyglycine in water to the diol-formylglycine, lowering the yield to around 85%[51].

Self-modifications

Besides the modification of other proteins, some enzymes can be used for self-modification such as human O6-alkylguanine-DNA alkyl transferase (hAGT)[52], cutinase[53] and halo alkane dehalogenase[54]. Structural analogs of the natural substrates temper the biological function of hAGT and cultinase. A single mutation in halo alkane dehalogenase (His272Phe) traps the protein at an intermediate state and allows covalent attachment of chemical probes[54]. Fusion proteins bearing these domains can be selectively modified *in vitro* or *in vivo*[55–57]. Compared with other approaches, the large size of these domains (21-33 kDa) is considered as the major drawback. This can influence the function and/or localization of the protein of interest by the interaction with other biomolecules. Nevertheless, hAGT is commonly used for cell imaging studies because of the high labeling efficiency and of cell permeable probes[55,58].

Ligases

A straightforward class of enzymes for modifying proteins after translation are the ligases (figure 2). Ting and coworkers have been involved in exploiting several enzymes for site-specific modifications. First, biotin ligase (BirA) was shown to accept also a ketone isostere of biotin as a cofactor[59]. Ligation of this biotin analog to proteins bearing the 15-amino-acid acceptor peptide (AP) was demonstrated *in vitro* and *in vivo*, followed by subsequent ketone-hydrazine conjugation. Second, the microbial lipoic acid ligase (LplA) was used to specifically attach an alkyl azide onto proteins with an engineered LplA acceptor peptide (LAP)[60]. Although only 33% could be converted[61], cell surface labeling with cyclo-octyne probes was demonstrated[60]. Mutants of LplA were shown to be more efficient[61] (up to 89%) and also transfer fluorinated aryl azide[62] and 7-hydroxycoumarin[63] to LAP proteins for photocrosslinking and life cell imaging, respectively. More recently the portfolio of lipoic acid ligase was extended to ligate a trans-cyclooctene[64]. The Diels-Alder cycloaddition allows rapid labeling of inner and outer cellular proteins, though the yield is unknown.

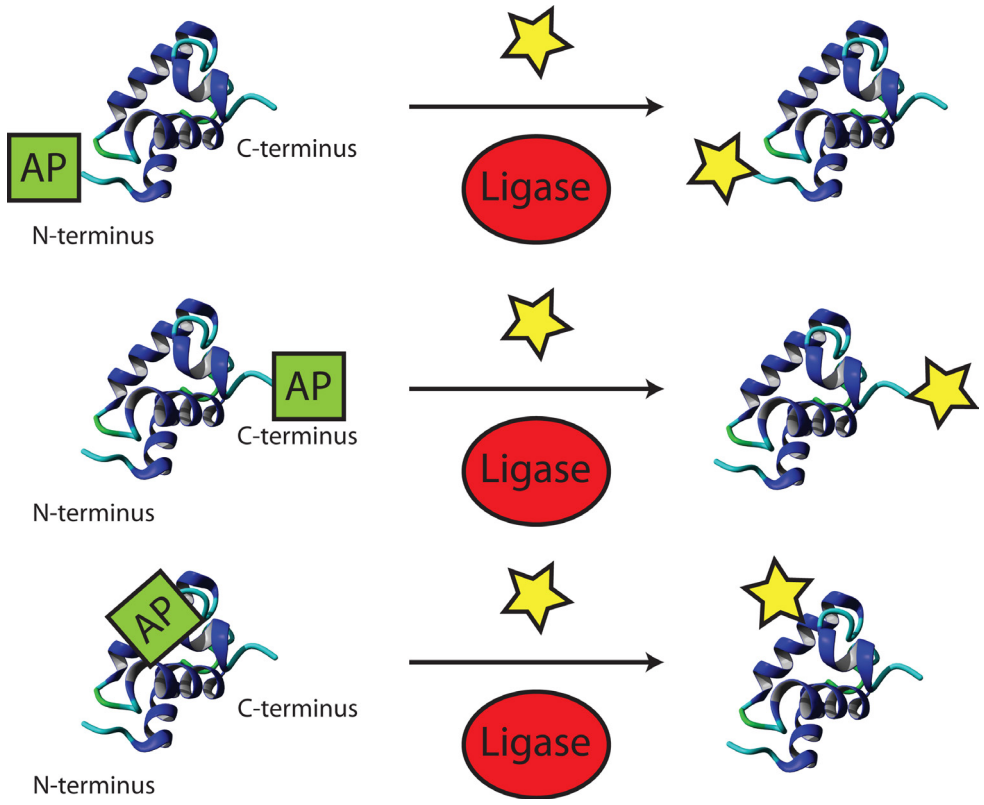

Figure 2. Protein modification by ligases at the N/C-terminus and in flexible loops.

Transferases

Another set of post-translational modifications is performed by phosphopantetheinyl transferases (PPTases)[65]. PPTases are categorized into Sfp-like (B. subtilis)[65], AcpS-like (E. coli)[66] and FAS2-like (S. cerevisiae)[67] subfamilies and transfer a phosphopantetheinyl (P-pant) group through a phosphodiester bond onto peptidyl/acyl carrier protein (PCP/ACP) domains. These typically 80–120 residues long domains are present on nonribosomal peptide synthetases (NRPSs), polyketide synthases (PKSs), and fatty acid synthases (FASs)[65].

Broad substrate specificity[68] and rapid conversion (>80% after 30 min)[69] was reported for Sfp-based labeling of proteins with phosphopantetheinylated analogs. In order to overcome possible size limitations, phage display screening identified several 11/12-residue peptide tags as replacement for the carrier domain, each allowing the labeling of N- or C-termini as well as flexible loops on target proteins[69,70]. Interestingly, orthogonal fluorescent labeling of cell surface receptors was demonstrated by using Sfp and AcpS selective peptide tags[70].

Transpeptidase

Instead of exploring the chemical space in which biomolecules can be modified by functional groups and subsequently incorporated in proteins of interest, some general applicable enzymatic modifications preexist in nature. Sortases function as transpeptidase anchoring proteins to the bacterial cell wall[71]. Upon recognition of the sorting motif LPXTG (or LPXTA) a catalytic cysteine cleaves the peptide bond between residue T and G, yielding a thioacyl intermediate[72]. Instead of hydrolysing a peptide bond (as in the case of cysteine proteases), sortases accept a N-terminal (oligo)glycine as a nucleophile, creating a new peptide bond between the two molecules (figure 3).

Sortases function at physiological conditions and have been used for protein labeling with various functionalities such as biotin, fluorophores, cross-linkers and multifunctional probes[73]. Target proteins are commonly labeled C-terminally with the LPXTG sorting motif, followed by a purification tag. Subsequent transpeptidation removes the purification tag and generates the labeled proteins in high yields. Interestingly, this approach has also been used to study the structure and function of a solvent-exposed loop within the ubiquitin C-terminal hydrolase 3 protein[74].

Besides introducing the sorting motif, proteins can also be equipped with a N-terminal (oligo)glycine for N-terminal conjugation. In this case, the sortase recognition element should be introduced onto the biomolecule. This approach has mostly been used for bacterial cell wall labeling with biotin, azide and fluorescent groups[73].

Alternatively, also both N- and C-terminal ligation has been demonstrated[75]. Selective labeling is achieved by using two sortases with different specificity (LPXTG & LPXTA), preventing the oligomerisation of proteins. Protein cyclisation occurs in cases where the N- and C-termini are in close proximity[76,77]. This is of particular interest in therapeutic drug design due to the enhanced conformational stability and increased resistance to proteolytic cleavage[78].

The fusion of two proteins can be achieved in a similar fashion, with each protein bearing one of the tags. Although genetic fusion of proteins is much more straightforward, in some cases this is not feasible. For instance when protein folding is affected, protein yields drop or proteins come from different hosts. In a recent study, 10 pairs of protein domains were generated with yields between 40-85%[79].

The labeling of proteins by sortases has been optimized and well described. One of the major drawbacks is the high concentration of sortase required. The poor reaction kinetics have been improved 140-fold using directed evolution by increasing the affinities for the sorting motif LPXTG as well as the (oligo)glycine peptide[80].

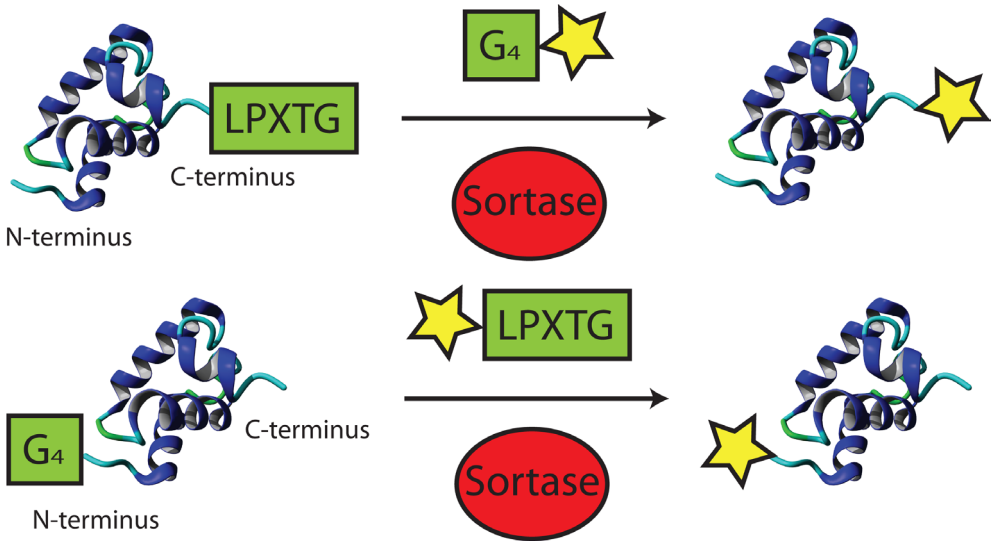

Figure 3. N- and C-terminal protein modification by sortases. Although sortase recognition sites have been engineered in flexible loops of proteins, the subsequent cleavage of the peptide backbone limits its therapeutic applications.

Protein splicing

Inteins, also known as protein introns, are protein domains expressed in frame of another protein[81]. Removal of the intein domain by self-excising, rejoins the two external host protein segments by formation of a native peptide bond, and restores the function of the host protein.

This process can be exploited for the N/C-terminal ligation of biomolecules (figure 4)[82]. The C-terminal labeling requires the formation of a thioester by nucleophilic attack of the intein N-terminal cysteine. The thiol can be exchanged in the presence of thiol reagents, resulting in cleavage of the intein. In a subsequent native chemical ligation reaction with a cysteine functionalized molecule, the thiol exchanges again followed by the generation of a peptide both by the S-N shift. The C-terminal intein mediated conjugation has been demonstrated for labeling with biotin[83], fluorophores[84] and lipids[85,86]. Moreover, semi synthetic proteins were produced by the ligation of cysteine bearing peptides, known as expressed protein ligation[87].

The N-terminal labeling also requires the exchange of thiols for cleaving off the intein. Now the intein C-terminal asparagine breaks the peptide bond, freeing an N-terminal cysteine on the protein of interest. Labeling of N-terminal cysteine is performed in the same NCL reaction with a thioester modified biomolecule and has been used to immobilize proteins on microarrays[88] as well as for *in vivo* labeling[89].

Inteins can, similarly to sortases, also facilitate the cyclisation of proteins[82]. The commercialized IMPACT kit allows straightforward production and purification of proteins with an N- and/or C-terminal modification for site-specific functionalization[15,90]. As the intein domain

is coexpressed, no other proteins are required. However, reactions in complex mixtures are challenging since thioesters can be inactivated by reactions with amines and by hydrolysis[91].

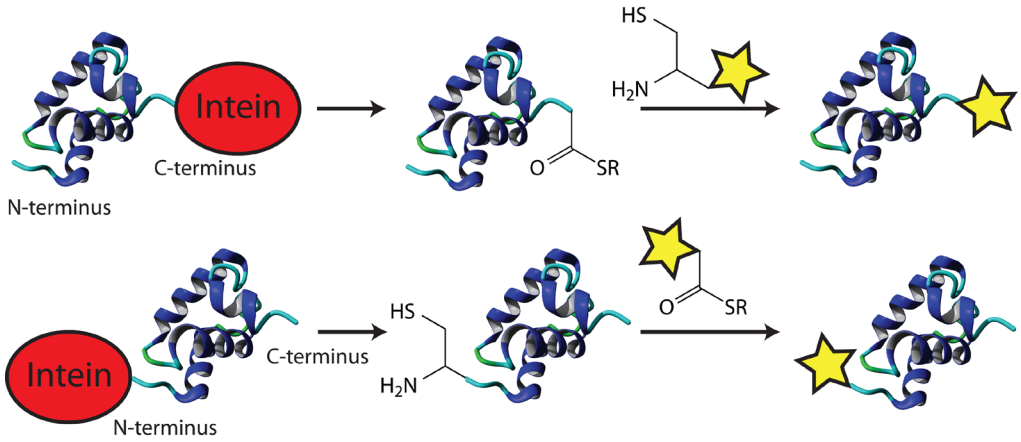

Figure 4. Intein-mediated conjugation of biomolecules.

Glycosylation

The covalent attachment of carbohydrate chains (glycans) to proteins is the most prevalent and complex PTM, also known as glycosylation[92]. Glycans can be N-linked to proteins via the asparagine or arginine side-chain, or O-linked via the hydroxyl group mostly on serine, threonine and tyrosine, and also hydroxylysine, or hydroxyproline side-chains[93]. Although the majority of the glycoproteins are present on the exterior surface of cells, the O-GlcNAc modification has also been reported for proteins in the cytosol and nucleus[94].

Glycosylation is important for protein folding and stability, thereby affecting the circulation lifetime in blood (discussed later on)[95]. Interestingly, the PTM itself can be used for subsequent modification of glycoproteins via bioorthogonal chemistry. For instance, the metabolic labeling of glycans is achieved by feeding cells or organisms with modified glycan precursors[96]. Several azido sugars including N-azidoacetylmannosamine (ManNAz), N-azidoacetylgalactosamine (GalNAz), N-azidoacetylglucosamine (GlcNAz) and 6-azidofucose (6AzFuc) have been incorporated into glycoproteins by the glycan biosynthetic machinery in both *in vitro* and *in vivo*[97]. In addition, attempts have been made to enzymatically label glycoproteins. For example the permissive mutant β-1,4-galactosyltransferase (Gal-T1 (Y289L)) introduces azido galactosamine (GalNAz) onto O-GlcNAc–modified glycoproteins[98,99]. The introduced azido group allows subsequent glycan-profiling and visualization of proteins of interest[98].

Although the glycan modification of glycoproteins expands the researcher's toolbox, the great structural complexity limits its applications today. Especially the glycan recognition

by the immune system affects the usefulness for therapeutic proteins[100]. Attempts to overcome these problems involve exploring the production of therapeutic glycoproteins in different hosts and addressing (chemo) enzymatic methods to derive homogeneous glycosylation patterns.

Applications for therapeutic antibodies

Traditionally, drugs have been small chemical entities based on natural and (semi)synthetic products[101]. Analogs of natural active compounds have been optimized for physicochemical and pharmacological properties allowing oral administration while maintaining therapeutic efficacy. The lack of specificity and/or the inability to block protein-protein interactions by these small chemical entities stimulated the development of protein based drugs[102]. Certain type of proteins such as hormones and antibodies naturally bear very high specificity for their target. Moreover, their natural appearance in the human body makes them reasonably safe as therapeutic compounds. Protein drugs, however, often suffer from other issues such as low stability, poor pharmacokinetics, limited efficacy and require a complex route of administration[103,104]. Over the years, research groups and pharmaceutical companies have made various attempts to improve these parameters by modifying therapeutic proteins using some of the above mentioned methods[105]. The second part will review these modifications.

Pharmacokinetics

In vivo responses of (protein) therapeutics are influenced by drug absorption, distribution, metabolism and excretion (ADME). Small sized proteins are predominantly cleared via glomerular filtration by the kidneys[106]. This results in a half-life of 2 hours for single-domain antibodies (15 kDa)[107] and 12-20 hours for Fab fragments (50 kDa)[108]. Proteins above the glomerular filtration cutoff (molecular weight >50 kDa and hydrodynamic radius >60 Å) are cleared by other pathways including proteolytic degradation, hepatic uptake and immune clearance[109]. Monoclonal antibodies, for instance, are 150 kDa and have long half-lives (7-23 days) by default[110].

The elimination of small proteins by the kidneys can thus be influenced by modifications affecting the size. The covalent attachment of water soluble polymers to proteins (such as polyethylene glycol; PEG) increases the hydrodynamic size and interestingly also reduces the immunogenicity by masking the protein from the immune system[111]. Several branched and non-branched PEG structures have been evaluated for the effect on renal clearance. Enhanced PK profiles for branched PEG conjugates have consistently been described for therapeutic proteins in the literature[112–114]. Recently for instance, single domain antibodies labeled with 2x20 kDa PEG were shown to be superior over 1x40 kDa and 4x10 kDa labeling without affecting the biological activity[114]. Biodistribution studies showed higher serum exposure of the antibody, though this was not the case for some tissues.

Although PEG is considered as the golden standard in drug delivery, antibody formation

against PEG conjugates was reported in 1983 already[115]. Interestingly, preexisting antibodies against PEG were found in healthy donors of the PEG-asparaginase clinical trial[116]. And even, a more rapid blood clearance of PEG conjugates was observed in patients with existing anti-PEG antibodies[116,117]. This may seriously affect the applications of PEG for drug delivery due to an expected reduced therapeutic efficacy in patients with antibodies against PEG.
These issues stimulated researchers to find alternative polymers including non-biodegradable poly(glycerol)s, poly(vinylpyrrolidone), poly(2-oxazoline)s, poly(N-(2-hydroxypropyl) methacrylamide), and biodegradable poly(amino acid)s. Promising results were reported for some alternatives, however the current understanding is very limited and requires additional (clinical) studies. A recent review by Knop et al. discusses PEG and potential alternatives in more detail[118].

Monoclonal antibodies on the other hand have already a long half-life. For therapeutic purposes, the IgG class has predominantly been used. Within the IgG class, the IgG subclasses 1-4 differ in the Fc region which affects effector functions such as phagocytic cell recruitment and complement activation through cellular IgG-Fc receptors, and in half-life by recycling via neonatal Fc receptor (FcRn)[119]. The strong effector effects and long half-life of subclass IgG1 are ideal for antibody based therapy in oncology[120]. Other treatments such as in Crohn's disease mainly depend on antigen neutralization. Here, the effector functions by the Fc region can give rise to side effects. This led to the development of a pegylated IgG1-Fab (Certolizumab pegol) next to the existing IgG1's infliximab and adalimumab, which misses the Fc region[121]. An additional benefit is the lack of active transport by FcRn across the human placenta and thus the antibody should be safe in pregnancy. Alternatively strategies to reduce/remove effector functions are IgG isotype switching to IgG2/4 and removal of glycosylation sites[122]. The latter can be achieved either by mutation of asparagine 297 in the CH2 domain (and additional glycosylation sites) or by expression of antibody (fragments) in prokaryotic hosts.

Distribution

Biodistribution is another factor determining the efficacy of antibody therapy, and varies per Ig class due to differences in the Fc region. The distribution of IgG class monoclonal antibodies is mainly confined to blood and extracellular fluid. Pegylation of antibody fragments was reported to influence the biodistribution[123]. Since the therapeutic response of antibody therapy depends on the drug concentration at the target site, many studies have analyzed impaired distribution in tumors[124–126]. Compared with normal tissue, the interstitial hydrostatic pressure and missing lymphatic draining restricts movement of antibodies[126]. Consequently, invasion of monoclonal antibodies occurs predominantly via diffusion across pores in the capillary and is limited by the molecular size. In addition, the 'binding site barrier' limits deep penetration of antibodies into tumors[127,128]. Diffusion and convection are restricted to the outer layer of cancer cells due to high

affinity, rapid internalization and subsequent metabolism of antibodies[129].

Taken together, tumor penetration can be improved by targeting smaller sized antibodies including single-domain antibodies and Fab fragments. These antibody fragments lack an Fc region and therefore have a reduced half-live. Whether the improved tumor penetration is sufficient to compensate for the shorter circulation time needs to be evaluated.

Clearance

The molecular weight of monoclonal antibodies is beyond the filtration cutoff of the kidneys. Still, the half-life between IgG subclasses ranges from 7 to 23 days[110]. The interaction between the Fc region and the FcRn receptor, has been suggested as one of the determining factors. Where normally the uptake of proteins by vascular endothelial cells would result in degradation in lysosomes, antibodies are recycled back into the circulation as a consequence of their interaction with the FcRn receptor[130]. Validation in FcRn knockout mice showed a 10-15x higher IgG elimination while other classes were not affected[131–133]. In addition, engineered tighter binding to the FcRn resulted in a 2-fold increase in the half-life in monkeys[134]. Other factors determining the clearance rate of antibodies are immunogenicity, proteolysis and glycosylation[135]. Interestingly, the production of hyperglycosylated antibodies fragments in engineered cell lines demonstrated longer half-lives as well as reduced proteolysis[109]. Alternatively, Fab fragments conjugated to PEG benefits, beside from the increased size, also from the reduced intracellular uptake and proteolytic degradation by masking sensitive sites[114].

Antibody drug conjugates (ADCs)

The next generation of biological medicines are the antibody drug conjugates (ADCs)[136]. Where 'naked' monoclonal antibodies rely on the recruitment of immune cells by the Fc region for its toxicity, ADCs bear a stable (or selective cleavable) linkage with a cytotoxic payload[137]. The release of the payload after absorption/internalization by the target cell minimizes exposure of healthy tissues[137]. More importantly, because of the cytotoxic payload, ADCs are more effective in the killing of cancer cells[138].

An interesting example is the monoclonal antibody trastuzumab (Herceptin), which targets Her2 over-expression on certain types of breast cancer[139]. Trastuzumab has been marketed since 1998 and predominantly inhibits tumor proliferation. Recently, ADC trastuzumab emtansine (Kadcyla) was approved by the FDA. The delivery of cytotoxic emtansine induces microtubule disruption, thereby making this construct more effective (54% longer median progression-free survival compared with trastuzumab plus docetaxel)[140,141]. Between 0 and 8 emtansine molecules are randomly conjugated via the SMCC crosslinker onto lysine residues on trastuzumab (3.5 on average)[140]. Because of the on average 100 lysines per antibody, this results in a heterogeneous mixture. A 2/3-fold faster clearance of trastuzumab emtansine compared

with the naked antibody has been attributed to deconjugation and proteolytic degradation of the ADC[142].

Better defined is the monoclonal antibody brentuximab vedotin (Adctris) for treating Hodgkin's lymphoma. Mild reduction by dithiothreitol (DTT) generates 8 thiol groups from four interchain disulfide bridges[143]. Monomethyl auristatin E (MMAE) is conjugated to 3-5 thiol groups (4 on average). Although labeling of brentuximab with 8 MMAE molecules has also been reported, the higher degree of labeling generally results in faster clearance/shorter half-life. Interestingly, the *in vivo* antitumor activity was comparable for ADCs bearing 4 or 8 MMAE molecules (at equal mg/kg/dose)[144].

Off target/side effects by ADCs can generally be explained by 3 situations: 1) The antibody is not specific enough causing accumulation in healthy tissue; 2) The cytotoxic agent is lost before it reaches the target cell; or 3) The heterogeneous population has altered specificities or pharmacokinetics. The drawbacks of producing monoclonal antibodies as heterogeneous product led to the site-specific incorporation of unnatural amino acids in monoclonal antibodies and antibody fragments[145–147]. A defined stoichiometry and stable linkage is expected to reduce the side effects of ADCs. In addition, optimal sites for conjugation can be selected to reduce the effect on the circulation time.

In order to demonstrate this, a noncleavable auristatin analog was conjugated to trastuzumab bearing the unnatural amino acid *p*-acetylphenylalanine (pAcF)[146]. The functionalized ADC was obtained in an overall yield of >95% and showed a similar clearance rate as the naked antibody.

Currently, the companies Allozyne, Ambrx and Sutro explore the incorporation of unnatural amino acids for its therapeutic applications. An overview of FDA approved ADCs is given in table 1.

Table 1. Overview of FDA approved ADCs.

mAb	Drug	Drugs/Ab (average)	Chemistry	Reducable	Trigger	Status (US)	Ref
Gemtuzumab ozogamicin	Calicheamicin	4-6 (5*)	Lysine	yes	pH	approved (2000) withdrawn (2010)	148
Brentuximab vedotin	Monomethyl auristatin E (MMAE)	3-5 (4)	Cysteine	no	protease	approved (2011)	143
Trastuzumab emtansine	Mertansine (DM1)	0-8 (3.5)	Lysine	no	none	approved (2013)	140

* For only 50% of the antibodies.

Bispecific antibodies

Next to ADCs, also the recruitment of T-cells by bispecific antibodies is effective for the treatment

of cancer. Bispecific antibodies recognize tumor specific antigens and T-cells at the same time[149]. In one strategy, random crosslinking has been applied to conjugate two antibodies together via hetero-bifunctional crosslinkers such as SPDP (succinimidyl-3(2-pyridylthiol)propionate)[150–152] and SMCC (Succinimidyl-4-(N-maleimidomethyl)cyclohexane-1-carboxylate)[153]. Monoclonal antibodies however bear two fragment antigen-binding sites (Fab fragment) both recognizing the same antigen. Selective reduction of disulfide bonds and subsequent oxidation was used to acquire monovalent bispecific antibody fragments (one Fab for each antigen)[154].

More recently, uniform bispecific antibodies were generated by first expressing two sets of half-antibodies which were unable to dimerize[155]. The bispecific antibodies were spontaneously formed by mixing the reduced half-antibodies under oxidizing conditions. In contrast, the only FDA approved bispecific antibody therapy (Catumaxomab) is directly produced in hybrid mouse/rat quadroma cell lines[156]. Due to the homology in the hinge region between mouse and rat antibodies, the 30-49% yield almost reached the statistical limit of 50% (m/m, **m/r**, **r/m** and r/r)[157]. Besides binding tumor cells via the EpCAM antigen and T-cells via the CD3 receptor, the intact Fc region of Catumaxomab recruits accessory cells to enhance the immune response against the tumor[158].

Next to the generation of full monoclonal antibodies, two Fab fragments bearing genetically encoded unnatural amino acids were conjugated to form an anti-HER2/anti-CD3 bispecific antibody[145]. The confined sites and defined chemistry allowed homogeneous products in a two-step process. Although effective tumor killing was observed *in vitro*, the efficacy *in vivo* still needs to be determined.

Nanoparticles

Based on antibody complexes in nature, immune complexes have emerged for the neutralization of antigens. Binding to tumor specific antigens blocks signaling cascades as well as causes down-regulation of the receptor[159]. Diverse set of scaffolds including avidin[160], gold[161], liposomes[162] and polymersomes[163–166] have been decorated with antibodies or antibody fragments. Recently, DNA scaffolds decorated with single-domain antibodies were demonstrated to allow various structures such as dimers and tetramers[147].

Besides immune complexes binding to antigens, the subsequent internalization has drawn attention for the delivery of drugs. Compared with current ADCs, nanocapsules facilitate the delivery of high drug concentrations by active (antibody binding) and passive targeting (EPR effect; beyond the scope of this review, see ref [167]). In order to remain in the blood circulation, nanoparticles need to meet several criteria including confined size, shape and chemical properties[168]. Antibody fragments are often used for the targeting of nanocapsules because no Fc region and subsequent signaling cascade is required. Since none of these nanomedicines have been FDA approved, an overview of decorated nanoparticles in clinical trials is given in table 2.

Table 2. Antibody decorated nanoparticles in clinical trials.

Name	Particle	Drug	Chemistry	Target	Antibody	Phase	Ref
Erbitux®ED-VsPAC	Bacterially-derived minicell	Paclitaxel	-	EGFR	mAb	II	169
SGT-53	Liposome	p53 gene	NA	Transferrin	scFv	Ib/II	170
MM-302	Liposome	Doxorubicin	NA	HER2	Fab	I	171
Lipovaxin-MM	Liposome	Melanoma antigens & IFNγ	-	DC-SIGN	sdAb	I	NA
SGT-94	Liposome	RB94 gene	NA	Transferrin	scFv	I	NA
C225-ILS-DOX	Liposome	Doxorubicin	Cysteine	EGFR	Fab (cetuximab)	I	172
MCC-465	Liposome	Doxorubicin	Lysine	Unknown	Fab_2	I*	173

* Clinical trial is performed in 2004, current status is not available.

Summary and Outlook

Site-specific modification of proteins has emerged as powerful tool to study proteins at the single amino acid level. Currently, the field is expanding towards applications for therapeutic proteins. Several studies have demonstrated the usefulness of unnatural amino acids in antibody drug conjugates. The time-consuming drug development and approval process has delayed the integration of these methods for therapeutic antibodies, but this can be expected in the near future.

In contrast to therapy, the approval process for diagnostic antibodies is shorter. The functionalization methods described in this review would be ideal to label antibodies with diagnostic tracers (radioactive, fluorescent or contrast agents), but will be even more important for the successful development of theranostics, a one-molecule combination of diagnosis and therapy.

Acknowledgements

This work was funded by the Focus & Massa project of the Utrecht University, the Netherlands. We thank Dr. S Oliveira for critical reading of the manuscript.

References

1. Sélo, I., Négroni, L., Créminon, C., Grassi, J. & Wal, J. M. Preferential labeling of alpha-amino N-terminal groups in peptides by biotin: application to the detection of specific anti-peptide antibodies by enzyme immunoassays. *J. Immunol. Methods* **199,** 127–38 (1996).
2. Chen, X., Muthoosamy, K., Pfisterer, A., Neumann, B. & Weil, T. Site-selective lysine modification of native proteins and peptides via kinetically controlled labeling. *Bioconjug. Chem.* **23,** 500–8 (2012).
3. Xu, G., Shin, S. B. Y. & Jaffrey, S. R. Chemoenzymatic labeling of protein C-termini for positive selection of C-terminal peptides. *ACS Chem. Biol.* **6,** 1015–20 (2011).
4. Kratz, H. *et al.* Straightforward thiol-mediated protein labelling with DTPA: Synthesis of a highly active 111In-annexin A5-DTPA tracer. *EJNMMI Res.* **2,** 17 (2012).
5. Shen, B.-Q. *et al.* Conjugation site modulates the in vivo stability and therapeutic activity of antibody-drug conjugates. *Nat. Biotechnol.* **30,** 184–9 (2012).
6. Shaunak, S. *et al.* Site-specific PEGylation of native disulfide bonds in therapeutic proteins. *Nat. Chem. Biol.* **2,** 312–3 (2006).
7. Stadtman, T. C. Emerging awareness of the critical roles of S-phosphocysteine and selenophosphate in biological systems. *Biofactors* **4,** 181–5 (1994).
8. Zhang, F. L. & Casey, P. J. Protein prenylation: molecular mechanisms and functional consequences. *Annu. Rev. Biochem.* **65,** 241–69 (1996).
9. Stepper, J. *et al.* Cysteine S-glycosylation, a new post-translational modification found in glycopeptide bacteriocins. *FEBS Lett.* **585,** 645–50 (2011).
10. Chalker, J. M. *et al.* Methods for converting cysteine to dehydroalanine on peptides and proteins. *Chem. Sci.* **2,** 1666 (2011).
11. Geoghegan, K. F. & Stroh, J. G. Site-directed conjugation of nonpeptide groups to peptides and proteins via periodate oxidation of a 2-amino alcohol. Application to modification at N-terminal serine. *Bioconjug. Chem.* **3,** 138–46
12. Kung, K. K.-Y., Wong, K.-F., Leung, K.-C. & Wong, M.-K. N-Terminal α-amino group modification of peptides by an oxime formation-exchange reaction sequence. *Chem. Commun. (Camb).* **49,** 6888–90 (2013).
13. Temming, R. P., Eggermont, L., van Eldijk, M. B., van Hest, J. C. M. & van Delft, F. L. N-Terminal dual protein functionalization by strain-promoted alkyne-nitrone cycloaddition. *Org. Biomol. Chem.* **11,** 2772–9 (2013).
14. Dawson, P. E., Muir, T. W., Clark-Lewis, I. & Kent, S. B. Synthesis of proteins by native chemical ligation. *Science* **266,** 776–9 (1994).
15. Ghosh, I. *et al.* Site-specific protein labeling by intein-mediated protein ligation. *Methods Mol. Biol.* **705,** 87–107 (2011).
16. Schoffelen, S. *et al.* Metal-free and pH-controlled introduction of azides in proteins. *Chem. Sci.* **2,** 701 (2011).
17. Gilmore, J. M., Scheck, R. A., Esser-Kahn, A. P., Joshi, N. S. & Francis, M. B. N-terminal protein modification through a biomimetic transamination reaction. *Angew. Chem. Int. Ed. Engl.* **45,** 5307–11 (2006).
18. Scheck, R. A., Dedeo, M. T., Iavarone, A. T. & Francis, M. B. Optimization of a biomimetic transamination reaction. *J. Am. Chem. Soc.* **130,** 11762–70 (2008).
19. Witus, L. S. *et al.* Site-specific protein transamination using N-methylpyridinium-4-carboxaldehyde. *J. Am. Chem. Soc.* **135,** 17223–9 (2013).
20. Chan, A. O.-Y. *et al.* Modification of N-terminal α-amino groups of peptides and proteins using ketenes. *J. Am. Chem. Soc.* **134,** 2589–98 (2012).
21. COHEN, G. N. & MUNIER, R. [Incorporation of structural analogues of amino acids in bacterial proteins]. *Biochim. Biophys. Acta* **21,** 592–3 (1956).
22. COWIE, D. B., COHEN, G. N., BOLTON, E. T. & DE ROBICHON-SZULMAJSTER, H. Amino acid analog incorporation into bacterial proteins. *Biochim. Biophys. Acta* **34,** 39–46 (1959).
23. Van Hest, J. C. & Tirrell, D. A. Efficient introduction of alkene functionality into proteins in vivo. *FEBS Lett.* **428,** 68–70 (1998).
24. Kiick, K. L., Saxon, E., Tirrell, D. A. & Bertozzi, C. R. Incorporation of azides into recombinant

proteins for chemoselective modification by the Staudinger ligation. *Proc. Natl. Acad. Sci. U. S. A.* **99,** 19–24 (2002).
25. Sletten, E. M. & Bertozzi, C. R. Bioorthogonal chemistry: fishing for selectivity in a sea of functionality. *Angew. Chem. Int. Ed. Engl.* **48,** 6974–98 (2009).
26. Schoffelen, S., Lambermon, M. H. L., van Eldijk, M. B. & van Hest, J. C. M. Site-specific modification of Candida antarctica lipase B via residue-specific incorporation of a non-canonical amino acid. *Bioconjug. Chem.* **19,** 1127–31 (2008).
27. Ibba, M., Kast, P. & Hennecke, H. Substrate specificity is determined by amino acid binding pocket size in Escherichia coli phenylalanyl-tRNA synthetase. *Biochemistry* **33,** 7107–12 (1994).
28. Ibba, M. & Hennecke, H. Relaxing the substrate specificity of an aminoacyl-tRNA synthetase allows in vitro and in vivo synthesis of proteins containing unnatural amino acids. *FEBS Lett.* **364,** 272–5 (1995).
29. Tang, Y. & Tirrell, D. A. Attenuation of the editing activity of the Escherichia coli leucyl-tRNA synthetase allows incorporation of novel amino acids into proteins in vivo. *Biochemistry* **41,** 10635–10645 (2002).
30. Kast, P. & Hennecke, H. Amino acid substrate specificity of Escherichia coli phenylalanyl-tRNA synthetase altered by distinct mutations. *J. Mol. Biol.* **222,** 99–124 (1991).
31. Döring, V. *et al.* Enlarging the amino acid set of Escherichia coli by infiltration of the valine coding pathway. *Science* **292,** 501–4 (2001).
32. Noren, C. J., Anthony-Cahill, S. J., Griffith, M. C. & Schultz, P. G. A general method for site-specific incorporation of unnatural amino acids into proteins. *Science* **244,** 182–8 (1989).
33. Bain, J. D., Diala, E. S., Glabe, C. G., Dix, T. A. & Chamberlin, A. R. Biosynthetic site-specific incorporation of a non-natural amino acid into a polypeptide. *J. Am. Chem. Soc.* **111,** 8013–8014 (1989).
34. Nowak, M. *et al.* Nicotinic receptor binding site probed with unnatural amino acid incorporation in intact cells. *Science (80-.).* **268,** 439–442 (1995).
35. Liu, D. R. & Schultz, P. G. Progress toward the evolution of an organism with an expanded genetic code. *Proc. Natl. Acad. Sci.* **96 ,** 4780–4785 (1999).
36. Young, T. S., Ahmad, I., Yin, J. A. & Schultz, P. G. An enhanced system for unnatural amino acid mutagenesis in E. coli. *J. Mol. Biol.* **395,** 361–74 (2010).
37. Liu, C. C. & Schultz, P. G. Adding New Chemistries to the Genetic Code. *Annu. Rev. Biochem.* **79,** 413–444 (2010).
38. Hohsaka, T., Ashizuka, Y., Murakami, H. & Sisido, M. Incorporation of Nonnatural Amino Acids into Streptavidin through In Vitro Frame-Shift Suppression. *J. Am. Chem. Soc.* **118,** 9778–9779 (1996).
39. Rodriguez, E. A., Lester, H. A. & Dougherty, D. A. In vivo incorporation of multiple unnatural amino acids through nonsense and frameshift suppression. *Proc. Natl. Acad. Sci. U. S. A.* **103,** 8650–5 (2006).
40. Karve, T. M. & Cheema, A. K. Small Changes Huge Impact: The Role of Protein Posttranslational Modifications in Cellular Homeostasis and Disease. *J. Amino Acids* **2011,** 1–13 (2011).
41. Resh, M. D. Trafficking and signaling by fatty-acylated and prenylated proteins. *Nat. Chem. Biol.* **2,** 584–590 (2006).
42. Casey, P. J. & Seabra, M. C. Protein prenyltransferases. *J. Biol. Chem.* **271,** 5289–92 (1996).
43. van't Hof, W. & Resh, M. D. Dual fatty acylation of p59(Fyn) is required for association with the T cell receptor zeta chain through phosphotyrosine-Src homology domain-2 interactions. *J. Cell Biol.* **145,** 377–89 (1999).
44. Heal, W. P., Wickramasinghe, S. R., Leatherbarrow, R. J. & Tate, E. W. N-Myristoyl transferase-mediated protein labelling in vivo. *Org. Biomol. Chem.* **6,** 2308–2315 (2008).
45. Kho, Y. *et al.* A tagging-via-substrate technology for detection and proteomics of farnesylated proteins. *Proc. Natl. Acad. Sci. U. S. A.* **101,** 12479–12484 (2004).
46. Greenberg, C. S., Birckbichler, P. J. & Rice, R. H. Transglutaminases: multifunctional cross-linking enzymes that stabilize tissues. *FASEB J.* **5,** 3071–7 (1991).
47. Lee, J.-H. *et al.* Glutamine (Q)-peptide screening for transglutaminase reaction using mRNA display. *Biotechnol. Bioeng.* **110,** 353–62 (2013).
48. Lin, C.-W. & Ting, A. Y. Transglutaminase-catalyzed site-specific conjugation of small-molecule probes to proteins in vitro and on the surface of living cells. *J. Am. Chem. Soc.* **128,** 4542–3 (2006).
49. Carrico, I. S., Carlson, B. L. & Bertozzi, C. R. Introducing genetically encoded aldehydes into

proteins. *Nat. Chem. Biol.* **3,** 321–2 (2007).
50. Wu, P. *et al.* Site-specific chemical modification of recombinant proteins produced in mammalian cells by using the genetically encoded aldehyde tag. *Proc. Natl. Acad. Sci. U. S. A.* **106,** 3000–5 (2009).
51. Rabuka, D., Rush, J. S., Dehart, G. W., Wu, P. & Bertozzi, C. R. Site-specific chemical protein conjugation using genetically encoded aldehyde tags. *Nat. Protoc.* **7,** 1052–1067 (2012).
52. Keppler, A. *et al.* A general method for the covalent labeling of fusion proteins with small molecules in vivo. *Nat. Biotechnol.* **21,** 86–9 (2003).
53. Mannesse, M. L. *et al.* Phosphonate analogues of triacylglycerols are potent inhibitors of lipase. *Biochim. Biophys. Acta* **1259,** 56–64 (1995).
54. Pries, F. *et al.* Histidine 289 is essential for hydrolysis of the alkyl-enzyme intermediate of haloalkane dehalogenase. *J. Biol. Chem.* **270,** 10405–11 (1995).
55. Gronemeyer, T., Chidley, C., Juillerat, A., Heinis, C. & Johnsson, K. Directed evolution of O6-alkylguanine-DNA alkyltransferase for applications in protein labeling. *Protein Eng. Des. Sel.* **19,** 309–16 (2006).
56. Bonasio, R. *et al.* Specific and covalent labeling of a membrane protein with organic fluorochromes and quantum dots. *Proc. Natl. Acad. Sci. U. S. A.* **104,** 14753–8 (2007).
57. Los, G. V & Wood, K. The HaloTag: a novel technology for cell imaging and protein analysis. *Methods Mol. Biol.* **356,** 195–208 (2007).
58. Gautier, A. *et al.* An engineered protein tag for multiprotein labeling in living cells. *Chem. Biol.* **15,** 128–36 (2008).
59. Chen, I., Howarth, M., Lin, W. & Ting, A. Y. Site-specific labeling of cell surface proteins with biophysical probes using biotin ligase. *Nat. Methods* **2,** 99–104 (2005).
60. Fernández-Suárez, M. *et al.* Redirecting lipoic acid ligase for cell surface protein labeling with small-molecule probes. *Nat. Biotechnol.* **25,** 1483–7 (2007).
61. Yao, J. Z. *et al.* Fluorophore targeting to cellular proteins via enzyme-mediated azide ligation and strain-promoted cycloaddition. *J. Am. Chem. Soc.* **134,** 3720–8 (2012).
62. Baruah, H., Puthenveetil, S., Choi, Y.-A., Shah, S. & Ting, A. Y. An engineered aryl azide ligase for site-specific mapping of protein-protein interactions through photo-cross-linking. *Angew. Chem. Int. Ed. Engl.* **47,** 7018–21 (2008).
63. Cohen, J. D., Thompson, S. & Ting, A. Y. Structure-guided engineering of a Pacific Blue fluorophore ligase for specific protein imaging in living cells. *Biochemistry* **50,** 8221–5 (2011).
64. Liu, D. S. *et al.* Diels-Alder cycloaddition for fluorophore targeting to specific proteins inside living cells. *J. Am. Chem. Soc.* **134,** 792–5 (2012).
65. Lambalot, R. H. *et al.* A new enzyme superfamily - the phosphopantetheinyl transferases. *Chem. Biol.* **3,** 923–36 (1996).
66. Lambalot, R. H. & Walsh, C. T. Cloning, overproduction, and characterization of the Escherichia coli holo-acyl carrier protein synthase. *J. Biol. Chem.* **270,** 24658–61 (1995).
67. Fichtlscherer, F., Wellein, C., Mittag, M. & Schweizer, E. A novel function of yeast fatty acid synthase. *Eur. J. Biochem.* **267,** 2666–2671 (2000).
68. Yin, J., Liu, F., Schinke, M., Daly, C. & Walsh, C. T. Phagemid encoded small molecules for high throughput screening of chemical libraries. *J. Am. Chem. Soc.* **126,** 13570–13571 (2004).
69. Yin, J. *et al.* Genetically encoded short peptide tag for versatile protein labeling by Sfp phosphopantetheinyl transferase. *Proc. Natl. Acad. Sci. U. S. A.* **102,** 15815–20 (2005).
70. Zhou, Z. *et al.* Genetically encoded short peptide tags for orthogonal protein labeling by Sfp and AcpS phosphopantetheinyl transferases. *ACS Chem. Biol.* **2,** 337–46 (2007).
71. Mazmanian, S. K., Liu, G., Ton-That, H. & Schneewind, O. Staphylococcus aureus sortase, an enzyme that anchors surface proteins to the cell wall. *Science* **285,** 760–3 (1999).
72. Marraffini, L. A., Dedent, A. C. & Schneewind, O. Sortases and the art of anchoring proteins to the envelopes of gram-positive bacteria. *Microbiol. Mol. Biol. Rev.* **70,** 192–221 (2006).
73. Popp, M. W.-L. & Ploegh, H. L. Making and breaking peptide bonds: protein engineering using sortase. *Angew. Chemie Int. Ed.* **50,** 5024–5032 (2011).
74. Popp, M. W., Artavanis-Tsakonas, K. & Ploegh, H. L. Substrate filtering by the active site crossover loop in UCHL3 revealed by sortagging and gain-of-function mutations. *J. Biol. Chem.* **284,** 3593–3602 (2009).
75. Antos, J. M. *et al.* Site-specific N- and C-terminal labeling of a single polypeptide using sortases of

different specificity. *J. Am. Chem. Soc.* **131,** 10800–1 (2009).
76. Antos, J. M. *et al.* A straight path to circular proteins. *J. Biol. Chem.* **284,** 16028–16036 (2009).
77. Wu, Z., Guo, X. & Guo, Z. Sortase A-catalyzed peptide cyclization for the synthesis of macrocyclic peptides and glycopeptides. *Chem. Commun.* **47,** 9218–9220 (2011).
78. Popp, M. W., Dougan, S. K., Chuang, T.-Y., Spooner, E. & Ploegh, H. L. Sortase-catalyzed transformations that improve the properties of cytokines. *Proc. Natl. Acad. Sci. U. S. A.* **108,** 3169–3174 (2011).
79. Levary, D. A., Parthasarathy, R., Boder, E. T. & Ackerman, M. E. Protein-Protein Fusion Catalyzed by Sortase A. *PLoS One* **6,** 6 (2011).
80. Chen, I., Dorr, B. M. & Liu, D. R. A general strategy for the evolution of bond-forming enzymes using yeast display. *Proc. Natl. Acad. Sci. U. S. A.* **108,** 11399–404 (2011).
81. Perler, F. B. *et al.* Protein splicing elements: inteins and exteins--a definition of terms and recommended nomenclature. *Nucleic Acids Res.* **22,** 1125–7 (1994).
82. Xu, M. Q. & Evans, T. C. Intein-mediated ligation and cyclization of expressed proteins. *Methods* **24,** 257–77 (2001).
83. Möhlmann, S., Bringmann, P., Greven, S. & Harrenga, A. Site-specific modification of ED-B-targeting antibody using intein-fusion technology. *BMC Biotechnol.* **11,** 76 (2011).
84. Wood, R. J. *et al.* Optimized conjugation of a fluorescent label to proteins via intein-mediated activation and ligation. *Bioconjug. Chem.* **15,** 366–72
85. Gottlieb, D., Grunwald, C., Nowak, C., Kuhlmann, J. & Waldmann, H. Intein-mediated in vitro synthesis of lipidated Ras proteins. *Chem. Commun.* 260–262 (2006).
86. Reulen, S. W. A., van Baal, I., Raats, J. M. H. & Merkx, M. Efficient, chemoselective synthesis of immunomicelles using single-domain antibodies with a C-terminal thioester. *BMC Biotechnol.* **9,** 66 (2009).
87. Muir, T. W., Sondhi, D. & Cole, P. A. Expressed protein ligation: a general method for protein engineering. *Proc. Natl. Acad. Sci. U. S. A.* **95,** 6705–6710 (1998).
88. Girish, A. *et al.* Site-specific immobilization of proteins in a microarray using intein-mediated protein splicing. *Bioorg. Med. Chem. Lett.* **15,** 2447–51 (2005).
89. Yeo, D. S. Y. *et al.* Cell-permeable small molecule probes for site-specific labeling of proteins. *Chem. Commun.* 2870–2871 (2003).
90. Southworth, M. W., Amaya, K., Evans, T. C., Xu, M. Q. & Perler, F. B. Purification of proteins fused to either the amino or carboxy terminus of the Mycobacterium xenopi gyrase A intein. *Biotechniques* **27,** 110–4, 116, 118–20 (1999).
91. Bracher, P. J., Snyder, P. W., Bohall, B. R. & Whitesides, G. M. The relative rates of thiol-thioester exchange and hydrolysis for alkyl and aryl thioalkanoates in water. *Orig. Life Evol. Biosph.* **41,** 399–412 (2011).
92. Walsh, G. & Jefferis, R. Post-translational modifications in the context of therapeutic proteins. *Nat. Biotechnol.* **24,** 1241–52 (2006).
93. Spiro, R. G. Protein glycosylation: nature, distribution, enzymatic formation, and disease implications of glycopeptide bonds. *Glycobiology* **12,** 43R–56R (2002).
94. Comer, F. I. & Hart, G. W. O-Glycosylation of Nuclear and Cytosolic Proteins: DYNAMIC INTERPLAY BETWEEN O-GlcNAc ANDO-PHOSPHATE . *J. Biol. Chem.* **275 ,** 29179–29182 (2000).
95. Solá, R. J. & Griebenow, K. Effects of glycosylation on the stability of protein pharmaceuticals. *J. Pharm. Sci.* **98,** 1223–45 (2009).
96. Saxon, E. & Bertozzi, C. R. Cell surface engineering by a modified Staudinger reaction. *Science* **287,** 2007–10 (2000).
97. Laughlin, S. T. & Bertozzi, C. R. Metabolic labeling of glycans with azido sugars and subsequent glycan-profiling and visualization via Staudinger ligation. *Nat. Protoc.* **2,** 2930–44 (2007).
98. Clark, P. M. *et al.* Direct in-gel fluorescence detection and cellular imaging of O-GlcNAc-modified proteins. *J. Am. Chem. Soc.* **130,** 11576–7 (2008).
99. Robert Aggeler, J. B. Q. L. B. A. Site-specific Labeling of Antibody N-glycans using a Click Chemistry-mediated Chemoenzymatic Approach. *J. Biomol. Tech.* **23,** S28 (2012).
100. Zhang, X.-L. Roles of glycans and glycopeptides in immune system and immune-related diseases. *Curr. Med. Chem.* **13,** 1141–7 (2006).
101. Newman, D. J. & Cragg, G. M. Natural products as sources of new drugs over the last 25 years. *J. Nat. Prod.* **70,** 461–477 (2007).

102. Leader, B., Baca, Q. J. & Golan, D. E. Protein therapeutics: a summary and pharmacological classification. *Nat. Rev. Drug Discov.* **7,** 21–39 (2008).
103. Brown, L. R. Commercial challenges of protein drug delivery. *Expert Opin. Drug Deliv.* **2,** 29–42 (2005).
104. Morishita, M. & Peppas, N. A. Is the oral route possible for peptide and protein drug delivery? *Drug Discov. Today* **11,** 905–10 (2006).
105. Jenkins, N. Modifications of therapeutic proteins: challenges and prospects. *Cytotechnology* **53,** 121–125 (2007).
106. Brater, D. C. Measurement of renal function during drug development. *Br. J. Clin. Pharmacol.* **54,** 87–95 (2002).
107. Harmsen, M. M. & De Haard, H. J. Properties, production, and applications of camelid single-domain antibody fragments. *Appl. Microbiol. Biotechnol.* **77,** 13–22 (2007).
108. Flanagan, R. J. & Jones, A. L. Fab antibody fragments: some applications in clinical toxicology. *Drug Saf. an Int. J. Med. Toxicol. drug Exp.* **27,** 1115–1133 (2004).
109. Solá, R. J. & Griebenow, K. Glycosylation of therapeutic proteins: an effective strategy to optimize efficacy. *BioDrugs Clin. Immunother. Biopharm. gene Ther.* **24,** 9–21 (2010).
110. Baker, K., Rath, T. & Blumberg, R. in *Mol. Cell. Mech. Antib. Act. SE - 8* (Nimmerjahn, F.) 189–219 (Springer New York, 2013). doi:10.1007/978-1-4614-7107-3_8
111. Veronese, F. M. & Mero, A. The impact of PEGylation on biological therapies. *BioDrugs Clin. Immunother. Biopharm. gene Ther.* **22,** 315–329 (2008).
112. Veronese, F. M., Caliceti, P. & Schiavon, O. Branched and Linear Poly(Ethylene Glycol): Influence of the Polymer Structure on Enzymological, Pharmacokinetic, and Immunological Properties of Protein Conjugates. *J. Bioact. Compat. Polym.* **12 ,** 196–207 (1997).
113. Leong, S. R. *et al.* Adapting pharmacokinetic properties of a humanized anti-interleukin-8 antibody for therapeutic applications using site-specific pegylation. *Cytokine* **16,** 106–19 (2001).
114. Vugmeyster, Y. *et al.* Pharmacokinetic, biodistribution, and biophysical profiles of TNF nanobodies conjugated to linear or branched poly(ethylene glycol). *Bioconjug. Chem.* **23,** 1452–62 (2012).
115. Richter, A. W. & Akerblom, E. Antibodies against polyethylene glycol produced in animals by immunization with monomethoxy polyethylene glycol modified proteins. *Int. Arch. Allergy Appl. Immunol.* **70,** 124–31 (1983).
116. Armstrong, J. K. *et al.* Antibody against poly(ethylene glycol) adversely affects PEG-asparaginase therapy in acute lymphoblastic leukemia patients. *Cancer* **110,** 103–111 (2007).
117. Ganson, N. J., Kelly, S. J., Scarlett, E., Sundy, J. S. & Hershfield, M. S. Control of hyperuricemia in subjects with refractory gout, and induction of antibody against poly(ethylene glycol) (PEG), in a phase I trial of subcutaneous PEGylated urate oxidase. *ARTHRITIS Res. Ther.* **8,** (2006).
118. Knop, K., Hoogenboom, R., Fischer, D. & Schubert, U. S. Poly(ethylene glycol) in drug delivery: pros and cons as well as potential alternatives. *Angew. Chem. Int. Ed. Engl.* **49,** 6288–308 (2010).
119. Jefferis, R., Pound, J., Lund, J. & Goodall, M. Effector mechanisms activated by human IgG subclass antibodies: clinical and molecular aspects. Review article. *Ann. Biol. Clin. (Paris).* **52,** 57–65 (1994).
120. Jefferis, R. Recombinant antibody therapeutics: the impact of glycosylation on mechanisms of action. *Trends Pharmacol. Sci.* **30,** 356–362 (2009).
121. Nesbitt, A. *et al.* Mechanism of action of certolizumab pegol (CDP870): in vitro comparison with other anti-tumor necrosis factor alpha agents. *Inflamm. Bowel Dis.* **13,** 1323–32 (2007).
122. Jiang, X.-R. *et al.* Advances in the assessment and control of the effector functions of therapeutic antibodies. *Nat. Rev. Drug Discov.* **10,** 101–11 (2011).
123. Pedley, R. B. *et al.* The potential for enhanced tumour localisation by poly(ethylene glycol) modification of anti-CEA antibody. *Br. J. Cancer* **70,** 1126–1130 (1994).
124. Di Paolo, A. & Bocci, G. Drug distribution in tumors: mechanisms, role in drug resistance, and methods for modification. *Curr. Oncol. Rep.* **9,** 109–14 (2007).
125. Klein, A. V & Hambley, T. W. Platinum drug distribution in cancer cells and tumors. *Chem. Rev.* **109,** 4911–20 (2009).
126. Thurber, G. M., Schmidt, M. M. & Wittrup, K. D. Factors determining antibody distribution in tumors. *Trends Pharmacol. Sci.* **29,** 57–61 (2008).
127. Fujimori, K., Covell, D. G., Fletcher, J. E. & Weinstein, J. N. Modeling analysis of the global and microscopic distribution of immunoglobulin G, F(ab')2, and Fab in tumors. *Cancer Res.* **49,** 5656–63 (1989).

128. Saga, T. *et al.* Targeting cancer micrometastases with monoclonal antibodies: a binding-site barrier. *Proc. Natl. Acad. Sci. U. S. A.* **92,** 8999–9003 (1995).
129. Rudnick, S. I. & Adams, G. P. Affinity and avidity in antibody-based tumor targeting. *Cancer Biother. Radiopharm.* **24,** 155–61 (2009).
130. Roopenian, D. C. & Akilesh, S. FcRn: the neonatal Fc receptor comes of age. *Nat. Rev. Immunol.* **7,** 715–725 (2007).
131. Ghetie, V. *et al.* Abnormally short serum half-lives of IgG in beta 2-microglobulin-deficient mice. *Eur. J. Immunol.* **26,** 690–6 (1996).
132. Junghans, R. P. & Anderson, C. L. The protection receptor for IgG catabolism is the beta2-microglobulin-containing neonatal intestinal transport receptor. *Proc. Natl. Acad. Sci. U. S. A.* **93,** 5512–6 (1996).
133. Israel, E. J., Wilsker, D. F., Hayes, K. C., Schoenfeld, D. & Simister, N. E. Increased clearance of IgG in mice that lack beta 2-microglobulin: possible protective role of FcRn. *Immunology* **89,** 573–8 (1996).
134. Datta-Mannan, A., Witcher, D. R., Lu, J. & Wroblewski, V. J. Influence of improved FcRn binding on the subcutaneous bioavailability of monoclonal antibodies in cynomolgus monkeys. *MAbs* **4,** (2012).
135. Vugmeyster, Y., Xu, X., Theil, F.-P., Khawli, L. A. & Leach, M. W. Pharmacokinetics and toxicology of therapeutic proteins: Advances and challenges. *World J. Biol. Chem.* **3,** 73–92 (2012).
136. Casi, G. & Neri, D. Antibody-drug conjugates: basic concepts, examples and future perspectives. *J. Control. Release* **161,** 422–8 (2012).
137. Dosio, F., Brusa, P. & Cattel, L. Immunotoxins and anticancer drug conjugate assemblies: the role of the linkage between components. *Toxins (Basel).* **3,** 848–83 (2011).
138. Chari, R. V. J. Targeted cancer therapy: conferring specificity to cytotoxic drugs. *Acc. Chem. Res.* **41,** 98–107 (2008).
139. Hudis, C. A. Trastuzumab--mechanism of action and use in clinical practice. *N. Engl. J. Med.* **357,** 39–51 (2007).
140. Lewis Phillips, G. D. *et al.* Targeting HER2-positive breast cancer with trastuzumab-DM1, an antibody-cytotoxic drug conjugate. *Cancer Res.* **68,** 9280–9290 (2008).
141. Hurvitz, S. A. *et al.* Phase II randomized study of trastuzumab emtansine versus trastuzumab plus docetaxel in patients with human epidermal growth factor receptor 2-positive metastatic breast cancer. *J. Clin. Oncol.* **31,** 1157–63 (2013).
142. Girish, S. *et al.* Clinical pharmacology of trastuzumab emtansine (T-DM1): an antibody-drug conjugate in development for the treatment of HER2-positive cancer. *Cancer Chemother. Pharmacol.* **69,** 1229–40 (2012).
143. Francisco, J. A. *et al.* cAC10-vcMMAE, an anti-CD30-monomethyl auristatin E conjugate with potent and selective antitumor activity. *Blood* **102,** 1458–1465 (2003).
144. Hamblett, K. J. *et al.* Effects of drug loading on the antitumor activity of a monoclonal antibody drug conjugate. *Clin. Cancer Res.* **10,** 7063–7070 (2004).
145. Kim, C. H. *et al.* Synthesis of bispecific antibodies using genetically encoded unnatural amino acids. *J. Am. Chem. Soc.* **134,** 9918–9921 (2012).
146. Axup, J. Y. *et al.* Synthesis of site-specific antibody-drug conjugates using unnatural amino acids. *Proc. Natl. Acad. Sci. U. S. A.* **109,** 16101–6 (2012).
147. Kazane, S. A. *et al.* Self-assembled antibody multimers through peptide nucleic acid conjugation. *J. Am. Chem. Soc.* **135,** 340–346 (2013).
148. Dowell, J. A., Korth-Bradley, J., Liu, H., King, S. P. & Berger, M. S. *Pharmacokinetics of gemtuzumab ozogamicin, an antibody-targeted chemotherapy agent for the treatment of patients with acute myeloid leukemia in first relapse. J. Clin. Pharmacol.* **41,** 1206–1214 (2001).
149. Chames, P. & Baty, D. Bispecific antibodies for cancer therapy: the light at the end of the tunnel? *MAbs* **1,** 539–47
150. Staerz, U. D., Kanagawa, O. & Bevan, M. J. Hybrid antibodies can target sites for attack by T cells. *Nature* **314,** 628–31
151. Karpovsky, B., Titus, J. A., Stephany, D. A. & Segal, D. M. Production of target-specific effector cells using hetero-cross-linked aggregates containing anti-target cell and anti-Fc gamma receptor antibodies. *J. Exp. Med.* **160,** 1686–701 (1984).
152. Perez, P., Hoffman, R. W., Shaw, S., Bluestone, J. A. & Segal, D. M. Specific targeting of cytotoxic T

cells by anti-T3 linked to anti-target cell antibody. *Nature* **316,** 354–6
153. Reusch, U. *et al.* Anti-CD3 x anti-epidermal growth factor receptor (EGFR) bispecific antibody redirects T-cell cytolytic activity to EGFR-positive cancers in vitro and in an animal model. *Clin. Cancer Res.* **12,** 183–90 (2006).
154. Shalaby, M. R. *et al.* Development of humanized bispecific antibodies reactive with cytotoxic lymphocytes and tumor cells overexpressing the HER2 protooncogene. *J. Exp. Med.* **175,** 217–25 (1992).
155. Spiess, C. *et al.* Bispecific antibodies with natural architecture produced by co-culture of bacteria expressing two distinct half-antibodies. *Nat. Biotechnol.* **31,** 753–8 (2013).
156. Shen, J. & Zhu, Z. Catumaxomab, a rat/murine hybrid trifunctional bispecific monoclonal antibody for the treatment of cancer. *Curr. Opin. Mol. Ther.* **10,** 273–284 (2008).
157. Lindhofer, H., Mocikat, R., Steipe, B. & Thierfelder, S. Preferential species-restricted heavy/light chain pairing in rat/mouse quadromas. Implications for a single-step purification of bispecific antibodies. *J. Immunol.* **155,** 219–25 (1995).
158. Linke, R., Klein, A. & Seimetz, D. Catumaxomab: clinical development and future directions. *MAbs* **2,** 129–36
159. Martinelli, E., De Palma, R., Orditura, M., De Vita, F. & Ciardiello, F. Anti-epidermal growth factor receptor monoclonal antibodies in cancer therapy. *Clin. Exp. Immunol.* **158,** 1–9 (2009).
160. Hutchins, B. M. *et al.* Site-specific coupling and sterically controlled formation of multimeric antibody fab fragments with unnatural amino acids. *J. Mol. Biol.* **406,** 595–603 (2011).
161. Dykman, L. A. & Khlebtsov, N. G. Gold nanoparticles in biology and medicine: recent advances and prospects. *Acta Naturae* **3,** 34–55 (2011).
162. Kontermann, R. E. Immunoliposomes for cancer therapy. *Curr. Opin. Mol. Ther.* **8,** 39–45 (2006).
163. Meng, F., Engbers, G. H. M. & Feijen, J. Biodegradable polymersomes as a basis for artificial cells: encapsulation, release and targeting. *J. Control. Release* **101,** 187–198 (2005).
164. Lin, J. J., Ghoroghchian, P. P., Zhang, Y. & Hammer, D. A. Adhesion of antibody-functionalized polymersomes. *Langmuir Acs J. Surfaces Colloids* **22,** 3975–3979 (2006).
165. Lee, J. S., Groothuis, T., Cusan, C., Mink, D. & Feijen, J. Lysosomally cleavable peptide-containing polymersomes modified with anti-EGFR antibody for systemic cancer chemotherapy. *Biomaterials* **32,** 9144–53 (2011).
166. Debets, M. F. *et al.* Nanobody-functionalized polymersomes for tumor-vessel targeting. *Macromol. Biosci.* **13,** 938–45 (2013).
167. Fang, J., Nakamura, H. & Maeda, H. The EPR effect: Unique features of tumor blood vessels for drug delivery, factors involved, and limitations and augmentation of the effect. *Adv. Drug Deliv. Rev.* **63,** 136–51 (2011).
168. Albanese, A., Tang, P. S. & Chan, W. C. W. The effect of nanoparticle size, shape, and surface chemistry on biological systems. *Annu. Rev. Biomed. Eng.* **14,** 1–16 (2012).
169. MacDiarmid, J. A. *et al.* Bacterially derived 400 nm particles for encapsulation and cancer cell targeting of chemotherapeutics. *Cancer Cell* **11,** 431–45 (2007).
170. Senzer, N. *et al.* Phase I Study of a Systemically Delivered p53 Nanoparticle in Advanced Solid Tumors. *Mol. Ther. J. Am. Soc. Gene Ther.* **21,** 1096–103 (2013).
171. Wickham, T. & Futch, K. A Phase I Study of MM-302, a HER2-targeted Liposomal Doxorubicin. *Patients with Adv. HER2-Positive Breast Cancer. Cancer Res* **72,** P5–18 (2012).
172. Mamot, C. *et al.* Tolerability, safety, pharmacokinetics, and efficacy of doxorubicin-loaded anti-EGFR immunoliposomes in advanced solid tumours: a phase 1 dose-escalation study. *Lancet Oncol.* **13,** 1234–1241 (2012).
173. Matsumura, Y. *et al.* Phase I and pharmacokinetic study of MCC-465, a doxorubicin (DXR) encapsulated in PEG immunoliposome, in patients with metastatic stomach cancer. *Ann. Oncol.* **15,** 517–525 (2004).

Chapter 3

Nanobodies and their therapeutic applications

Remko van Vught, Paul van Bergen en Henegouwen, Roland J Pieters, Eefjan Breukink

Abstract

Monoclonal antibodies (mAb) have emerged as protein-based drugs for the treatment of Crohn's disease, rheumatoid arthritis and various forms of cancer. Extended knowledge has become available over the years in an attempt to improve monoclonal antibody therapies. One of the remaining drawbacks of mAbs is the limited tumor penetration impeded by their size. In order to overcome this issue, research groups and companies have explored (therapeutic) applications of the smaller sized antibody fragments. One unique antibody fragment is the VH domain of heavy-chain antibodies of camelids (VHH, also known as nanobody or sdAb). Here, the properties and therapeutic applications of nanobodies will be reviewed.

From native antibodies to single domain antibody fragments

The adaptive immune system is essential for the protection against pathogenic hosts and toxins. After invasion, molecular determinants specific for the pathogen induce the primary response and specific memory cells for future challenges. The neutralization can occur via various mechanisms but all require specific binding of an antibody, also known as immunoglobulin (Ig). Although several types of antibodies with distinct functions exist (IgA, IgD, IgE, IgG and IgM), the IgG subtype is predominantly involved in therapeutic applications.

Antibodies of the IgG subtype are monomeric, y-shaped proteins, composed of two identical heavy and two identical light peptide chains (Fig. 1)[1]. Binding by the antibody occurs via one of the two antigen binding sites, after which effector functions are mediated by the Fc domain[2]. The Fc domain can activate the complement system (classical pathway), but also neutralize the pathogen via antibody-dependent cell-mediated cytotoxicity (ADCC) or intracellular antibody-mediated proteolysis (IAMP). In addition, binding to the neonatal Fc receptor (FcRn) rescues the antibody from degradation, resulting in long half-lives (7-21 days). These effector functions are ideal for many therapeutic applications but can also be unwanted and give rise to side effects when only antigen neutralization is required. Moreover, in case of imaging, the long half-life and effector functions are also undesirable. There are various ways to silence the Fc functions. Removal of glycosylation of the Fc domain impairs the binding to Fc receptors[3]. Another approach is to remove the Fc domain by proteolysis (Fab), or by genetic engineering.

Antibody proteolysis by papain results in antibody fragments of 55 kDa bearing only one light domain and a part of the heavy chain (Fab fragment), and therefore have only one antigen binding region (Fig. 1)[1]. Genetic engineering of the variable regions from both heavy and light chain results in the formation of only the antigen-binding region (Fv). The introduction of a flexible linker between both domains prevents the dissociation of the two chains, resulting in the single-chain variable fragment (scFv). The scFv was demonstrated to be expressed and secreted from *Escherichia coli* and some of them retained high affinities for their antigens[4]. More problematic is the reduced solubility and stability, resulting in aggregation. Although the affinity for the antigen is retained for both Fab and scFv fragments, the avidity is lost compared with mAb and the smaller protein size changes the pharmacokinetics. Where mAb have a long half-life, this is reduced to 10-20 hours for Fab fragments[5] and to <1 hour for scFv fragments[6]. This renders antibody fragments less effective for therapy, but in combination with deep tissue penetration makes them more suitable for imaging.

A special class of antibodies, the heavy-chain antibodies (HcAbs, Fig. 1), were discovered in camelids (camels, dromedaries, alpaca's and llamas)[7]. HcAbs are fully functional antibodies, devoid of a light chain and first constant domain CH1, and are present next to the classical antibodies in these animals. Other functional HcAbs have been found in primitive fish

species including ratfish, nurse and wobbegong sharks[8]. In contrast, non-functional heavy chain antibodies have been described as the gamma heavy chain disease in humans[9]. The antibody binding fragment of camelid HcAbs is the single chain domain VHH (Fig. 1)[10]. The VHH domain is only 15 kDa and harbors favorable antigen binding properties including high affinity, solubility and stability. Interestingly, more potent VHHs are commonly selected by hypermutation in phage display screening[11]. VHHs are commercialized by the Belgian company Ablynx(r) under the name of nanobodies, referring to the small size[12].

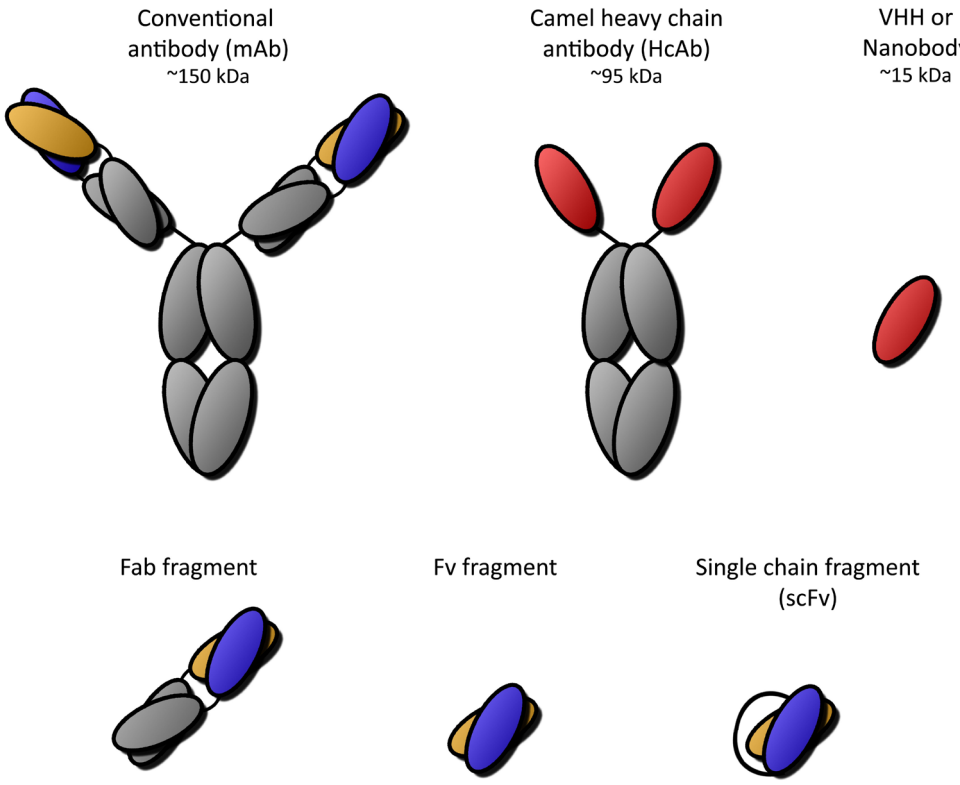

Figure 1. Schematic representation of antibodies and their antibody fragments. The heavy (VH) and light (VL) variable domain were depicted in blue and yellow, whereas the VH domain of heavy-chain antibodies of camelids was depicted in red. Fab fragments lacking the Fc domain are generated from conventional antibodies by Papain proteolysis. Genetic engineering of the variable regions from both heavy and light chain results in the formation of only the antigen-binding region (Fv), which can be stabilized by a flexible linker (scFv). Genetic engineering of the variable region of HcAbs results in a single variable domain (VHH, also known as nanobody or sdAb).

Structural analysis of nanobodies

Single chain fragments derived from classical antibodies carry both the heavy (VH) and light (VL) variable domain. Nanobodies are homologous to the human VH3 domain but lack the VL

domain[10]. Instead, amino acid substitutions at positions 37, 44, 45, and 47 (Kabat numbering) are found to compensate for the hydrophobic VL interface (framework 2). In addition, the Leu11 is replaced by a serine as a consequence of the missing CH1 domain in the camel heavy chain immunoglobulins. Another striking difference as compared with the classical VH3 domain is the extended complementarity determining region (CDR) 3 in nanobodies. The longer CDR3 can form a fingerlike structure to interact with cavities of target proteins[13]. This allows nanobodies to bind 'hidden' epitopes such as active sites, in contrast to the more surficial epitopes of classical antibodies. A good example is the crystal structure of lysozyme with its substrate and of lysozyme in complex with a nanobody (Fig. 2)[14]. Here, half of the extended CDR3 (blue) interacts with its own Vh region, while the other half invades the active site of lysozyme.

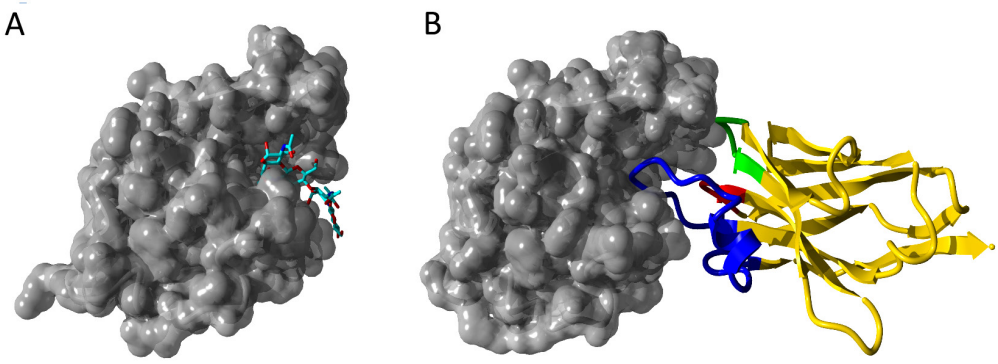

Figure 2. Crystal structures of lysozyme in complex with its substrate (a) and a nanobody (b). CDR3 of the nanobody (in blue) penetrates deeply into the active site of lysozyme. CDR1 and CDR2 are shown in red and green, respectively.

Compared with classical antibodies, certain nanobodies have been demonstrated to remain functional during or after incubation at high temperatures (up to 90°C) and after incubation at extreme pH conditions[15,16]. This increased stability has predominantly been explained by the efficient folding capacity and to a minor extent by the resistance against denaturation. Hydrophilic residues in the VL interacting region are important for the thermostability, as demonstrated by *in vitro* evolution of VH domains[17]. Next to this, the nanobody requires only the refolding of one single domain and not both the VH and VL domain. The lack of the VL domain is also advantageous for engineering multivalency (Fig 3). The fusion of two (or more) nanobodies results in increased affinity (avidity) when both antibody fragments bind the same target protein at the same epitope (bivalent) or different epitopes (biparatopic). The latter case has been shown to enhance internalization by receptor mediated clustering[18]. Alternatively, the two (or more) nanobodies can also bind different targets (bispecific). The usefulness of bispecific

nanobodies has clearly been demonstrated for therapeutic applications[19]. In this example, two nanobodies target the cancer antigen EGFR and one nanobody binds to albumin, resulting in a prolonged half-life of up to 2 days.

The high homology of nanobodies with human VH3 gives them a low immunogenic potential[20]. Additional humanization can further minimize the immunogenicity and is therefore recommended for applications in the clinic. Recently, a general approach to derive humanized nanobodies was published[21].

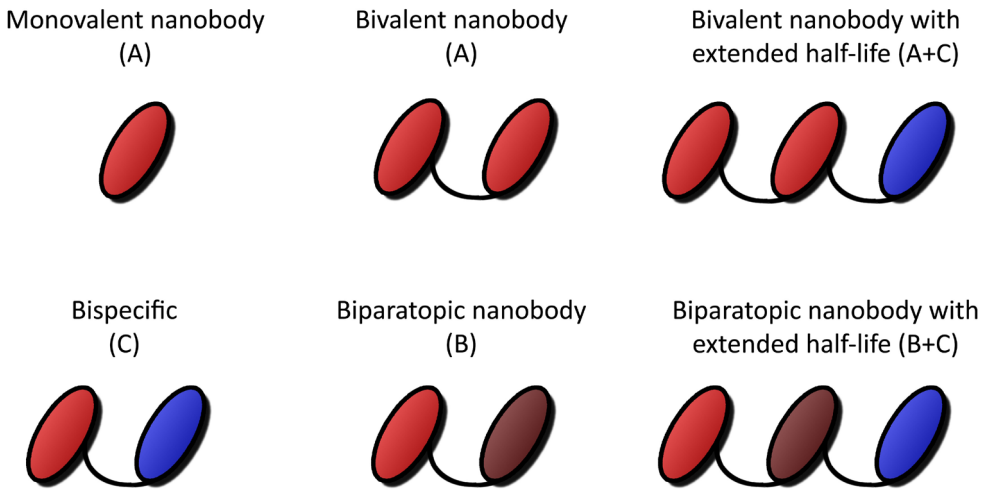

Figure 3. Schematic representation of multivalent nanobodies. Several combinations of nanobodies have been produced in mono-, bi- or trivalent formats (A) monospecific: binding the same epitope of the same target, (B) biparatopic: binding two different epitopes of the same target, (C) bispecific: binding two different targets, or in combination with an anti-Albumin nanobody for extended half-life (in blue).

Applications

The beneficial features of nanobodies stimulated research groups and companies to explore possible (therapeutic) applications. Of these, the small size and subsequent short half-life (2 hours) can be seen as both an advantage and a disadvantage[22]. For imaging agents, high specificity, high affinity and high tumor to background ratio (TBR) are required. The first two facilitate high accumulation at the target site. In order to localize tumors, the tumor specific signal must be higher than the signal obtained from background noise. The non-specific signal reduces rapidly over time by the high blood clearance, consequently increases the TBR and enables imaging within 4 hours post injection. This makes nanobodies ideal imaging agents, as has been demonstrated for several imaging modalities including PET, SPECT, MRI and optical imaging[23]. Still, nanobody-based imaging agents (and those based on proteins in general) hardly reach intracellular targets and targets in the brain. Detection at sites close to the kidneys and

bladder can also be challenging due to the high accumulation of nanobodies at those organs.

The situation is different for therapeutic applications. Due to their short *in vivo* half-life, the therapeutic efficacy of nanobodies is restricted to a single and short treatment protocol. This is exemplified by nanobody applications where nanobodies are binding to soluble ligands, as is the case with the vWF where nanobodies can be used to prevent blood clotting. Several methods have been developed to prolong the circulation of nanobodies including binding to serum proteins[24], pegylation[25] and fusion to IgFc[26]. Depending on the application, one is preferred over the other, while all have some adverse effects. The recent progress of several therapeutic applications will be discussed in more detail.

Neutralization

One well described application is the neutralization of scorpion and snake venom by nanobodies. The venom consists of small highly toxic peptides that diffuse rapidly through blood and tissue[27]. Most antivenoms are immunoglobulin fragments which suffer from low potency and induce adverse effects (e.g. anaphylactic shock). In contrast to the small size peptides (~7 kDa), the antibody fragments are much larger and therefore diffuse slower throughout the body. Nanobodies are smaller (~15 KDa) and thus more suitable. Potent nanobody binders can be selected by phage display screening. For example, neutralizing nanobodies were raised against the AahII peptide (LD_{50} <3 ng) of the North African scorpion Aah (Androctonus australis hector)[28]. Of the 12 nanobodies evaluated in this study, some were 'best in class' and one exceeded the neutralizing potency of all previous antibody fragments.

In another study, nanobodies were raised against ART 2.2, a toxin-related ectoenzyme on leukocytes[29]. Nanobodies could specifically block the enzymatic and cytotoxic activities of ART 2.2 while ecto-enzymes ART1 and ART2.1 remained functional. The full *in vivo* inhibition of ART 2.2 was evident from as early as 15 minutes to up to 6 hours. Interestingly, fusion to the Fc-domain of mouse IgG1 prolonged the nanobody-based blockade to up to 7 days[26]. The larger size, however affected the diffusion of the fusion protein, which now requires 2 hours to fully block the activity of ART 2.2.

Several groups have attempted to neutralize the rotavirus, the cause of severe diarrhea under infants and young children. The stability of nanobodies to extreme pH's permits oral application and administration to mice and protection against diarrhea was demonstrated[30]. In addition, the administration of Lactobacilli expressing the nanobody on their surface was also explored[31]. These bacteria reduced the disease duration and severity, and thus comprise a promising tool for the treatment of rotavirus-induced diarrhea.

Besides this, nanobodies have also been described for the neutralization of HIV-1[32,33]. Recently, broad neutralization was reported for the L8CJ3 nanobody (96 of 100 tested HIV-1 strains)[34]. L8CJ3 primarily binds the CD4 binding site of HIV-1 envelope proteins, the same site that

potent neutralizing antibodies from patients target. The potent L8CJ3 nanobody can be either used for passive immunization or prevention via an anti-retroviral-containing gel. Nanobodies are of particular interest for anti-retroviral-containing gels because of the temperature and pH stability as well as their low cost of production as compared with mAb.

Cascade inhibition

The short half-life of nanobodies is an attractive feature for the temporary inhibition of several threatening events including sepsis, immune system blocking and blood-clotting. The latter is of particular interest because of the small therapeutic window of traditional drugs. Blocking the blood-clotting cascade is complicated by a dose-limiting risk of bleeding complications which can be life threatening. Recently, several nanobodies targeting the activated form of the von Willebrand factor (vWF) have been described. One of them (ALX-0081) has been evaluated as an antithrombotic agent and successfully passed phase I clinical trials[35]. ALX-0081 binds after administration only to the activated vWF and thus limits the bleeding risk. In addition, the overdose potential is generally low because of the rapid clearance of the unbound drug by the kidneys and possible application of serum purified vWF as antidote.

Systemic inflammation in rheumatoid arthritis however requires a long therapeutic efficacy. Next to the existing monoclonal antibody therapies infliximab (Remicade), adalimumab (Humira) or certolizumab pegol (Cimzia), nanobodies have been developed against TNF-alpha. One of them, the trivalent nanobody ATN-103, neutralizes TNF-alpha and binds to albumin to increase the half-life[36].

Receptor antagonism

In cancer, the uncontrolled cell division can be caused by the overexpression of a number of receptors which efficiently triggers downstream cascades upon ligand binding. This process can be inhibited by antibodies binding either the ligand or the receptor, subsequently preventing downstream signaling. Several monoclonal antibodies have been developed including rilotumumab (AMG102; Amgen) and TAK-701 (Millennium) against hepatocyte growth factor (HGF) and cetuximab (Erbitux) and panitumumab (Vectibix) against the epidermal growth factor receptor (EGFR) (see http://www.antibodysociety.org/news/approved_mabs.php).

Hepatocyte growth factor (HGF) is the only known ligand for the HGF receptor (also known as the c-MET receptor), is overexpressed in tumors, and can therefore be used as antigen[37]. Recently, two anti-HGF nanobodies have been fused to an albumin binding nanobody and were evaluated *in vivo*[38]. The two nanobodies showed a high accumulation in the tumor with half-lives of ~2 days. Interestingly, mice treated with the anti-HGF nanobodies had a dose-dependent benefit of the therapy, of which >50 % were cured without side effects when receiving the highest dose (100 µg per mouse).

In contrast, other receptors including EGFR from the family of receptor tyrosine kinases (RTKs) can be activated by multiple ligands[39]. It can be expected that, in order to receive maximal beneficial outcome, downstream signaling of the receptor needs to be fully blocked. Predictive diagnostic tools have mainly focused on the EGFR expression levels, but this does not necessarily correlate with the therapeutic outcome. More important are mutations in the EGFR and K-*ras* genes resulting in receptor activation and downstream signaling[40]. Where monovalent anti-EGFR nanobodies already reduced EGF binding and receptor activation, bivalent nanobodies were more potent in blocking EGF induced signaling and cell proliferation[19]. The efficacy of this bivalent construct fused to an anti-albumin nanobody was evaluated *in vivo* and showed inhibition of tumor growth. Furthermore, biparatopic anti-EGFR nanobodies, where the nanobodies bind different epitopes on EGFR, demonstrated more efficient inhibition of tumor growth[18]. This is the result of nanobody induced clustering of EGF receptors and efficient receptor downregulation. Still, despite the faster and deeper tumor penetration[24], this biparatopic nanobody could not match the efficacy of cetuximab. Nanobodies are missing an Fc domain and therefore lack antibody-dependent cell-mediated cytotoxicity (ADCC) and complement-dependent cytotoxicity (CDC).

Fusion to an effector domain

Next to blocking receptor signaling, nanobodies can also be fused to an effector domain for the treatment of cancer. An anti-carcinoembryonic antigen (CEA) nanobody fused to enterobacter cloacae β-lactamase accumulates mainly at the tumor site[41]. Administration of the prodrug (7-(4-carboxybutanamido) cephalosporin mustard) 24 hours later, demonstrated a dose-dependent therapeutic response with a complete cure at the highest dose. Despite the promising results, high accumulation of nanobodies in the kidneys could cause severe side effects when the prodrug is converted. This therapy is therefore predominantly suitable in combination with prodrugs which have slow renal clearance.

Alternatively, a toxin domain can be fused to antibody (fragments) creating an immunotoxin. The targeted delivery of PE38 has been well described in the literature and is under evaluation in three separate clinical trials. Recently, a nanobody based immunotoxin has been described for targeting the vascular endothelial growth factor receptor 2 (VEGFR2)[42]. This anti-VEGFR2-PE38 conjugate showed efficient binding and tumor growth inhibition of 293KDR cells *in vitro*, but lacked evaluation *in vivo*. Toxic side effects of PE38 fusion proteins have been attributed to binding the antigen on healthy cells and non-specific liver damage, thereby limiting the therapeutic dose.

Targeted delivery

Nanobodies as targeting moieties on drug carriers have been described in combination with

several delivery platforms including micelles, liposomes and polymersomes (see table 1). Drug carriers allow the specific delivery of high amounts of drugs with limited specificity, poor pharmacokinetics or low potency[43]. Increased half-lives of drug carriers by pegylation is the result of shielding it from the immune system[44]. The subsequent selective accumulation of drug carriers in tumors is caused by an incomplete vasculature and lacking lymphatic drainage, also known as the enhanced permeability and retention effect (EPR)[45]. Nanobody decoration of these carriers allows additional receptor mediated internalization, resulting in downregulation of the receptor and delivery of the drug inside the cell[46].

In a recent study, a dual target liposomal formulation was evaluated for the inhibition of tumor growth[47]. The anti-EGFR nanobody decorated liposome efficiently recognized and downregulated the EGF receptor. The encapsulated anti-IGF-1R kinase inhibitor beneficially inhibited tumor cell proliferation *in vitro*[48]. Evaluation in tumor xenograft models showed good correlation between the inhibition of tumor growth *in vitro* and *in vivo*.

Another example is the delivery of drugs into the brain. Most drugs cannot enter the brain directly and require carriers to facilitate transport over the blood-brain barrier (BBB). Of all the nanobodies raised against brain vascular endothelial cells, one was found to interact with the alpha(2,3)-sialoglycoprotein receptor, to undergo transcytosis and was subsequently released at the basolateral side[49]. Interestingly, nanobodies expressed on M13 phages were able to transport the whole phage particle into the brain *in vivo*[50]. Although this approach demonstrates delivery over the BBB, the low efficiency limits therapeutic applications.

Table 1: Overview of nanobody based drug carriers.

Particle	Drug	Target	Size	Remarks	Ref
Albumin	Multikinase inhibitor 17864-L(x)-a	EGFR	100 nm		51
Albumin	Multikinase inhibitor 17864-L(x)-a	c-Met	100 nm		52
Gold	-	HER2	60 nm		53
Liposome	Anti-IGF-1R kinase inhibitor AG538	EGFR	100 nm	Dual-active nanomedicine	48
Microbubble	-	VCAM-1	2200 nm	Imaging only, but applicable for therapy (see ref [54])	55
Polymeric micel	Doxirubicin	EGFR			56
Polymersome	-	PlexinD1	100 nm		57

Alternatively, drugs can also be directly conjugated to nanobodies. In contrast to the delivery via carriers, these antibody drug conjugates must bear very high potency to establish therapeutic efficacy. Since nanobodies are rapidly cleared from the body, high exposure of the drug to the kidneys can be considered as major drawback. Photosensitizers (PS) however require activation

and have been conjugated to antibody (fragments) to selectively induce cell death upon irradiation[58–60]. Compared with free PS, this approach reduces photosensitivity in patients but can be further improved by using antibody fragments with even shorter half-lives. Recently, the PS IRDye700DX was conjugated to nanobodies and delivered to EGFR overexpressing cells[48]. A biparatopic nanobody demonstrated high phototoxicity upon activation by light, probably due to efficient internalization. Evaluation in tumor xenograft models is required to assess the therapeutic efficacy of these constructs *in vivo*.

Image and therapy combined

The removal of tumors in surgical procedures is often complex. Surgeons predominantly resect tumor tissue while incomplete removal would result in the return of the tumor. Image guided surgery can assist surgeons by real-time visualization of the tumor. Anti-EGFR nanobodies labeled with IRDye800CW were shown to have tumor to background ratios (TBR) of >2 in orthotopic tongue tumors[61]. Interestingly, besides the tumor also metastases in cervical lymph nodes could be detected. In a comparable study, nanobodies against HER2 were analyzed in a breast cancer model and had TBRs of 2.5[62].

Advances in photodynamic therapy could also be employed for image guided therapy. The development of new fluorescent photosensitizers opens up possibilities for *in vivo* imaging. Recently it was proposed that these probes could first assist surgeons with the resection of tumors[63]. Subsequent irradiation of the surrounding tissue would eradicate remaining cancer cells.

Another approach is the photothermal therapy using gold nanoparticles. These particles absorb at wavelengths across the near-infrared window, convert this into thermal energy and destroy surrounding tissue by these elevated temperatures (40 – 46 °C)[64]. Although gold nanoparticles of 100 nm have shorter half-lives than their smaller counterparts, they have the highest total mass accumulation in tumor tissue[65]. Targeted gold nanoparticles against HER2 positive cancers caused efficient photothermal destruction upon stimulation[53]. Whether this approach is also effective *in vivo,* still needs to be determined.

Outlook

Nanobodies are, because of the favorable biochemical and physical properties, a unique class of antibody fragments. To date, 7 nanobodies are under evaluation in clinical trials, of which 3 are currently in phase II. With several nanobodies in the pipeline of Ablynx and research contributions made by academia, more can be expected in the near future. Besides ‘naked’ nanobodies, also drug conjugates and nanoparticles decorated with nanobodies have a good future prospective. The size and stability of nanobodies allows straightforward manipulation and the directed conjugation of drugs without impairing the antigen binding properties. This new

field of site-specific conjugation can not only facilitate access to homogenous protein drugs but also enables routes to combine diagnostics and therapy.

Acknowledgements
This work was funded by the Focus & Massa project of the Utrecht University, the Netherlands.

References

1. Padlan, E. A. Anatomy of the antibody molecule. *Mol. Immunol.* **31,** 169–217 (1994).
2. Jefferis, R., Lund, J. & Pound, J. D. IgG-Fc-mediated effector functions: molecular definition of interaction sites for effector ligands and the role of glycosylation. *Immunol. Rev.* **163,** 59–76 (1998).
3. Zheng, K., Bantog, C. & Bayer, R. The impact of glycosylation on monoclonal antibody conformation and stability. *MAbs* **3,** 568–576 (2011).
4. Fernández, L. A. Prokaryotic expression of antibodies and affibodies. *Curr. Opin. Biotechnol.* **15,** 364–373 (2004).
5. Flanagan, R. J. & Jones, A. L. Fab antibody fragments: some applications in clinical toxicology. *Drug Saf.* **27,** 1115–1133 (2004).
6. Janda, K. D. & Treweek, J. B. Vaccines targeting drugs of abuse: is the glass half-empty or half-full? *Nat. Rev. Immunol.* (2011). doi:10.1038/nri3130
7. Hamers-Casterman, C. *et al.* Naturally occurring antibodies devoid of light chains. *Nature* **363,** 446–448 (1993).
8. Flajnik, M. F. & Kasahara, M. Origin and evolution of the adaptive immune system: genetic events and selective pressures. *Nat. Rev. Genet.* **11,** 47–59 (2010).
9. Alexander, A. *et al.* gamma Heavy chain disease in man: cDNA sequence supports partial gene deletion model. *Proc. Natl. Acad. Sci. U. S. A.* **79,** 3260–4 (1982).
10. Muyldermans, S., Atarhouch, T., Saldanha, J., Barbosa, J. A. & Hamers, R. Sequence and structure of VH domain from naturally occurring camel heavy chain immunoglobulins lacking light chains. *Protein Eng.* **7,** 1129–1135 (1994).
11. Tanha, J., Dubuc, G., Hirama, T., Narang, S. A. & MacKenzie, C. R. Selection by phage display of llama conventional VH fragments with heavy chain antibody VHH properties. *J. Immunol. Methods* **263,** 97–109 (2002).
12. Kolkman, J. A. & Law, D. A. Nanobodies - From llamas to therapeutic proteins. *Drug Discov. Today Technol.* **7,** (2010).
13. Lauwereys, M. *et al.* Potent enzyme inhibitors derived from dromedary heavy-chain antibodies. *EMBO J.* **17,** 3512–3520 (1998).
14. Desmyter, A. *et al.* Crystal structure of a camel single-domain VH antibody fragment in complex with lysozyme. *Nat. Struct. Biol.* **3,** 803–811 (1996).
15. Van der Linden, R. H. *et al.* Comparison of physical chemical properties of llama VHH antibody fragments and mouse monoclonal antibodies. *Biochim Biophys Acta* **1431,** 37–46 (1999).
16. Dumoulin, M. *et al.* Single-domain antibody fragments with high conformational stability. *Protein Sci.* **11,** 500–515 (2002).
17. Barthelemy, P. A. *et al.* Comprehensive analysis of the factors contributing to the stability and solubility of autonomous human VH domains. *J. Biol. Chem.* **283,** 3639–54 (2008).
18. Roovers, R. C. *et al.* A biparatopic anti-EGFR nanobody efficiently inhibits solid tumour growth. *Int. J. Cancer* **129,** 2013–24 (2011).
19. Roovers, R. C. *et al.* Efficient inhibition of EGFR signalling and of tumour growth by antagonistic anti-EGFR Nanobodies. *Cancer Immunol. Immunother.* **56,** 303–317 (2006).
20. Cortez-Retamozo, V. *et al.* Efficient tumor targeting by single-domain antibody fragments of camels. *Int. J. Cancer* **98,** 456–462 (2002).
21. Vincke, C. *et al.* General strategy to humanize a camelid single-domain antibody and identification of a universal humanized nanobody scaffold. *J. Biol. Chem.* **284,** 3273–3284 (2009).
22. Harmsen, M. M. & De Haard, H. J. Properties, production, and applications of camelid single-domain antibody fragments. *Appl. Microbiol. Biotechnol.* **77,** 13–22 (2007).
23. Chakravarty, R., Goel, S. & Cai, W. Nanobody: The "Magic Bullet" for Molecular Imaging? *Theranostics* **4,** 386–398 (2014).
24. Tijink, B. M. *et al.* Improved tumor targeting of anti-epidermal growth factor receptor Nanobodies through albumin binding: taking advantage of modular Nanobody technology. *Mol. Cancer Ther.* **7,** 2288–2297 (2008).
25. Vugmeyster, Y. *et al.* Pharmacokinetic, biodistribution, and biophysical profiles of TNF nanobodies conjugated to linear or branched poly(ethylene glycol). *Bioconjug. Chem.* **23,** 1452–62 (2012).
26. Scheuplein, F. *et al.* A recombinant heavy chain antibody approach blocks ART2 mediated deletion

of an iNKT cell population that upon activation inhibits autoimmune diabetes. *J. Autoimmun.* **34,** 145–154 (2010).
27. Harrison, R. A. *et al.* Research strategies to improve snakebite treatment: Challenges and progress. *J. Proteomics* **74,** 1768–1780 (2011).
28. Abderrazek, R. Ben *et al.* Identification of potent nanobodies to neutralize the most poisonous polypeptide from scorpion venom. *Biochem. J.* **424,** 263–272 (2009).
29. Koch-Nolte, F. *et al.* Single domain antibodies from llama effectively and specifically block T cell ecto-ADP-ribosyltransferase ART2.2 in vivo. *FASEB J.* **21,** 3490–3498 (2007).
30. Garaicoechea, L. *et al.* Llama-derived single-chain antibody fragments directed to rotavirus VP6 protein possess broad neutralizing activity in vitro and confer protection against diarrhea in mice. *J. Virol.* **82,** 9753–9764 (2008).
31. Pant, N. *et al.* Lactobacilli expressing variable domain of llama heavy-chain antibody fragments (lactobodies) confer protection against rotavirus-induced diarrhea. *J. Infect. Dis.* **194,** 1580–1588 (2006).
32. Forsman, A. *et al.* Llama antibody fragments with cross-subtype human immunodeficiency virus type 1 (HIV-1)-neutralizing properties and high affinity for HIV-1 gp120. *J. Virol.* **82,** 12069–12081 (2008).
33. Strokappe, N. *et al.* Llama antibody fragments recognizing various epitopes of the CD4bs neutralize a broad range of HIV-1 subtypes A, B and C. *PLoS One* **7,** (2012).
34. McCoy, L. E. *et al.* Potent and broad neutralization of HIV-1 by a llama antibody elicited by immunization. *J. Exp. Med.* **209,** 1091–1103 (2012).
35. Ulrichts, H. *et al.* Antithrombotic drug candidate ALX-0081 shows superior preclinical efficacy and safety compared with currently marketed antiplatelet drugs. *Blood* **118,** 757–765 (2011).
36. Kratz, F. & Elsadek, B. Clinical impact of serum proteins on drug delivery. *J. Control. Release* **161,** 429–45 (2012).
37. Maulik, G. *et al.* Role of the hepatocyte growth factor receptor, c-Met, in oncogenesis and potential for therapeutic inhibition. *Cytokine Growth Factor Rev.* **13,** 41–59 (2002).
38. Vosjan, M. J. W. D. *et al.* Nanobodies Targeting the Hepatocyte Growth Factor: Potential New Drugs for Molecular Cancer Therapy. *Mol. Cancer Ther.* **11,** 1017–1025 (2012).
39. Vecchione, L., Jacobs, B., Normanno, N., Ciardiello, F. & Tejpar, S. EGFR-targeted therapy. *Exp. Cell Res.* **317,** 2765–2771 (2011).
40. Pantaleo, M. A. *et al.* Molecular imaging of EGFR: it's time to go beyond receptor expression. *J. Nucl. Med.* **50,** 1195–6; author reply 1196, 1197 (2009).
41. Cortez-Retamozo, V. *et al.* Efficient cancer therapy with a nanobody-based conjugate. *Cancer Res.* **64,** 2853–2857 (2004).
42. Behdani, M. *et al.* Development of VEGFR2-specific Nanobody Pseudomonas exotoxin A conjugated to provide efficient inhibition of tumor cell growth. *N. Biotechnol.* **30,** 205–209 (2013).
43. Zamboni, W. C. *et al.* Best Practices in Cancer Nanotechnology: Perspective from NCI Nanotechnology Alliance. *Clin. Cancer Res.* **18,** 3229–3241 (2012).
44. Howard, M. D., Jay, M., Dziubla, T. D. & Lu, X. PEGylation of Nanocarrier Drug Delivery Systems: State of the Art. *J. Biomed. Nanotechnol.* **4,** 133–148 (2008).
45. Fang, J., Nakamura, H. & Maeda, H. The EPR effect: Unique features of tumor blood vessels for drug delivery, factors involved, and limitations and augmentation of the effect. *Adv. Drug Deliv. Rev.* **63,** 136–151 (2011).
46. Fay, F. & Scott, C. J. Antibody-targeted nanoparticles for cancer therapy. *Immunotherapy* **3,** 381–394 (2011).
47. Van Der Meel, R. *et al.* Tumor-targeted Nanobullets: Anti-EGFR nanobody-liposomes loaded with anti-IGF-1R kinase inhibitor for cancer treatment. *J. Control. Release* **159,** 281–289 (2012).
48. Van der Meel, R. *et al.* Inhibition of Tumor Growth by Targeted Anti-EGFR/IGF-1R Nanobullets Depends on Efficient Blocking of Cell Survival Pathways. *Mol. Pharm.* **10,** 3717–3727 (2013).
49. Abulrob, A., Sprong, H., Van Bergen en Henegouwen, P. & Stanimirovic, D. The blood-brain barrier transmigrating single domain antibody: mechanisms of transport and antigenic epitopes in human brain endothelial cells. *J. Neurochem.* **95,** 1201–1214 (2005).
50. Muruganandam, A., Tanha, J., Narang, S. & Stanimirovic, D. Selection of phage-displayed llama single-domain antibodies that transmigrate across human blood-brain barrier endothelium. *FASEB J.* **16,** 240–242 (2002).

51. Altintas, I. *et al.* Nanobody-albumin nanoparticles (NANAPs) for the delivery of a multikinase inhibitor 17864 to EGFR overexpressing tumor cells. *J. Control. Release* **165,** 110–118 (2013).
52. Heukers, R. *et al.* Targeting hepatocyte growth factor receptor (Met) positive tumor cells using internalizing nanobody-decorated albumin nanoparticles. *Biomaterials* **35,** 601–10 (2014).
53. Van de Broek, B. *et al.* Specific cell targeting with nanobody conjugated branched gold nanoparticles for photothermal therapy. *ACS Nano* **5,** 4319–4328 (2011).
54. Yan, F. *et al.* Therapeutic Ultrasonic Microbubbles Carrying Paclitaxel and LyP-1 Peptide: Preparation, Characterization and Application to Ultrasound-Assisted Chemotherapy in Breast Cancer Cells. *Ultrasound Med. Biol.* **37,** 768–779 (2011).
55. Hernot, S. *et al.* Nanobody-coupled microbubbles as novel molecular tracer. *J. Control. Release* **158,** 346–353 (2012).
56. Talelli, M. *et al.* Intrinsically active nanobody-modified polymeric micelles for tumor-targeted combination therapy. *Biomaterials* **34,** 1255–1260 (2013).
57. Debets, M. F. *et al.* Nanobody-functionalized polymersomes for tumor-vessel targeting. *Macromol. Biosci.* **13,** 938–45 (2013).
58. Soukos, N. S. *et al.* Epidermal growth factor receptor-targeted immunophotodiagnosis and photoimmunotherapy of oral precancer in vivo. *Cancer Res.* **61,** 4490–4496 (2001).
59. Savellano, M. D. & Hasan, T. Photochemical targeting of epidermal growth factor receptor: a mechanistic study. *Clin. Cancer Res.* **11,** 1658–1668 (2005).
60. Kuimova, M. K. *et al.* Fluorescence characterisation of multiply-loaded anti-HER2 single chain Fv-photosensitizer conjugates suitable for photodynamic therapy. *Photochem. Photobiol. Sci.* **6,** 933–939 (2007).
61. Van Driel, P. B. a a *et al.* Intraoperative fluorescence delineation of head and neck cancer with a fluorescent Anti-epidermal growth factor receptor nanobody. *Int. J. Cancer* (2013). doi:10.1002/ijc.28601
62. Kijanka, M. *et al.* Rapid optical imaging of human breast tumour xenografts using anti-HER2 VHHs site-directly conjugated to IRDye 800CW for image-guided surgery. *Eur. J. Nucl. Med. Mol. Imaging* **40,** 1718–1729 (2013).
63. Heukers, R., van Bergen En Henegouwen, P. M. P. & Oliveira, S. Nanobody-photosensitizer conjugates for targeted photodynamic therapy. *Nanomedicine* (2014). doi:10.1016/j.nano.2013.12.007
64. Roti Roti, J. L. Cellular responses to hyperthermia (40-46 degrees C): cell killing and molecular events. *Int. J. Hyperthermia* **24,** 3–15 (2008).
65. Perrault, S. D., Walkey, C., Jennings, T., Fischer, H. C. & Chan, W. C. W. Mediating tumor targeting efficiency of nanoparticles through design. *Nano Lett.* **9,** 1909–1915 (2009).

Chapter 4

Intein-mediated functionalization of nanobodies

Remko van Vught, Sabrina Oliveira, Rob Roovers, Paul van Bergen en Henegouwen, Roland Pieters, Eefjan Breukink

Abstract

Nanobodies are the variable domains of heavy chain only antibodies and have emerged potent targeting modalities for therapeutic, diagnostic and research(-driven) applications. Their functionalization with biomolecules is often performed via non-selective chemistries resulting in heterogeneous protein mixtures as well as reduction (or complete loss) of antigen recognition. Intein-mediated functionalization of nanobodies has been described to overcome these limitations. Yet, this does not always result in quantitative functionalization of the nanobody. In order to improve this reaction, the nanobody-intein fusion protein was optimized and analyzed for its thiol-mediated cleavage using different thiol-containing compounds. Cysteamine was identified as a novel substrate for this reaction that allows subsequent functionalization of the nanobodies as demonstrated by labeling with fluorescent probes and PEG as well as conjugation to liposomes.

1. Introduction

Antibodies are known for their specific interaction with their antigen and have therefore emerged as tools in many biomedical fields. Over 30 monoclonal antibodies have been marketed for treatment of autoimmune diseases and various cancers. A new class, the antibody drug conjugates (ADCs), target toxic drugs which otherwise would have limited specificity and thus major side effects[1–3]. Antibodies are also used in the field of molecular imaging for the identification/localization of diseases[4]. For this purpose, PET, SPECT, MRI and optical imaging probes need to be conjugated to a validated antibody[5].

Next to the full monoclonal antibodies, there has been an increasing interest in antibody fragments because of the shorter retention time in the body and the lack of an immunological response against it[6]. In addition, these antibody fragments can be produced in prokaryotic hosts, optimized via phage display and genetically fused for multivalency[7]. The potential applications and straightforward production led to the development of several antibody fragments including monovalent antibody fragments (Fab), single-chain antibody fragments (scFv), and single-domain antibodies (sdAb)[6]. While Fabs are the result of papain digested monoclonal antibodies and scFvs are the genetic fusion of the heavy and light variable domains, sdAbs are derived from heavy-chain only antibodies (HcAbs) found in camelids (camels, dromedaries and llamas) and primitive fish (ratfish, nurse and wobbegong sharks)[8,9].

Single-domain antibodies are the smallest antibody fragments (~15 kDa) of naturally occurring antibodies[8,9]. In addition, sdAbs possess unique features such as high affinity, solubility and thermal stability as a result of the lack of the light chain[10,11]. Since several years, sdAbs derived from llama's are being commercialized by Ablynx under the name nanobodies (or VHH) for their therapeutic applications. The half-life of nanobodies (1-2 hrs) can be prolonged for up to 2 days by genetic fusion to an anti-Albumin nanobody[12]. This allows for short to medium term therapeutic applications such as inflammation and immunology. Their short half-life is also very suitable for molecular imaging[13–15]. Nanobodies diffuse rapidly throughout the body, allowing fast binding to their antigen and clearance from the blood. As a result of this, nanobodies can be used for molecular imaging within 1-3 hrs post injection, in contrast to > 24 hrs for monoclonal antibodies[16].

The conjugation of drugs or reporter molecules to nanobodies has mostly been performed by random coupling to its lysines. Nanobodies bear on average 4-6 lysine residues that can be modified by using NHS ester based ligation. Compared with monoclonal antibodies, their relative large surface area involved in antigen recognition renders this approach less suitable. The labeling of lysine(s) in one of the complementarity determining regions (CDRs) can be catastrophic for antigen binding. In addition, this random conjugation leads to a heterogeneous population and complicates further downstream processing and applications. This led to the development of several approaches of site-specific modification via the incorporation of

unnatural amino acids[17–19], the use of sortases[20], or intein-based conjugation[21,22]. The latter is of particular interest since it allows the site-specific integration of multiple chemical handles[22].

Inteins originate as expressed protein domains in frame of another protein[23]. Self-excision releases the intein domain and restores the function of the host protein by fusing the ends. This self-excision process can be exploited for site-specific modification of the N- or C-terminus of nanobodies via expressed protein ligation (EPL)[24]. Since the N-terminus is in close proximity to the CDRs, it is potentially involved in antigen binding and thus not suitable for the conjugation of biomolecules. The C-terminus of nanobodies however, is rarely involved and can be used for EPL. First, the native peptide bond is converted to a thioester, after which a cysteine (analog) can be ligated which restores the native peptide bond (also known as native chemical ligation)[24,25].

Previously, nanobodies were coupled via EPL onto the surface of liposomes[21]. In this approach, nanobodies bearing a reactive thioester were first isolated. These reactive nanobodies were subsequently decorated onto cysteine modified liposomes, resulting in immunoliposomes. More recently, the decoration of polymersomes with dual functionalized nanobodies was demonstrated[22]. In this study, a peptide bearing both the cysteine and an azide group were first ligated to the nanobody. Although both functional groups could be used for the coupling of biomolecules, the authors consistently reached a labeling efficiency of only 50 %. Since both reactions are normally quantitative, this observation was attributed to the low EPL efficiency. Although the non-reacted nanobodies could be separated from the decorated polymersomes, this would be more challenging when small biomolecules were attached. We therefore set out to optimize the EPL reaction. As for all (chemical) reactions, the reaction speed is temperature and concentration dependent. Since ambient temperatures are preferred, the fusion protein was concentrated by an elastin-like polypeptide (ELP) tag. ELPs were previously demonstrated to reversibly aggregate in response to increasing temperature and ionic strength, and thus readily concentrate the protein[26,27]. Next to this, the native chemical ligation reaction is dependent on a reactive thioester[28]. Thioesters however, are also susceptible to hydrolysis by water and therefore need to be readily converted into the desired product. Circumvention of this intermediate step could also improve the EPL efficiency.

In this paper, we first optimized the expression of the nanobody-intein-ELP fusion protein. In the subsequent intein-mediated cleavage experiments we analyzed the reactivity of several thiol compounds. Of these, cysteamine was very efficient and demonstrated a nearly quantitative conversion in a thiol-maleimide reaction. The thiol-functionalized nanobody was furthermore analyzed in binding studies and by conjugation to liposomes.

2. Materials and methods

2.1 Chemical and reagents

Lipids 1,2-dipalmitoyl-*sn*-glycero-3-phosphocholine (DPPC), cholesterol (Chol), 1,2-distearoyl-sn-glycero-3-phosphoethanolamine-N-[maleimide(polyethylene glycol)-2000] (DSPE-PEG-MAL, average PEG molecular mass of 2000 amu), L-α-Phosphatidylethanolamine-N-(lissamine rhodamine B sulfonyl) (Rho-PE) were from Avanti Polar Lipids (Alabaster AL). Ampicillin, cysteine, cysteamine, sodium 2-sulfanylethanesulfonate (Mesna), 4-(2-hydroxyethyl)-1-piperazineethanesulfonic acid (HEPES), coomassie brilliant blue r, tris(2-carboxyethyl)phosphine (TCEP), bovine serum albumin (BSA), DNAse, and lysozyme were from Sigma-Aldrich (St. Louis, MO, USA). Isopropyl β-D-1-thiogalactopyranoside (IPTG) and Ni-NTA beads were from Thermo Fisher Scientific (Waltham, MA, USA). Tetracycline was obtained from OPG Farma (BUVA, Uitgeest, the Netherlands). PBS was from Lonza (Basel, Switzerland). IRDye 800CW Maleimide and IRDye 800CW NHS were obtained from LI-COR Biosciences (Lincoln, NE, USA). Bugbuster and sodium chloride (NaCl) were from Merck KGaA (Darmstadt, Germany). PEG10k-Maleimide was from JenKem Technology USA (Allen, Texas, USA) Lipid stocks were dissolved in chloroform and stored at -20 °C in the dark after purging with nitrogen gas. The exact concentration of the DPPC and DSPE-PEG stocks were determined by the inorganic phosphate determination[29].

2.2 Cell culturing

The human epidermoid carcinoma cell line A431 (CRL-1555) and mouse fibroblast cell line NIH 3T3 2.2 (abbreviated 3T3 2.2) were cultured in Dulbecco's Modified Eagle's Medium (DMEM; Gibco, Invitrogen, United Kingdom) supplemented with 8 % fetal bovine serum (FBS) (v/v). The cell culture media was supplemented with antibiotics to a final concentration 100 U/mL penicillin, 100 µg/mL streptomycin, and 2 mM L-glutamine (PAA, Germany). All cell lines were kept in culture at 37 °C in a humidified atmosphere containing 5 % CO_2. The cell lines were consistently found to be free of mycoplasma (MycoAlert Mycoplasma Detection Kit, Lonza).

2.3 Plasmids and expression of anti-EGFR nanobodies

The antagonistic anti-EGFR nanobody EGa1 (described previously Roovers et al.[30]) was fused to a c-terminal intein domain and elastin-like polypeptide (intein-ELP, kind gift from Carlos Filipe, McMaster University, Canada). Briefly, the EGa1 nanobody in pTXB1 (kind gift from William Leenders, Radboud University Nijmegen, the Netherlands) was transferred to the intein-ELP contstruct by using the sites XbaI and BsiWI. Subsequently, the HIS_6-tag and VSV-tag in between the nanobody and intein were replaced by an $S(GGGG)_4S(GGGG)_4S$ linker. The final construct was verified by sequencing (Macrogen Europe). E. coli BLR(DE3) cells were transformed with the adapted pTXB1 construct and selected using 100 mg/mL ampicillin and 12.5 mg/mL tetracycline.

The expression of the fusion protein was optimized by inducing cultures between OD_{600} 0.5 - 0.6 with 0.3 mM IPTG for 2, 4 and 20 hrs at 25, 30 and 37 °C. Samples were separated on SDS-PAGE gel, blotted on nitrocellulose membrane, detected using monoclonal anti-polyHistidine–Peroxidase antibody (A7058, Sigma-Aldrich, the Netherlands) and quantified using ImageJ 1.47.

The fusion protein was expressed according to the optimized expression conditions and induced in the logarithmic fase by the addition of 0.3 mM IPTG for 20 hrs at 25 °C. The harvested cultures were lysed in 1:50 bugbuster supplemented with lysozyme and DNAse and incubated for 15 min at room temperature (RT). The supernatant was collected by centrifugation at 19 000xg at 4 °C and incubated with in PBS equilibrated Ni-NTA beads (1 ml beads per liter culture) for 1 h at 4 °C. The beads were washed three times with PBS after which the protein was eluted in 250 mM imidazole in PBS. Protein in the collected fractions was precipitated by addition of NaCl to an end concentration of 2 M.

2.4 Intein-mediated cleavage

For analysis of the intein-mediated cleavage, a different construct was employed bearing nanobody, HIS_6-tag, intein and chitin binding domain (pTXB1.0). The fusion protein was expressed and purified under the same conditions. Instead of precipitation by NaCl, the eluted protein was bound to chitin functionalized beads (NEB, Ipswich, MA, USA). Briefly, the fusion protein was purified from a 400 mL culture by lysis with 8 mL bugbuster and incubation with 2 mL slurry Ni-NTA for 1 hr at 4 °C. The protein was subsequently eluted using 1 mL 250 mM imidazole in PBS of which 400 µL was mixed with 2 mL slurry chitin beads in 10 mL buffer (20 mM phosphate buffer pH 7.0, 500 mM sodium chloride) and incubated for 1 hr at 4 °C. The chitin beads were washed twice with 10 mL buffer and resuspended in 1 mL buffer. For the intein-mediated cleavage, 200 µL suspension with protein loaded chitin beads was mixed with 150 µL 150 mM cysteamine or analog, and incubated at RT for 1, 4 or 21 hrs. Samples were taken at the indicated time points and stored at -20 °C. The next day, all samples were 1:1 (v/v) diluted in 2x Laemmli sample buffer without DTT. Proteins samples were separated by SDS-PAGE, blotted on nitrocellulose membrane, detected using monoclonal anti-polyHistidine–Peroxidase antibody and quantified using ImageJ 1.47.

For the intein-mediated cleavage by cysteamine, the pellet was resuspended in ice-cold cleavage buffer (20 mM phosphate buffer pH 7.0, 250 mM cysteamine) and incubated overnight at 4 °C. The salt concentration of the mixture was again raised to 2 M to precipitate the cleaved ELP. The supernatant was dialyzed against PBS, supplemented with 2 mM $CaCl_2$ and incubated with with 0.00025 % enterokinase (w/w; NEB) overnight at 37 °C to completely remove the leader sequence. The supernatant containing the thiol-functionalized nanobody was further purified by size exclusion using an in PBS equilibrated Superdex 75 10/300 GL column (GE Healthcare Europe GmbH, Munich, Germany). The purified protein was stored at 4 °C until further use.

2.5 Nanobody labeling

Nanobodies were reduced by addition of 5 mM TCEP for 5 min at RT, desalted against PBS using Zeba Spin Desalting columns (Thermo Fisher Scientific, Perbio Science Nederland B.V., Etten-Leur, the Netherlands) and incubated with the indicated equivalents of maleimide labeled PEG10k, IRDye 800CW NHS or IRDye 800CW Maleimide for overnight at RT. In case of the IRDye 800CW, the samples were again desalted against PBS to remove the excess of dye. The samples were 1:1 (v/v) diluted in 2x laemmli sample buffer without DTT, separated by SDS-PAGE, coomassie stained and detected using ODYSSEY CLx (Li-COR Biosciences).

2.6 Determination of the affinity towards A431 cells

Cells (8000/well) were seeded 2 days in advance. Prior to the assay, cells were washed with chilled buffer (DMEM without phenol red, supplemented with 25 mM HEPES and 1 % BSA, pH 7.2) and incubated for 30 min at 4 °C. A serial dilution of VHHs in buffer was incubated for 1.5 hrs at 4 °C. The non-bound VHHs were removed by three times washing with buffer, after which the bound fraction was detected by using the Odyssey scanner. The background subtracted fluorescent signal was plotted and analyzed using GraphPad Prism 5.02 software.

2.7 Preparation of liposomes

Rhodamine-labeled liposomes were prepared as described previously (Broekgaarden et al.[31]) according to the lipid-film technique. In short, lipids in chloroform were premixed at DPPC:Chol:DSPE-PEG-mal:Rho-PE molar ratios of 76.8:15:8:0.2, respectively. The lipids were desiccated under nitrogen gas, after which the lipid-film was dried under vacuum for 30 min. Subsequently, the lipid-film was hydrated with physiological buffer composed of 0.88 % (w/v) sodium chloride, 10mM HEPES (pH 7.4, 0.292 osmol/kg). Liposomes were sized by sonication and extrusion through 0.2 µm aluminum oxide filters (Whatman, GE Healthcare, Little Chalfont, United Kingdom). Nanobodies were reduced by addition of 5 mM TCEP for 5 min at RT, desalted against PBS using Zeba Spin Desalting columns (Thermo Fisher Scientific) and incubated with liposomes for 1 h at RT followed by incubation overnight at 4°C (nanobody to total lipid (TL) ratio employed was 1:100 mol/mol). Non-reacted maleimide groups on DSPE-PEG-MAL were quenched by addition of BME at equimolar concentration (relative to the DSPE-PEG-MAL) and incubated for 1 h at RT. The non-coupled nanobodies and BME were removed by 2× ultracentrifugation at 200,000 ×g for 40 min at 4 °C, after which the total lipid concentration was determined (Rouser et al.[32]) and liposomes were stored at 4 °C until further use.

2.8 Cell assays

For each experiment, 2000 cells per well were seeded in 96-wells plates (Greiner Bio-One, Alphen a/d Rijn, the Netherlands) one day in advance. Cells were incubated for 48 hrs with

200 µM TL (unless mentioned otherwise) in DMEM supplemented with 8 % FBS (v/v) at 37 °C. After 48 hrs, all samples were washed twice with DMEM. To determine the viability, cells were incubated 2 - 3 hrs with DMEM (without phenol red) supplemented with 1:10 (v/v) Alamar Blue (Life Technologies, Thermo Fisher Scientific). Rhodamine as well as the conversion of the Alamar Blue to its fluorescent analog were measured with a FluoStar Optima fluorescent plate reader (BMG Labtech GmbH, Ortenberg, Germany). The cell viability was calculated in percentage (%) relative to untreated cells after background subtraction. Data was plotted using GraphPad Prism 5.02 software.

2.9 Fluorescent imaging

A431 cells were grown on gelatin coated coverslips for 2 days. Cells were incubated with 125 µM TL for 30 min at 37 °C, washed once with DMEM and chased in DMEM for 110 min at 37 °C. Subsequently, transferrin alexa 488 conjugate (Life Technologies) was incubated for 10 min at 37 °C after which the cells were washed twice with ice-cold PBS and fixed with 4 % formaldehyde (w/v) at 4 °C. The cell nuclei were stained with 4',6-diamidino-2-phenylindole (DAPI, Roche, Basel, Switzerland) and images were acquired using a Zeiss LSM 700 inverted confocal microscope (Zeiss, Oberkochen, Germany).

3. Results

Examples of EPL for the functionalization of nanobodies have all used the commercialized impact kit bearing the chitin binding domain (CBD) for purification. In order to optimize the EPL efficiency we explored the possibility of a tandem purification protocol, combining HIS_6-tag purification with reversible precipitation by an elastin-like polypeptide (ELP). Although this does not affect the intein working mechanism, there are some relevant changes (Scheme 1). First, tandem purification of the fusion protein reduces the initial impurities. Second, the EPL is now performed in one step, at high concentration and in solution instead of in suspension with chitin beads. Third, the cleaved intein-ELP domain can be easily separated from the functionalized nanobody by ELP precipitation.

3.1 Intein nanobody fusion: expression & purification

As recommended by the impact kit, we first optimized the expression of the VHH-intein-ELP fusion protein. Expression at low temperatures is known to reduce solubility problems as well as to decrease the *in vivo* cleavage of the intein. We therefore analyzed the protein expression at 25 °C, 30 °C and 37 °C (Fig. 1a). Expression of the intact fusion protein was most optimal when induced for 20 hrs at either RT or 30 °C. In contrast, expression at 37 °C resulted in only 48.4 % of the maximum protein yield. To determine whether this observation could be explained by the *in vivo* cleavage of the intein, the amount of free VHH was also quantified

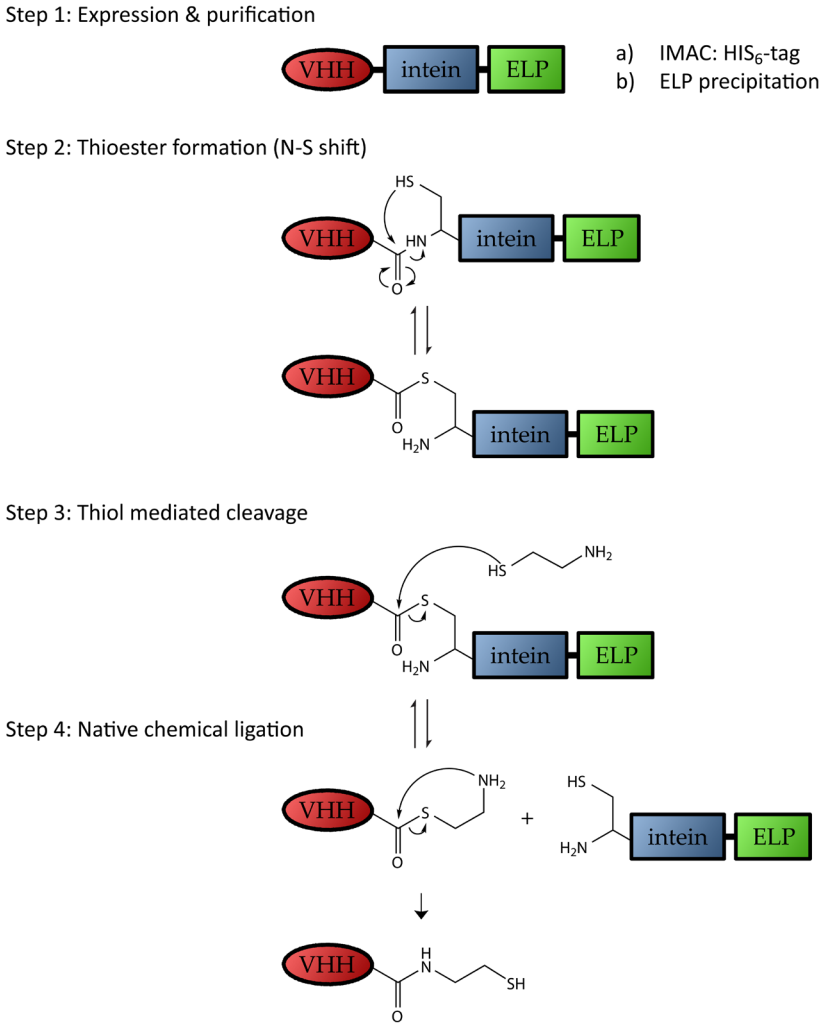

Scheme 1. Overview of the expression and purification of the nanobody-intein fusion protein (VHH-intein-ELP). Step 1, the expression and tandem purification by employing the HIS_6-tag followed by ELP precipitation. Step 2, intein-based rearrangement of a native peptide into a (less stable) thioester. Step 3, exchange of the thioester by addition of a thiol reagent (in this example with cysteamine). This results in splicing of the VHH from the intein-ELP domains. Step 4, rearrangement of the thioester into a native peptide bond by native chemical ligation.

(Fig. 1b). No free VHH could be detected after 2 hrs. The amount of free VHH after 20 hrs was nearly identical for all temperatures. Interestingly, minor formation of free VHH (<2 %) was observed after 4 hrs at 25 °C, while this was 8.6 % and 11.2 % for expression at 30 °C and 37 °C, respectively. We therefore concluded that expression at 25 °C for 20 hrs was the most optimal and that protein expressed at 37 °C was probably (more) prone to degradation by proteases.

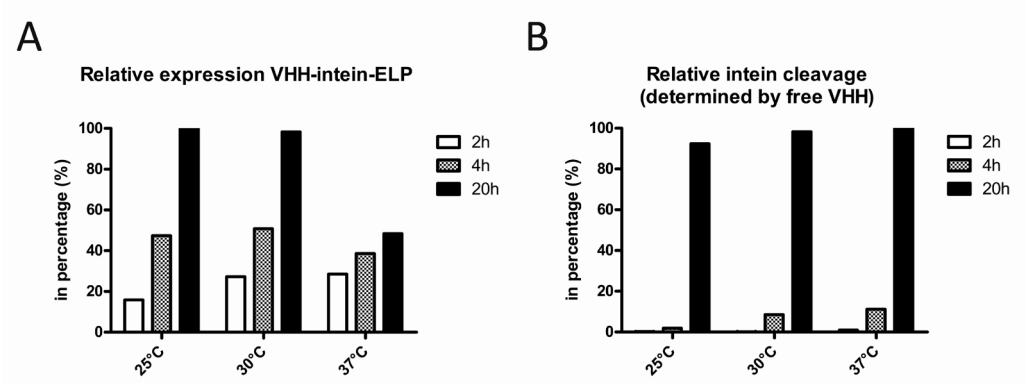

Figure 1. Expression of the nanobody-intein fusion (VHH-intein-ELP). Relative expression levels of VHH-intein-ELP 2, 4 or 20 hrs after induction by 0.3 mM IPTG (A) and the relative *in vivo* cleavage during expression (B). Cell lysates were separated using a non-reducing 15% SDS-PAGE gel, blotted onto nitrocellulose membranes and the VHH-intein-ELP and free VHH were detected by an anti-HIS_6 monoclonal antibody.

3.2 Intein-mediated cleavage/ligation

The thiol-mediated cleavage of intein fusion proteins is commonly employed using sodium 2-sulfanylethanesulfonate (Mesna) to obtain the target protein with a reactive thioester. Mesna is not only very nucleophilic at neutral pH, but also a good leaving group for the subsequent native chemical ligation reaction with a cysteine bearing peptide. Yet, these two steps (3 and 4 in Scheme 1) are not always quantitative as described previously[22]. The intein-mediated cleavage was therefore evaluated for several thiol compounds (Fig. 2). Of these, cysteine (Cys) and cysteamine (CA) can perform the intein cleavage and ligation in one reaction. Mesna and 2-mercaptoethanol (BME) can only cleave intein fusion proteins since these compounds lack an amino group and thus allow the ligation of different cysteine bearing peptides. The intein-mediated cleavage was most efficient with BME, followed by Mesna and CA, and slowest with Cys. Despite the slower onset, the total intein cleavage by CA after 21 hrs was comparable to Mesna. Since CA also performs the native chemical ligation reaction, we explored the potential for CA to introduce a reactive thiol group at the C-terminus of nanobodies.

In the subsequent EPL with 250 mM cysteamine we efficiently produced VHH bearing a C-terminal thiol group (VHH-CA), as shown in figure 3a (lane 1). Despite our efforts we observed some minor contamination, probably due to degradation of the intein-ELP domain. These impurities were removed by size exclusion chromatography (Fig. 3).

A

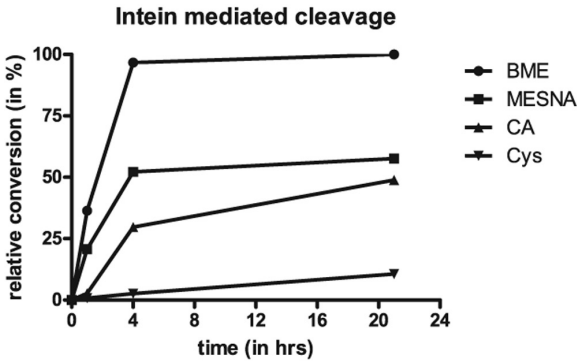

B

Compound name	Abbrev.	pKa (thiol)	pKa (amine)
2-Mercaptoethanol	BME	9.72	
Sodium 2-sulfanylethanesulfonate	Mesna	9.1	
Cysteine	Cys	8.7	10.2
Cysteamine	CA	8.27	10.53

Figure 2. Evaluation of intein-mediated cleavage by 2-mercaptoethanol (BME), sodium 2-sulfanylethanesulfonate (Mesna), cysteamine (CA) and cysteine (Cys). (A) The relative conversion at RT after 1, 4, 21 hrs. The fusion protein was immobilized on beads after which the VHH in the supernatant was separated on SDS-PAGE gel, blotted and detected by an anti-HIS_6 monoclonal antibody. (B) An overview of the relevant pKa's of the compounds[36].

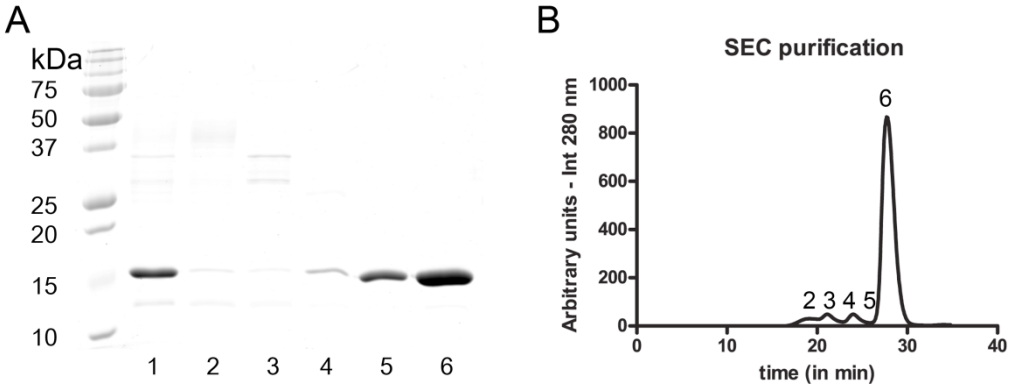

Figure 3. Expression and purification of the nanobody bearing a reactive thiol group (VHH-CA). (A) SDS-PAGE analysis of protein samples of VHH-CA before (lane 1) and after size exclusion chromatography (SEC) using a Superdex 75 10/300 GL column (lanes 2-6). (B) The corresponding SEC profile during purification of VHH-CA using an ÄKTA Prime and detector at 280 nm.

3.3 Nanobody labeling

To confirm the presence and assess the reactivity of the C-terminal thiol group we incubated VHH-CA with increasing concentrations of PEG10k-Maleimide. The attachment of PEG10k-Maleimide was visualized on SDS-PAGE gel as a shift towards higher molecular weight (Fig. 4a). The unmodified VHH-CA migrates at approximately 15 kDa, consistent with the molecular weight of a single VHH-CA molecule (15.76 kDa). The addition of PEG10k-Maleimide results in a concentration dependent shift. Quantification of the SDS-PAGE gel identified conversion rates of 75 % and 92 % for 5 and 15 equivalents, respectively (Fig. 4b). Next to the desired conjugate, only minor impurities were detected including the VHH-CA bearing multiple modifications as well as the unmodified VHH-CA.

The reactivity and functionality of VHH-CA was furthermore studied by labeling with IRDye 800CW. As a control, EPL was performed with Mesna to produce the VHH without a C-terminal thiol group (VHH-Mesna). Both proteins were labeled with 4 equivalents of IRDye 800CW Maleimide. Next to this, VHH-Mesna was also randomly labeled with 1 or 4 equivalents IRDye 800CW NHS. The fluorescent signal per VHH was analyzed by SDS-PAGE gel (Fig. 4c). The labeling of VHH-Mesna with IRDye 800CW Maleimide was less efficient compared with the NHS conjugates. In contrast, the fluorescent signal of VHH-CA-Mal was comparable to VHH-Mesna-4eq-NHS, indicating the presence of a reactive thiol group on VHH-CA. To evaluate whether attachment of the labeling affects the binding properties of the VHH, binding assays were employed on the EGFR overexpressing cells (A431, under non-internalizing conditions; at 4 °C) (Fig. 4c & 4d). The highest binding affinity was observed for VHH-CA after directional labeling with IRDye 800CW Maleimide. Random labeling with
IRDye 800CW NHS resulted in a lower affinity. Despite the high Bmax of VHH-Mesna-4eq-NHS, the affinity was decreased 5.9-fold compared with VHH-CA-Mal. In contrast, only a 1.8-fold decrease in affinity was observed for VHH-Mesna when labeled with 1 equivalent IRDye 800CW NHS, however the Bmax and thus total fluorescent signal was 2.8-fold lower than VHH-CA. The random labeling of this VHH therefore appears to decrease the affinity in a concentration dependent manner.

3.4 Liposomes

Another platform to examine the functionality of VHH-CA is the conjugation to liposomes. Nanobodies have previously been decorated onto liposomes via random conjugation (SATA modification)[33,34] or EPL using cysteine modified liposomes[21]. Here, the VHH-CA was directly conjugated to liposomes bearing DSPE-PEG-Maleimide and rhodamine as fluorescent marker (VHH-Rho-L). To assess the inherent toxicity and their antagonistic properties (anti-EGFR VHH competes with EGF) these liposomes were incubated with A431 (EGFR positive) and 3T3 2.2 (EGFR negative) cells at various concentrations (Fig. 5a). No inhibition of cell proliferation was

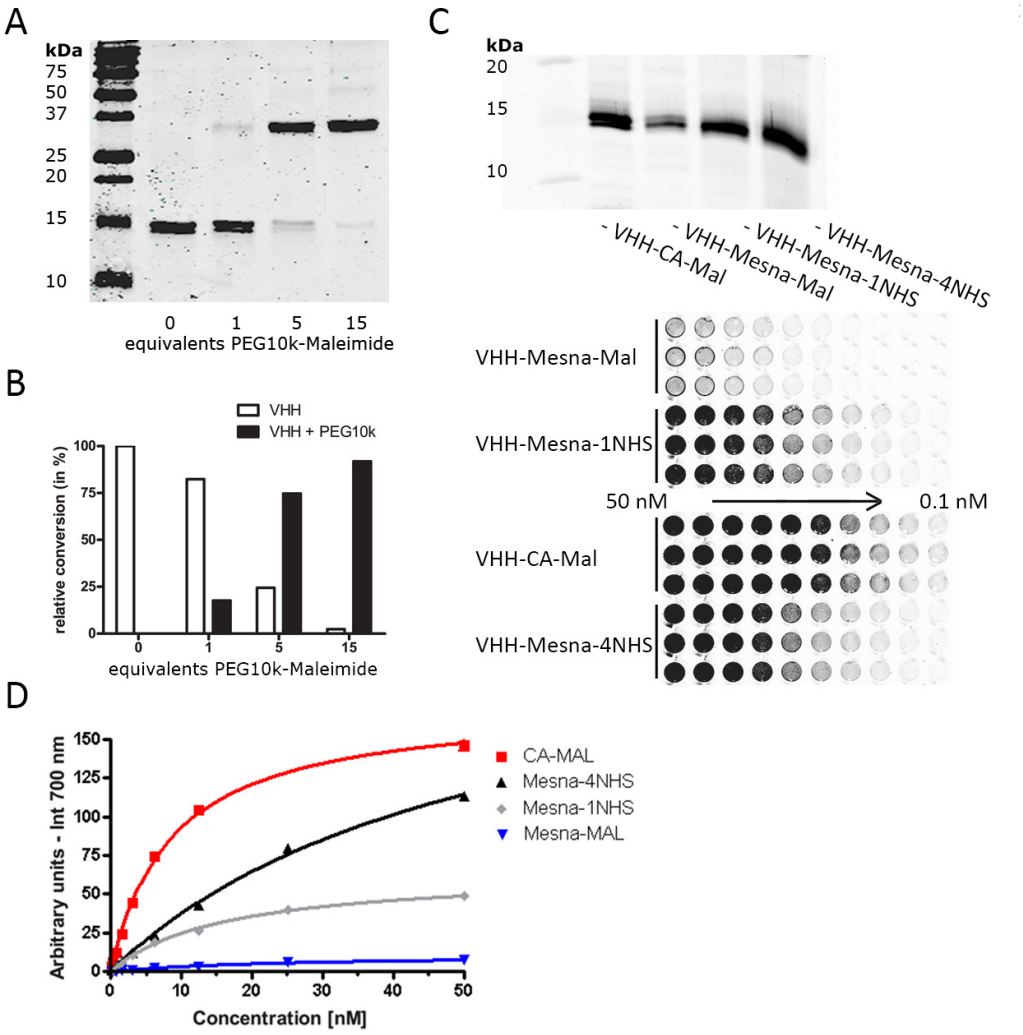

		CA-MAL	Mesna-4NHS	Mesna-4NHS	Mesna-MAL
Best-fit values	Bmax	173.80	236.80	64.77	11.19 AU
	Kd	8.73	53.36	16.26	24.80 nM
Std. Error	Bmax	3.07	10.88	2.02	0.63 AU
	Kd	0.40	3.99	1.20	2.90 nM

Figure 4. Characterization of the thiol-modified nanobody (VHH-CA). (A) The reactivity of the C-terminal thiol group was analyzed by conjugation to PEG10k-Maleimide and migration on SDS-PAGE gel. (B) The quantification of the thiol maleimide conversion was plotted. (C) In addition, the VHH-CA was modified with IRDye 800CW Maleimide and analyzed for the binding properties towards A431 cells (EGFR positive cells, antigen of the VHH; EGa1). As control, VHH modified with Mesna was also conjugated to IRDye 800CW Maleimide or IRDye 800CW NHS (1 or 4 equivalents to VHH). (D) The detected fluorescent signal was plotted and fitted according to the one site binding (hyperbola) equation using graphpad 5.02.

observed after 48 hrs of incubation with both liposomal formulations (+/- VHH, VHH-Rho-L and Rho-L respectively). In a follow up experiment we tested whether these liposomes interact with cells by assaying the rhodamine fluorescence of the exposed cells after incubation for 48 hrs (Fig. 5b). A concentration dependent rhodamine fluorescence signal was observed for the VHH-Rho-L when incubated with A431 cells. In contrast, only a low fluorescence signal was detected for the non-targeted liposomes (Rho-L). Incubation of both liposomal formulations with 3T3 2.2 cells resulted in a low background signal. The decoration of nanobodies on the surface of liposomes therefore provides specific interaction with EGFR positive cells.

The interaction of liposomes with A431 cells was furthermore confirmed by fluorescent microscopy (Fig. 5c). Rhodamine-labeled liposomes were incubated for 30 min, followed by a chase for 2 hrs to provide time for internalization. After 2 hrs, membrane-bound liposomes were removed by an acid wash (not the internalized liposomes). Unlike the liposomes without targeting moiety (Rho-L), the VHH-Rho-L liposomes were clearly visualized. In order to reveal the localization of the liposomes, the cells were stained with transferrin-alexa488. Transferrin is rapidly internalized via receptor-mediated endocytosis and localizes at early endosomes. No co-localization of the liposomes and transferrin was observed, indicating that the liposomes were not present in endosomes. Further experiments are required to establish the localization and rate of internalization of these liposomes over time.

4. Discussion

Over the years, nanobodies have been explored for their diagnostic and therapeutic applications[9]. In order to improve the EPL of nanobodies we developed a new construct, replacing the chitin binding domain by an elastin-like polypeptide. Expression at 25 °C and 30 °C yielded the maximum amount of fusion protein. The *in vivo* cleavage of the VHH-intein-ELP fusion protein was apparent for all tested temperatures after 20 hrs. In contrast, shorter inductions suffered less from this effect. The *in vivo* cleavage after 4 hrs of induction was temperature dependent and is in agreement with the impact kit manual (NEB manual E6901).

Although the *in vivo* cleavage lowers the overall yield, the target protein is lost during purification and thus does not affect the EPL efficiency. More important is the inactivation by hydrolysis and amidation after purification. From this point, the non-functionalized protein cannot be separated from the functionalized protein and decreases the EPL yield.

We therefore evaluated several cysteine analogs to perform the thiol-mediated cleavage (and the subsequent NCL). This reaction is known to depend on the C-terminal residue of the target protein as well as the reactivity of the thiol group. In a direct comparison with cysteine for instance, NCL with a selenocysteine bearing peptide (more nucleophilic and lower pKa) was 1000-fold faster at pH 5.0[35]. The more efficient EPL with cysteamine compared with cysteine can possibly be explained by the lower pKa (8.27 vs 8.7)[36]. In contrast, BME has a

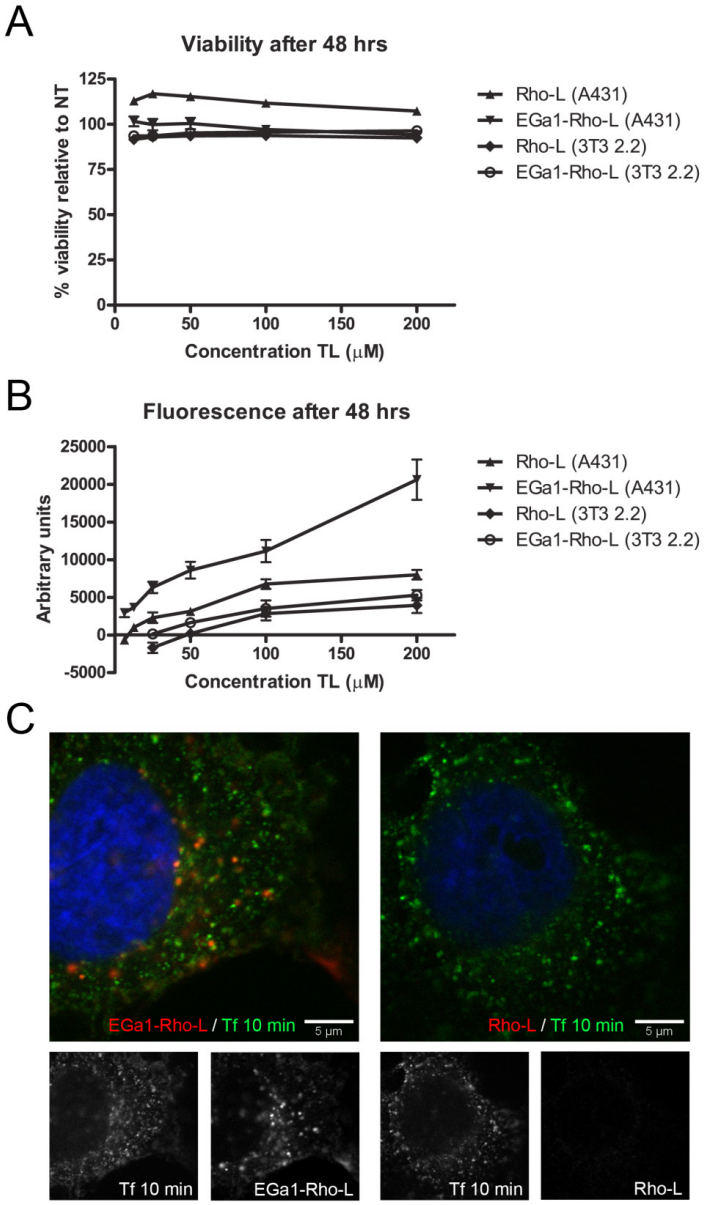

Figure 5. Analysis of rhodamine-labeled liposomes decorated with or without VHH-CA (VHH-Rho-L and Rho-L, respectively). (A) To determine the toxicity, liposomes were incubated at various concentrations for 48 hrs with cells, after which the cell viability was determined with Alamar Blue. (B) Specific binding and uptake by the cells was determined by the detection of rhodamine fluorescence after incubation of the liposomal formulation for 48 hrs. (C) The specific uptake was further analyzed by confocal laser scanning microscopy. A431 cells grown on gelatin coated glass slides were incubated with 125 μM TL of liposomes (red) for 30 min and chased with DMEM medium for 110 min. Transferrin alexa 488 (green) conjugated was incubated for 10 min, after which the cells were washed with ice-cold PBS, PBS (pH 5.0; acid wash) and fixed by addition of 4 % paraformaldehyde. Cell nuclei were stained with DAPI (blue). Color channels were enhanced to improve visualization. Data from two experiments are presented as mean ± SEM (n=6).

much higher pKa (9.72) than cysteamine but was remarkably faster. The intein-mediated cleavage by thiols therefore does not solely depend on a low pKa and the degree of formation of the corresponding thiolate at neutral pH (6-8), but also on other functional groups in the molecule, possibly affecting the thiol nucleophilicity. Furthermore, the positively charged amino group of cysteamine for instance might directly interact with the thiolate and/or prevent nucleophilical attack of the thioester. Another possibility is that the alcohol group of BME, may act as a general base and aid in the partial deprotonation of the thiol group.

Although the intein-mediated cleavage is most efficient in the presence of BME, cysteamine is the preferred choice for the introduction of a reactive thiol group. The labeling of proteins via cysteines has drawn much attention. Thiol groups are more nucleophicic than amines and are often present in proteins as disulfide bonds. An additional cysteine allows for site-directed conjugation to maleimide groups, as a consequence of the 1000-fold selectivity over amines at neutral pH[37]. One major drawback however is non-native disulfide bond formation causing protein misfolding. EPL with cysteamine overcomes this problem by introducing the thiol group after protein folding.

Here we demonstrated the conjugation of VHH-CA to PEG10k-Maleimide in a concentration dependent manner. Near quantitative conversion was observed when 15 equivalents of PEG10k-Maleimide were employed. Despite the large amount of PEG10k-Maleimide only minor fractions of multiple modifications of VHH-CA were observed. The large amount of PEG10k-Maleimide required and limited generation of side products can be explained by: A) a lower reactivity of PEG10k-Maleimide as a result of the long polymer, B) the selectivity of maleimide groups for thiols and C) the single modified VHH is efficiently 'masked' by PEG (as described for therapeutic proteins) and prevents a second modification.

Next to the reactivity of VHH-CA also the functional integrity was evaluated. Nanobodies are well known for their high stability, though modifications can affect the binding properties. This was indeed the case for random modification of VHH-Mesna. The attachment of IRDye 800CW through lysines decreased the affinity and was concentration dependent. Site-directed conjugation of VHH-CA was less invasive. The limited reactivity of amines towards maleimide resulted in the labeling of only a minor fraction of the VHH-Mesna. Direct comparison of VHH-CA and VHH-Mesna therefore indicates the presence of the reactive thiol group after EPL.

Liposomes as drug delivery platform are employed for many therapeutic applications. Next to the passive targeting by the enhanced permeability and retention effect (EPR), nanobodies can facilitate the active targeting of liposomes. Long term exposure (48 hrs) of liposomes to cells revealed no toxicity or growth inhibition for both formulations. In contrast, nanobodies randomly decorated on liposomes were previously reported to downregulate EGFR and cause growth inhibition. High TL concentrations were required to obtain effective growth inhibition. Differences in e.g. lipid composition, chemistry employed to decorated liposome with

nanobodies, quenching of maleimide groups and cell lines, complicated the comparison and prevented the identification of the determining factor.

Specific uptake by A431 cells was observed for VHH decorated liposomes (VHH-Rho-L), while this was not the case for non-targeted liposomes (Rho-L) or when EGFR negative cells were employed. This specific uptake was furthermore confirmed by microscopy and was only visible for the targeted liposomes (VHH-Rho-L). Colocalization with transferrin and thus early endosomes was not observed. Since the membrane bound liposomes were removed by an acid wash, the rhodamine fluorescence signal probably resides further downstream the degradation pathway in late endosomes or lysosomes.

5. Conclusion

In conclusion, we have demonstrated that nanobodies can be efficiently functionalized by EPL. This requires a modified intein construct as well as a reactive cysteine analog for the one step thiol-mediated cleavage and native chemical ligation. The EPL of nanobodies with cysteamine resulted in VHH-CA and could be quantitatively labeled with PEG10k-Maleimide. More importantly, VHH-CA remains functional after labeling with IRDye 800CW Maleimide and was decorated on liposomes. In a next step, nanobodies can be site-specifically conjugated to a liposomal platform for the active delivery of drugs.

Acknowledgements

This work was funded by the Focus & Massa project of the Utrecht University, the Netherlands.

References

1. Casi, G. & Neri, D. Antibody-drug conjugates: basic concepts, examples and future perspectives. *J. Control. Release* **161,** 422–8 (2012).
2. Sassoon, I. & Blanc, V. Antibody-drug conjugate (ADC) clinical pipeline: a review. *Methods Mol. Biol.* **1045,** 1–27 (2013).
3. Panowksi, S., Bhakta, S., Raab, H., Polakis, P. & Junutula, J. R. Site-specific antibody drug conjugates for cancer therapy. *MAbs* **6,** 34–45
4. Wu, A. M. & Olafsen, T. Antibodies for molecular imaging of cancer. *Cancer J.* **14,** 191–7 (2008).
5. Olafsen, T. & Wu, A. M. Antibody vectors for imaging. *Semin. Nucl. Med.* **40,** 167–81 (2010).
6. Holliger, P. & Hudson, P. J. Engineered antibody fragments and the rise of single domains. *Nat. Biotechnol.* **23,** 1126–36 (2005).
7. Fernández, L. A. Prokaryotic expression of antibodies and affibodies. *Curr. Opin. Biotechnol.* **15,** 364–73 (2004).
8. Hamers-Casterman, C. *et al.* Naturally occurring antibodies devoid of light chains. *Nature* **363,** 446–8 (1993).
9. Muyldermans, S. Nanobodies: natural single-domain antibodies. *Annu. Rev. Biochem.* **82,** 775–97 (2013).
10. Muyldermans, S., Atarhouch, T., Saldanha, J., Barbosa, J. A. & Hamers, R. Sequence and structure of VH domain from naturally occurring camel heavy chain immunoglobulins lacking light chains. *Protein Eng.* **7,** 1129–35 (1994).
11. Harmsen, M. M. & De Haard, H. J. Properties, production, and applications of camelid single-domain antibody fragments. *Appl. Microbiol. Biotechnol.* **77,** 13–22 (2007).
12. Tijink, B. M. *et al.* Improved tumor targeting of anti-epidermal growth factor receptor Nanobodies through albumin binding: taking advantage of modular Nanobody technology. *Mol. Cancer Ther.* **7,** 2288–97 (2008).
13. Devoogdt, N. *et al.* Molecular imaging using Nanobodies: a case study. *Methods Mol. Biol.* **911,** 559–67 (2012).
14. Oliveira, S. *et al.* Rapid visualization of human tumor xenografts through optical imaging with a near-infrared fluorescent anti-epidermal growth factor receptor nanobody. *Mol. Imaging* **11,** 33–46 (2012).
15. Kijanka, M. *et al.* Rapid optical imaging of human breast tumour xenografts using anti-HER2 VHHs site-directly conjugated to IRDye 800CW for image-guided surgery. *Eur. J. Nucl. Med. Mol. Imaging* **40,** 1718–1729 (2013).
16. Vaneycken, I. *et al.* Immuno-imaging using nanobodies. *Curr. Opin. Biotechnol.* **22,** 877–81 (2011).
17. Noren, C. J., Anthony-Cahill, S. J., Griffith, M. C. & Schultz, P. G. A general method for site-specific incorporation of unnatural amino acids into proteins. *Science* **244,** 182–8 (1989).
18. Liu, C. C. & Schultz, P. G. Adding New Chemistries to the Genetic Code. *Annu. Rev. Biochem.* **79,** 413–444 (2010).
19. Axup, J. Y. *et al.* Synthesis of site-specific antibody-drug conjugates using unnatural amino acids. *Proc. Natl. Acad. Sci.* **109,** 16101–16106 (2012).
20. Witte, M. D. *et al.* Preparation of unnatural N-to-N and C-to-C protein fusions. *Proc. Natl. Acad. Sci. U. S. A.* **109,** 11993–8 (2012).
21. Reulen, S. W. A., van Baal, I., Raats, J. M. H. & Merkx, M. Efficient, chemoselective synthesis of immunomicelles using single-domain antibodies with a C-terminal thioester. *BMC Biotechnol.* **9,** 66 (2009).
22. Debets, M. F. *et al.* Nanobody-functionalized polymersomes for tumor-vessel targeting. *Macromol. Biosci.* **13,** 938–45 (2013).
23. Perler, F. B. *et al.* Protein splicing elements: inteins and exteins--a definition of terms and recommended nomenclature. *Nucleic Acids Res.* **22,** 1125–7 (1994).
24. Xu, M. Q. & Evans, T. C. Intein-mediated ligation and cyclization of expressed proteins. *Methods* **24,** 257–77 (2001).
25. Dawson, P. E., Muir, T. W., Clark-Lewis, I. & Kent, S. B. Synthesis of proteins by native chemical ligation. *Science* **266,** 776–9 (1994).
26. MacEwan, S. R. & Chilkoti, A. Elastin-like polypeptides: biomedical applications of tunable

biopolymers. *Biopolymers* **94,** 60–77 (2010).
27. Ge, X. *et al.* Self-cleavable stimulus responsive tags for protein purification without chromatography. *J. Am. Chem. Soc.* **127,** 11228–9 (2005).
28. Johnson, E. C. B. & Kent, S. B. H. Insights into the mechanism and catalysis of the native chemical ligation reaction. *J. Am. Chem. Soc.* **128,** 6640–6 (2006).
29. Rouser, G., Fleischer, S. & Yamamoto, A. Two dimensional thin layer chromatographic separation of polar lipids and determination of phospholipids by phosphorus analysis of spots. *Lipids* **5,** 494–496 (1970).
30. Roovers, R. C. *et al.* Efficient inhibition of EGFR signaling and of tumour growth by antagonistic anti-EFGR Nanobodies. *Cancer Immunol. Immunother.* **56,** 303–317 (2007).
31. Broekgaarden, M., de Kroon, A. I. P. M., Gulik, T. M. van & Heger, M. Development and in vitro proof-of-concept of interstitially targeted zinc- phthalocyanine liposomes for photodynamic therapy. *Curr. Med. Chem.* **21,** 377–91 (2013).
32. Rouser, G., Fkeischer, S. & Yamamoto, A. Two dimensional then layer chromatographic separation of polar lipids and determination of phospholipids by phosphorus analysis of spots. *Lipids* **5,** 494–6 (1970).
33. Oliveira, S. *et al.* Downregulation of EGFR by a novel multivalent nanobody-liposome platform. *J. Control. Release* **145,** 165–75 (2010).
34. Van der Meel, R. *et al.* Inhibition of tumor growth by targeted anti-EGFR/IGF-1R nanobullets depends on efficient blocking of cell survival pathways. *Mol. Pharm.* **10,** 3717–27 (2013).
35. Hondal, R. J., Nilsson, B. L. & Raines, R. T. Selenocysteine in native chemical ligation and expressed protein ligation. *J. Am. Chem. Soc.* **123,** 5140–1 (2001).
36. Lide, D. R. CRC Handbook of Chemistry and Physics, 84th Edition, 2003-2004. *Handb. Chem. Phys.* **53,** 2616 (2003).
37. Kratz, H. *et al.* Straightforward thiol-mediated protein labelling with DTPA: Synthesis of a highly active 111In-annexin A5-DTPA tracer. *EJNMMI Res.* **2,** 17 (2012).

Chapter 5

Epidermal growth factor receptor-targeted liposomes with zinc phthalocyanine for photodynamic therapy

Remko van Vught*, Mans Broekgaarden*, Thomas M. van Gulik, Paul van Bergen en Henegouwen, Roland Pieters, Eefjan Breukink, Michal Heger

*** Authors contributed equally**

Abstract

Photodynamic therapy (PDT) is a non-invasive treatment modality based on the activation of a photosensitizer (PS) for the production of reactive oxygen species (ROS) and subsequent induction of cell death. Current PDT treatments focus on cancers that are ineligible or are recalcitrant to standard therapies. However, the commonly employed PSs exhibit suboptimal photophysical and photochemical properties and pharmacokinetics, and as a result are ineffective and cause skin phototoxicity. Liposomal encapsulation of PSs not only reduces skin accumulation but also passively targets liposomes to tumor cells. In order to further improve tumor targeting, we developed and characterized a novel liposomal formulation that contains zinc phthalocyanine (ZnPC) as PS and anti-epidermal growth factor (EGFR) nanobodies to facilitate active targeting. These tumor-targeting liposomes (TTLs) specifically bound to and were internalized by EGFR-overexpressing cancer cells. The uptake was significantly reduced in control liposomes lacking the anti-EGFR nanobodies and in murine fibroblasts that lack EGFR. The TTLs further exhibited superior PDT efficacy in EGFR-overexpressing cancer cells compared with control liposomes and fibroblasts incubated with TTLs. Lastly, the photokilling efficacy was dependent on the drug-light interval, whereby long drug-light intervals were associated with reduced photokilling efficacy.

1. Introduction

Photodynamic therapy (PDT) is a non-to-minimally invasive treatment modality that is standardly employed for several types of superficially located solid tumors (e.g., basal cell- and squamous cell carcinomas in the skin, early central stage lung tumors, and esophageal malignancies) producing complete response rates of 70-85 % [1–3]. PDT is also used as a last-line treatment option for tumors that respond poorly to surgery, chemotherapy, and/or radiotherapy, including recurrent superficial urothelial carcinomas[4], nasopharyngeal carcinomas[5] and non-resectable extrahepatic cholangiocarcinomas[6,7]. Unfortunately, the mean complete response rate of these tumors to PDT is also relatively poor, namely 41 % in urothelial carcinomas[4] and 56 % in nasopharyngeal carcinomas[8]. Non-resectable extrahepatic cholangiocarcinomas are only treated palliatively to extend patients' life expectancy[7], as there is currently no curative treatment available.

PDT entails the topical, oral, or systemic administration of a PS, accumulation of the PS in the tumor, and subsequent irradiation of the tumor with high-power resonant light to activate the PS, i.e., to bring PS electrons to a triplet state[9,10]. The triplet state electrons mainly transfer their energy to molecular oxygen (O_2) as they decay to ground state, yielding singlet oxygen ($^1O_2$) in the process. Alternatively, triplet state electrons are transferred to O_2 to produce superoxide anion ($O_2^{\bullet-}$), albeit this mechanism is less common for the PSs that are used for PDT. Both types of reactive oxygen species (ROS) are capable of oxidizing biomolecules and, when produced excessively such as during PDT, induce lethal oxidative stress in light-exposed cancer cells. Consequently, PDT causes cellular demise, shutdown of intratumoral vasculature, and an anti-tumor immune response, altogether resulting in removal of the tumor[11].

Despite the notable therapeutic efficacy with respect to superficial tumors, there are several factors that have restricted the implementation of PDT for cancers that are recalcitrant to or ineligible for standard therapy. First, patients have to remain shielded from light to prevent skin phototoxicity[12], which stems from the profound accumulation of (orally or systemically administered) PS in the skin. As a result, several treatment centers, including ours, have discontinued the use of PDT for terminally ill patients, given that forcing these patients to remain inside for an extended period of time is unethical. Second, most of the currently approved PSs have suboptimal photophysical and photochemical properties, as a result of which the treatment outcomes are suboptimal, particularly in larger tumors[12]. Third, cancer cells activate cell survival mechanisms following PDT that enable the tumor to cope with extensive oxidative stress and ensure tumor survival[13].

Accordingly, we have developed a comprehensive tumor treatment strategy for the abovementioned PDT-recalcitrant solid tumors that is based on the use of third-generation PSs (liposome-encapsulated metallated phthalocyanines)[14]. The PS-encapsulating liposomes are targeted to three pharmacologically relevant locations in the tumor, namely tumor cells, endothelium[15], and interstitium[16] in order to inflict different types of damage and ensure

considerable tumor lethality following PDT. The development and testing of the PS-encapsulating, interstitium-targeting liposomes (ITLs)[16] has been described elsewhere.

This study focuses on the development of tumor-targeting liposomes (TTLs) that contain zinc phthalocyanine (ZnPC) as PS[16,17]. Active targeting of TTLs was facilitated by anti-EGFR nanobodies[18,19], the variable domain of heavy chain only antibodies derived from camelids[20,21]. These antibody fragments are highly stable and relatively easy manipulated for (site-specific) conjugation to drug carriers[22]. Based on the previously established knowledge on ITLs and ETLs, TTLs were developed and characterized. The tumor-specific uptake of TTLs by EGFR-overexpressing cancer cells was quantified and visualized by confocal microscopy, after which in vitro proof-of-concept was demonstrated with respect to PDT efficacy.

2. Materials and Methods

2.1 Chemicals and reagents

The 1,2-dipalmitoyl-*sn*-glycero-3-phosphocholine (DPPC), cholesterol (chol), L-α-phosphatidylethanolamine, distearoyl methoxypolyethylene glycol conjugate maleimide (DSPE-PEG-MAL, average PEG molecular mass of 2,000 amu), L-α-Phosphatidylethanolamine-N-(lissamine rhodamine B sulfonyl) (Rho-PE) and 1-palmitoyl-2-{6-[(7-nitro-2-1,3-benzoxadiazol-4-yl)amino]hexanoyl}-*sn*-glycero-3-phosphocholine (NBD-PC) were from Avanti Polar Lipids (Alabaster, AL, USA). ZnPC (97% purity), 4-(2-hydroxyethyl)-1-piperazineethanesulfonic acid (HEPES), bovine serum albumin (BSA), cysteamine, DNAse, lysozyme, ampicillin, coomassie brilliant blue r, tris(2-carboxyethyl)phosphine hydrochloride (TCEP), and pyridine were from Sigma-Aldrich (St. Louis, MO, USA). Isopropyl β-D-1-thiogalactopyranoside (IPTG) and Ni-NTA beads were from Thermo Fisher Scientific (Waltham, MA, USA). Tetracycline was obtained from OPG Farma (BUVA, Uitgeest, the Netherlands). Sterile PBS was from Lonza (Basel, Switzerland). Enterokinase was obtained from New England Biolabs (P8070S, Ipswich, MA, USA). Chloroform, 2-mercaptoethanol (BME), bugbuster and NaCl were from Merck KGaA (Darmstadt, Germany).

Lipid stocks were dissolved in chloroform and stored at -20 °C in the dark after purging with nitrogen gas. The concentration of the lipid stocks was determined by the inorganic phosphate determination modified from Rouser et al.[23]. ZnPC was dissolved in pyridine at a concentration of 178 μM.

2.2 Cell culture

The human epidermoid carcinoma cell line A431 (CRL-1555) and the mouse fibroblast cell line NIH 3T3 2.2 were cultured in Dulbecco's modified Eagle's medium (DMEM, Gibco, Life Technologies, Thermo Fisher Scientific) supplemented with 8% fetal bovine serum (FBS) (v/v), antibiotics (100 U/mL penicillin, 100 μg/mL streptomycin), and 2 mM L-glutamine (PAA, Cölbe,

Germany) under standard culture conditions (at 37 °C in a humidified atmosphere containing 95 % O_2 and 5 % CO_2). Cells were regularly screened for mycoplasma infection (MycoAlert Mycoplasma Detection Kit, Lonza Benelux, Breda, the Netherlands) and all experiments were performed on mycoplasma-free cells.

2.3 Preparation, isolation, and purification of anti-EGFR nanobodies

The antagonistic anti-EGFR nanobody EGa1 (Roovers et al.[18]) was fused to a c-terminal intein domain and elastin-like polypeptide[24] (kind gift from Carlos Filipe, McMaster University, Canada). E. coli BLR(DE3) cells were transformed with the adapted pTXB1 construct (kind gift from William Leenders, Radboud University Nijmegen, the Netherlands) and selected using 100 µg/mL ampicillin and 12.5 µg/mL tetracycline. Expression of the fusion protein was induced in the logarithmic phase (OD_{600} = 0.5) by addition of 1 mM IPTG for 16 hrs at 25 °C. The harvested cultures were lysed in 1:50 bugbuster supplemented with lysozyme and DNAse and incubated for 15 min at room temperature (RT). The supernatant was collected by centrifugation at 19,000 ×g at 4 °C and incubated with Ni-NTA beads equilibrated in PBS (1 mL beads per liter culture) for 1 h at 4 °C. The beads were washed three times with 10 column volumes PBS after which the protein was eluted with 1 column volume 250 mM imidazole in PBS. Protein in the collected fractions was precipitated by addition of NaCl to a final concentration of 2 M. The pellet was resuspended in ice-cold cleavage buffer (20 mM phosphate buffer, pH = 7.0, containing 250 mM cysteamine) and incubated overnight at 4 °C. Again, the protein was precipitated by the addition of NaCl (2M final concentration). The supernatant that contained the functionalized nanobody was dialyzed against PBS, supplemented with 2 mM $CaCl_2$, incubated with 0.00025 % enterokinase (w/w) for 16 hrs at 37 °C (to remove the non-processed leader sequence), concentrated and loaded per 0.5 mL onto an in PBS equilibrated Superdex 75 10/300 GL column (GE Healthcare, Munich, Germany). The purified protein was stored at 4 °C until further use.

2.4 Protein analysis by SDS-PAGE

The nanobody conjugation to DSPE-PEG-MAL was assayed prior to liposome preparation. DSPE-PEG-MAL was dried under vacuum followed by addition of the nanobody and incubation for 20 hrs at RT. The protein/lipid samples were subsequently separated by reducing 15% SDS-PAGE gel to analyze the attachment of DSPE-PEG-MAL. The protein was visualized using coomassie brilliant blue r stain, detected with an ODYSSEY CLx scanner and quantified by densitometric analysis using ImageJ 1.47 (National Institutes of Health, Bethesda, MD).

2.5 Preparation of liposomes

ZnPC-encapsulating liposomes were prepared as described previously[16] according to the lipid-film technique. Lipids in chloroform were premixed at DPPC:chol:DSPE-PEG-MAL molar ratios of

77:15:8, respectively, and ZnPC was added to the lipid mixture at a ZnPC:lipid ratio of 0.003[16]. To fluorescently label the liposomes, Rho-PE or NBD-PC were added to the lipid mixture at the expense of DPPC at 0.2 and 5 mol%, respectively. The lipids were desiccated under nitrogen gas, after which the lipid film was vacuum exsiccated for 30 min. Subsequently, the lipid film was hydrated with physiological buffer composed of 0.88 % (w/v) NaCl, 10 mM HEPES, pH = 7.4, 0.292 osmol/kg. Liposomes were sized by brief sonication and extrusion through 0.2 µm aluminum oxide filters (Whatman, GE Healthcare, Little Chalfont, United Kingdom).

The C-terminal thiol on the nanobodies were reduced by 5 mM TCEP for 5 min at RT, desalted against PBS using Zeba Spin desalting columns (Thermo Fisher Scientific), and incubated with liposomes for 1 h at RT in the dark followed by incubation at 4 °C overnight in the dark. The nanobody:total lipid ratios used were 2 or 10 nMol/µMol. The non-reacted maleimide groups on DSPE-PEG-MAL were quenched by addition of BME at equimolar concentration (relative to the DSPE-PEG-MAL) and incubated for 1 h at RT. To study the effect of non-reacted maleimide groups on PDT efficacy, a part of the liposome batch was not quenched by BME and only incubated for 1 h at RT. The non-coupled nanobodies and BME were removed by 2× ultracentrifugation at 200,000 ×g for 40 min at 4 °C, after which the total lipid concentration was determined (Rouser et al. [23]). Liposomes were analyzed for size and polydispersity index by dynamic light scattering (DLS, 10 times for 1 min) using the Zetasizer 3000 (Malvern Instruments, Malvern, UK), and stored in the dark at 4 °C.

2.6 In vitro cell association studies

For the cell association studies, A431 cells were seeded in 96-wells plates (Greiner Bio-One, Alphen a/d Rijn, the Netherlands) at a density of 16,000/well and cultured for 24 hrs. Next, cells were washed once with phenol red-lacking but otherwise fully supplemented DMEM (DMEM-PR) and incubated with ZnPC-TTLs in medium (concentrations indicated separately per experiment) for 1 h under standard culture conditions. After incubation, the cells were washed twice with DMEM and once with 2 mM phosphate buffer pH 7.0, after which the plates were vacuum exsiccated for 15 min to remove residual fluid. The fluorescent intensity of ZnPC was detected with an ODYSSEY CLx scanner and quantified using Image Studio 3.1 (Li-COR Biosciences, UK).

2.7 In vitro photodynamic therapy

For the PDT optimization experiments, cells were seeded in 96-wells plates at a density of 4,000 cells/well and cultured for 24 hrs. Next, cells were incubated for 10 min with 125 µM total lipid concentration including cholesterol (TL) in medium, washed twice with DMEM-PR, washed again twice with DMEM-PR or PBS (to evaluate the effect of medium on PDT efficacy) and treated by PDT. For the remaining experiments, cells were seeded in 96-wells plates at a density of 2,000 cells/well and cultured for 24 hrs. In the time course experiment, cells were incubated for 10 or

30 min with 125 μM TL at the indicated time points, washed twice with DMEM-PR and treated by PDT. In the 30 min exposure experiments, cells were cultured for 22 hrs and incubated for 30 min with 62.5, 125 or 250 μM TL, washed twice with DMEM-PR, cultured for 1.5 hrs (to facilitate internalization of the liposomes) and treated by PDT. In other experiments, cells were cultured for 22 hrs and incubated for 10 min with 125 μM TL (unless mentioned otherwise), washed twice with DMEM-PR, cultured for 2 hrs (to facilitate internalization of the liposomes) and treated by PDT. For PDT treatment, all plates were subjected to a light dose of 10 J/cm^2 at 670 ± 10 nm during 42 min (1 LED per well, 4-mW/cm^2 as measured with an Orion Laser power/energy monitor, Ophir Optronics LTD, Jerusalem, Israel). After PDT, the plates were immediately returned to the incubator. The cell viability was assayed the next day (section 2.8).

2.8 Cell viability assays

Viability assays using Alamar Blue reagent were performed according to the manufacturer's protocol (AbD Serotec, Oxford, United Kingdom). Briefly, cells were incubated for 2-3 hrs with phenol red-lacking but otherwise fully supplemented DMEM (DMEM-PR) containing 1:10 (v/v) Alamar Blue (Life Technologies). The conversion of the Alamar Blue to its fluorescent analogue was measured with a FluoStar Optima fluorescence plate reader (BMG Labtech GmbH, Ortenberg, Germany). Cell viability was expressed as a percentage of dead cells relative to untreated cells after background subtraction. Data were plotted using GraphPad Prism 5.02 software.

2.9 Confocal laser scanning microscopy

A431 cells were seeded on fibronectin-coated microscope coverslips in 6-wells plates at 2.0×10^5 cells/mL. Cells reached subconfluence during overnight incubation. The cells were exposed to ZnPC-TTLs labeled with or without nanobody for 10 min, after which cells were washed twice in PBS and received fresh medium. Cells were placed at culture conditions for 3.5 hrs, after which cells received fresh serum-free DMEM supplemented with 50 nM Mitotracker Red CMX-ROS (Molecular Probes/Life Technologies, Eugene, OR, USA). After 30 min of incubation, cells were washed twice with PBS, after which the coverslips were mounted on microscope slides with Vectashield mounting medium with DAPI (Vectashield, Burlingame, CA, USA). Slides were dried for 1 h and sealed with nail polish. Confocal laser scanning microscopy was performed on a Leica SP8 Confocal microscope system (Leica Microsystems, Wetzlar, Germany). Cells were analyzed for fluorescence of DAPI (λ_{ex} = 405 nm, λ_{em} = 415-500 nm), Mitotracker Red CMXROS (λ_{ex} = 579 nm, λ_{em} = 589-700 nm), and ZnPC (λ_{ex} = 660 nm, λ_{em} = 670-750 nm). Images were processed in Leica Application Software using the Advanced Fluorescence module (Leica Microsystems).

3. Results and discussion

3.1 Preparation and characterization of liposomes

Over the years, several lipid-based drug delivery systems, including liposomal formulations, have been developed and validated for PDT[25]. The PS-encapsulating liposomal formulations can be targeted to the tumor passively via the enhanced permeability and retention effect[26] (e.g., ITLs[16], actively by using cationic liposomes that are avidly taken up by the tumor endothelium (e.g., ETLs[15]), or actively by the use of charged component lipids or liposome-conjugated ligands that recognize overexpressed epitopes on cancer cells (e.g., TTLs, this paper). For PS-containing TTLs, the use of nanobodies has never been investigated for selective cancer cell targeting. Consequently, PEGylated ZnPC-encapsulating TTLs containing anti-EGFR nanobodies (EGa1) were developed, characterized, and tested on EGFR-overexpressing cancer cells. In addition, we developed an intein based fusion protein for site-directed conjugation (Scheme 1), rather than decoration the liposomes with randomly oriented nanobody[19].

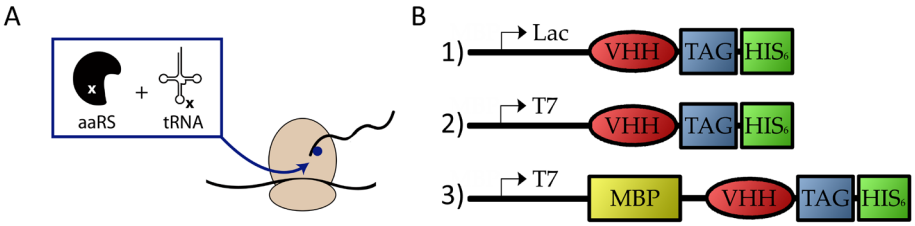

Scheme 1. Schematic representation of tumor-targeting liposomes for photodynamic therapy (PDT). (A) A reactive thiol group was introduced at the C-terminus of an anti-EGFR nanobody (VHH-SH) by incubating the nanobody-intein-ELP fusion protein with cysteamine. The VHH-SH protein was subsequently conjugated to maleimide-PEG functionalized liposomes containing the photosensitizer zinc phthalocyanine (ZnPC) in the bilayer. (B) The tumor-targeting liposomes are expected to bind to and be internalized by cancers cells. Subsequent illumination of the photosensitizer-replete cancer cells will lead to the photochemical generation of reactive oxygen species that cause cell death.

The EGa1 nanobody was expressed as fusion protein that contained an intein and elastin-like polypeptide (ELP) domain and incubated with cysteamine to release the intein and ELP and thereby introduced a C-terminal thiol group for conjugation (VHH-SH). To assess the conjugation efficiency to DSPE-PEG-MAL, we incubated VHH-SH with increasing concentrations of DSPE-PEG-MAL and analyzed the protein and protein-lipid complex migration on SDS-PAGE gel (Fig 1a). The unmodified VHH-SH migrated at approximately 15 kDa, corresponding to the molecular weight of a single VHH-SH molecule (15.76 kDa). The conjugation of VHH-SH to DSPE-PEG-MAL was confirmed by a band shift towards higher molecular weights (~22 kDa). The band density increased up to 5 equivalents DSPE-PEG-MAL in a concentration-dependent manner, signifying an increasing degree of conjugation. Next to labeling of VHH-SH with a single DSPE-PEG-MAL molecule, multiple modifications were visible. The incubation with 2.5 equivalents DSPE-PEG-MAL yielded the highest conversion rate of single modified VHH-SH (80.41%) with a minimum extent of multiple modifications.

The conjugation of VHH-SH to liposomes was also confirmed by SDS-PAGE analysis (Fig 1b). Only a minor fraction of uncoupled VHH-SH was detected after conjugation, which was removed by ultracentrifugation (not shown, only visible after adjusting the brightness/contrast of the image). Despite the preferential conjugation to the reactive thiol (band at ~22 kDa), random labeling was observed. This was probably the result of the excess of DSPE-PEG-MAL, which first reacted with the thiol group and subsequently with lysine residues on the

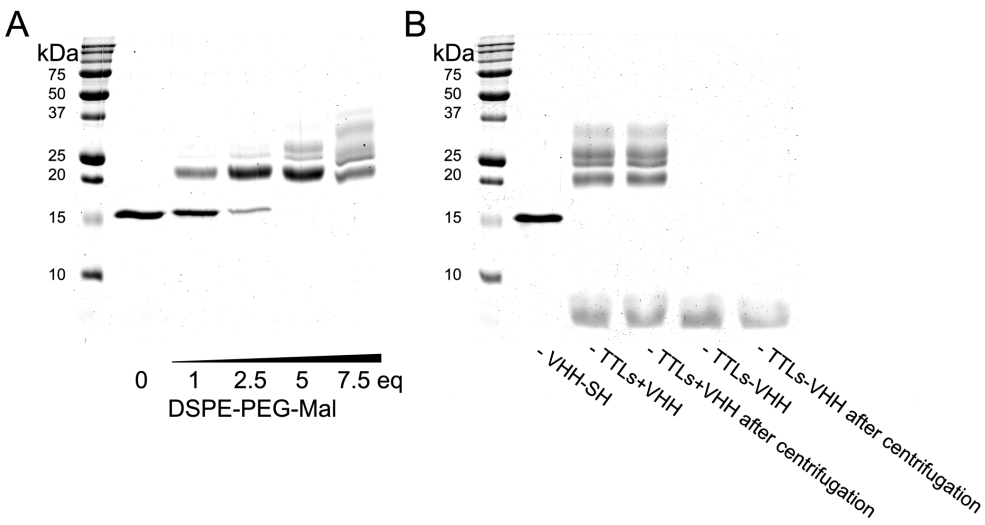

Figure 1. Preparation and characterization of nanobodies and nanobody-targeted liposomes. (A) The conjugation of VHH-SH to DSPE-PEG-MAL was analyzed by protein migration on SDS-PAGE gel. VHH-SH was incubated with increasing concentrations of DSPE-PEG-MAL overnight at room temperature. Samples were 1:1 diluted with 4x laemmli sample buffer to quench the free maleimide groups. (B) Liposomes containing DSPE-PEG-MAL were incubated with VHH-SH. The unbound VHH-SH was removed by 2x ultracentrifugation, after which the liposomes were separated by SDS-PAGE gel.

surface of VHH-SH. Unconjugated liposomes showed no band corresponding to unmodified VHH-SH but displayed a band in the front of the gel, corresponding to DSPE-PEG-MAL.

The prepared liposomes were analyzed by DLS (Table 1). Sonication and extrusion through 0.2 μM filters resulted in a mean size of 90-130 nm for all liposomal formulations.

Table 1. Liposomal characteristics of non-targeted liposomes (TTLs-VHH) or targeted liposomes (TTLs+1/5VHH and TTLs+VHH). The TTLs+1/5VHH liposomes have only 20% of the nanobodies on the liposomal surface compared with the standard TTLs (TTLs+VHH) and were employed to determine the concentration-dependent effect of nanobodies on PDT efficacy. Data are presented as mean ± SD of two separately prepared batches of liposomes.

Formulation	Size [nm]	PDI
TTLs - VHH	88.4 ± 3.2	0.21 ± 0.06
TTLs + 1/5VHH	107.8 ± 14.6	0.31 ± 0.05
TTLs + VHH	134.1 ± 4.2	0.26 ± 0.08

3.2 In vitro binding and uptake of TTLs

Binding and uptake of TTLs by cancer cells is essential for the outcome after PDT since most effective ROS damage occurs within the cell. The recognition of VHH-targeted liposomes by EGFR-(over)expressing cells was determined in cell association studies. Towards this end, A431 cells (human epidermoid carcinoma cell line expressing high levels of EGFR) were incubated with VHH-decorated (TTLs+VHH) and non-targeted, control liposomes (TTLs-VHH) containing ZnPC (Fig 2a). The fluorescent signal was quantified and plotted as a function of total lipid (TL) concentration (Fig 2b). Concentration-dependent binding and uptake of liposomes by A431 cells was observed for both formulations, although the association between cells and TTLs was considerably more pronounced than for control liposomes. The non-specific uptake of TTLs-VHH liposomes by A431 cells was probably the result of the long incubation time (1 h), which was necessary because at shorter incubation times the ZnPC fluorescence was below the detection limit. This is not surprising given the high triplet state quantum yield of ZnPC[17], causing a large fraction of singlet state electrons to undergo intersystem crossing to the triplet state at the expense of fluorescence. Accordingly, the long incubation time do not necessarily reflect binding affinity as much as they reflect the technical limitations of the detection system, as evidenced by the 4-fold greater fluorescence signal of TTLs+VHH liposomes versus the TTLs-VHH liposomes.

The binding and internalization of TTLs by EGFR-overexpressing cells was further studied by confocal fluorescence microscopy. In order to mimic the *in vivo* situation, where continuous perfusion limits the exposure of liposomes to target cells, the NBD-labeled liposomes were incubated for 10 min followed by a chase for 0.5 or 4 hrs (Fig 3).

This short exposure is expected to not only reduce the non-specific uptake, but to visualize the active targeting of these liposomes. Membrane association of targeted NBD-liposomes was

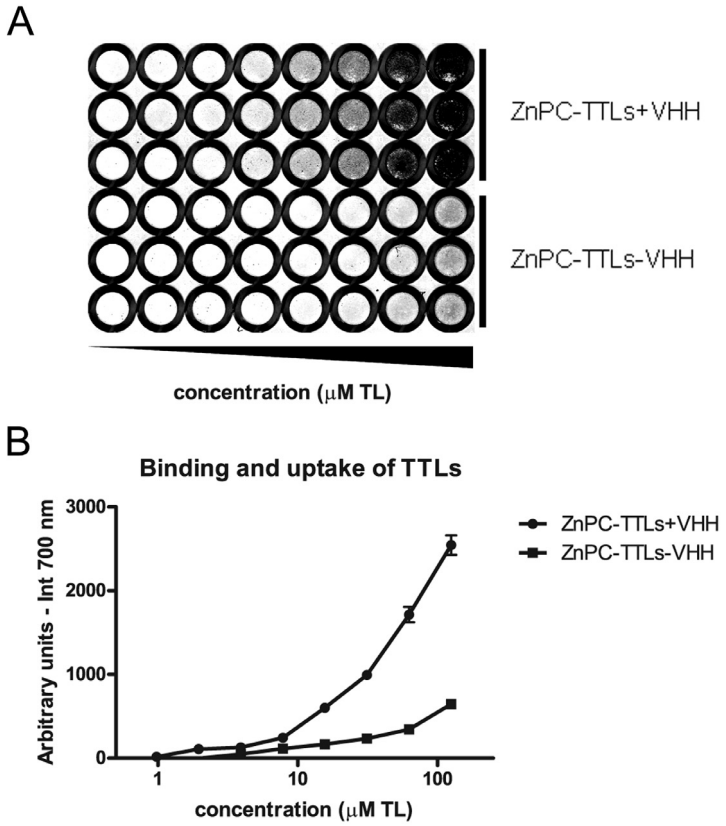

Figure 2. Binding and uptake of TTLs by A431 cells. (A) The A431 cells were incubated with increasing concentration of liposomes for 1 h at 37 °C. The fluorescent intensity at 700 nm of ZnPC was detected with an Odyssey CLx scanner. (B) The fluorescent intensity was quantified by Image Studio 3.1. Data from two experiments are presented as mean ± SEM (n=6).

only evident for A431 cells and not 3T3 2.2 cells, which lack EGFR expression. Similarly, minimal membrane association was visible for non-targeted NBD-liposomes. NBD-labeled liposomes were rapidly internalized by A431 cells since the NBD label was dispersed throughout the cells, exhibiting colocalization with mitochondria after only 30 min. Despite the reduction in NBD fluorescence after 4 hrs the colocalization with mitochondria was still evident. This loss of fluorescence was probably the result of the limited chemical or biological stability of NBD (e.g., metabolism of the phospholipid). The fluorescence was significantly higher for the TTLs in A431 cells compared with control liposomes as well as the 3T3 2.2 cells, corroborating the association data reported in figure 2 and the binding specificity of TTLs.

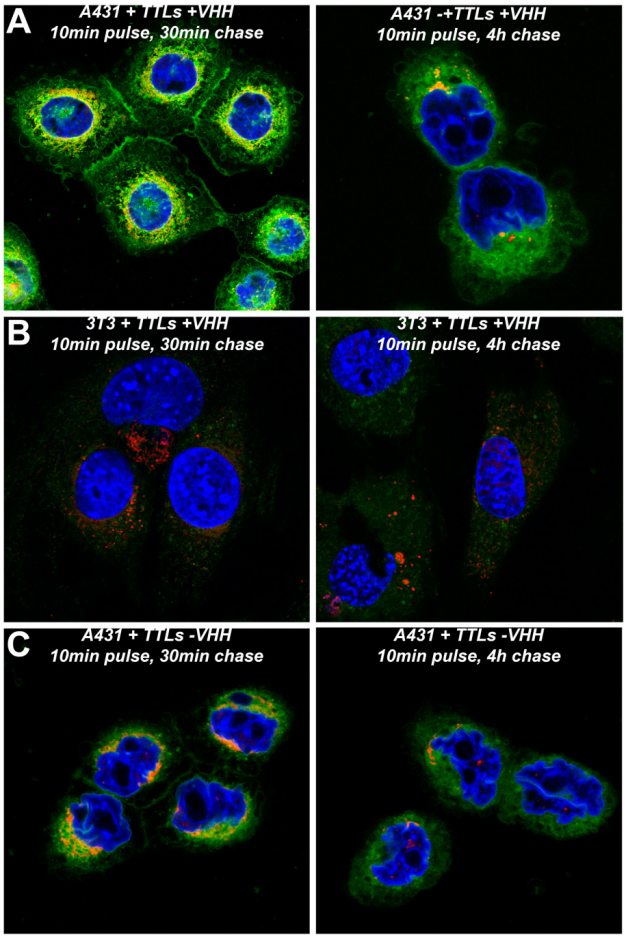

Figure 3. Confocal laser scanning microscopy on A431 cells stained with DAPI (blue, nuclei), NBD (green), and Mitotracker Red CMXROS (red, mitochondria). Images are depicted as overlays of the three channels. EGFR-overexpressing A431 (A) and EGFR-null 3T3 2.2 (B) cells were incubated for 10 min at 37 °C with targeted NBD-liposomes (TTLs+VHH) and chased for 0.5 or 4 hrs. As control, A431 cells were incubated with non-targeted NBD-liposomes (TTLs-VHH) and chased for 0.5 or 4 hrs (C).

In addition to NBD localization, the localization of ZnPC was investigated to determine its intracellular dispersion (Fig 4). After incubation for 10 min and a 4-h chase, the specific uptake of liposomes by A431 cells was mainly observed for the TTLs+VHH liposomes. Co-staining of the cells with Mitotracker Red CMXROS showed that ZnPC was not strictly confined to mitochondria but also other intracellular locations. Previously, localization of ZnPC in the Golgi complex was reported for several cell lines[27–29]. In addition, localization of ZnPC in mitochondria was also described (after prolonged incubation/chase) and was important for the effective induction of apoptotic cell death after PDT treatment[29].

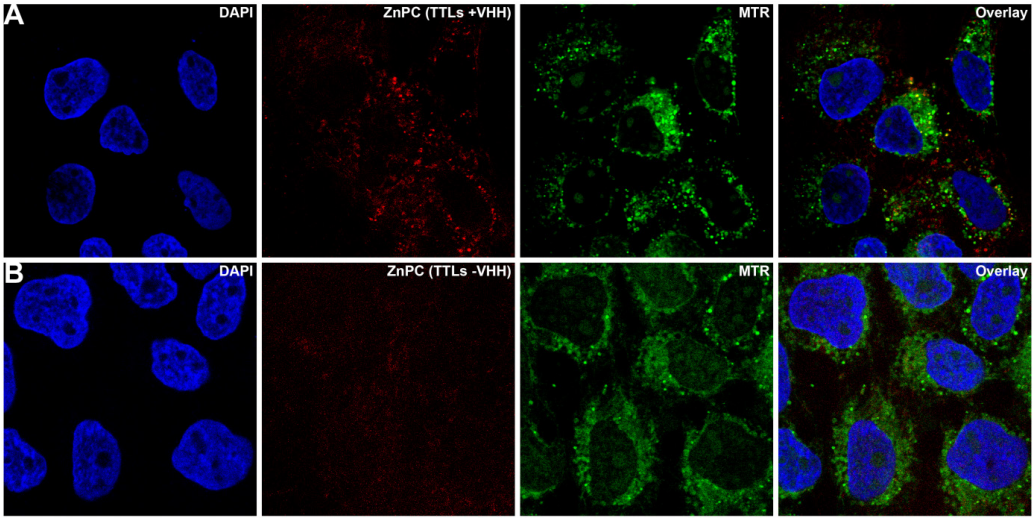

Figure 4. Confocal laser scanning microscopy of A431 cells stained with DAPI (blue, nuclei), ZnPC (red) delivered by TTLs, and Mitotracker Red CMXROS (green, mitochondria). Overlays are depicted in the last panel. ZnPC was imaged after a 10-min incubation and 4-h chase with targeted liposomes (A; TTLs+VHH) or non-targeted, control liposomes (B; TTLs-VHH).

3.3 In vitro PDT efficacy

In an effort to evaluate the *in vitro* PDT efficacy of TTLs, we first analyzed the dark toxicity. Incubation of A431 cells with various concentrations of TTLs (TTLs+VHH and TTLs-VHH) without PDT treatment had no detrimental effect on cell viability (Fig 5a). This demonstrates that all components (ZnPC, nanobody, PEGylated liposomes) were not toxic to A431 cells at the assayed concentrations.

Subsequently, PDT efficacy was evaluated after illumination of the A431 (Fig 5b) and 3T3 2.2 (Fig 5c) cells. Cells were incubated for 10 min with liposomes directly followed by several washing steps and PDT treatment. The treatment with TTLs was most effective (Fig 5b). A third liposomal formulation bearing only 20 % of VHH on the surface (TTLs+1/5VHH), incubated with A431 cells at equimolar final lipid concentrations, did not affect cell viability after illumination and its PDT efficacy was comparable to the TTLs-VHH liposomal formulation, indicating that a relatively high nanobody surface density is required for the successful photokilling of cancer cells.

In the next step, we determined whether quenching of free, non-reacted maleimide groups on the liposomal surface with 2-mercaptoethanol (BME) is necessary for effective PDT treatment. During the production of the liposomes, a part from the same batch was taken and not quenched by BME. Compared with the BME-quenched formulation, a clear reduction in PDT efficacy was observed for the non-quenched TTLs+VHH liposomes while the other formulations remained non-toxic after light exposure. This effect was probably the result of association of

proteins in the medium to the liposomal surface, thereby preventing the association with cells due to either blocking of the recognition domain on the nanobody or due to steric hindrance. Accordingly, the influence of DMEM medium (supplemented with FBS) on PDT efficacy was addressed by incubating cells with liposomes in medium followed by PDT in PBS (Fig 5c, third column). The PDT efficacy was increased for all formulations, but markedly more for the TTLs+VHH liposomes. In contrast, no toxicity was observed in 3T3 2.2 cells under any of the above mentioned conditions. These results are in agreement with the binding and uptake experiments (Fig 2) and stress the beneficial effect of active targeting of nanobody-conjugated liposomes.

The observation that PDT is more efficient in PBS might implicate that a large fraction of the liposomes resides on the cell surface after 10 min incubation and was less effective due to scavengers in medium. As stated before, PDT is expected to be more efficient when the PS is located in the cell and thus might benefit from a chase before illumination to provide time for increased internalization of the PS. In order to study this effect, cells were incubated at different time points for 10 min with liposomes and chased (0 - 24 hrs), after which the PDT efficacy in medium was determined (Fig 5d). Time-dependent PDT efficacy was observed for both liposomal formulations. Interestingly, an increase in effectivity was observed for the TTLs+VHH liposomes by delaying illumination, which might be attributed to the internalization and dispersion dynamics of ZnPC as was shown for NBD-PC (Fig 3). However, a decrease in PDT efficacy was observed from 8 hrs and onwards (instead of a static effectivity after complete uptake). This phenomenon was probably the result of ZnPC distribution to intracellular loci where the consequences of ROS formation are less detrimental to cell viability. Contrastingly, the TTLs-VHH liposomes demonstrated an increasing efficacy over time, albeit never reaching the cytotoxicity levels of the TTLs. Whether this non-specific uptake results in differential intracellular distribution of ZnPC compared with the TTLs+VHH liposomes and hence the differential PDT efficacy, still needs to be determined. The timing of PDT in both formulations affected the therapeutic outcome and warrants additional experiments to further investigate the translational importance of drug-light intervals. Most interesting would be to evaluate whether a similar effect can be observed *in vivo* since the incubation time and concentration would be less defined.

The optimized conditions were further employed to evaluate concentration-dependent effects. Both liposomal formulations were incubated for 10 min, chased for 2 hrs, followed by PDT treatment (Fig 5e). As expected, the TTLs+VHH liposomes were more effective at all examined concentrations due to their active targeting component. Only minimal non-specific toxicity was observed for TTLs-VHH liposomes or for TTLs+VHH liposomes when incubated with the 3T3 2.2 cells. The broad therapeutic window was at its maximum at a lipid concentration of 31.3 µM, resulting in 74.9 % difference in cell viability compared with TTLs-VHH liposomes.

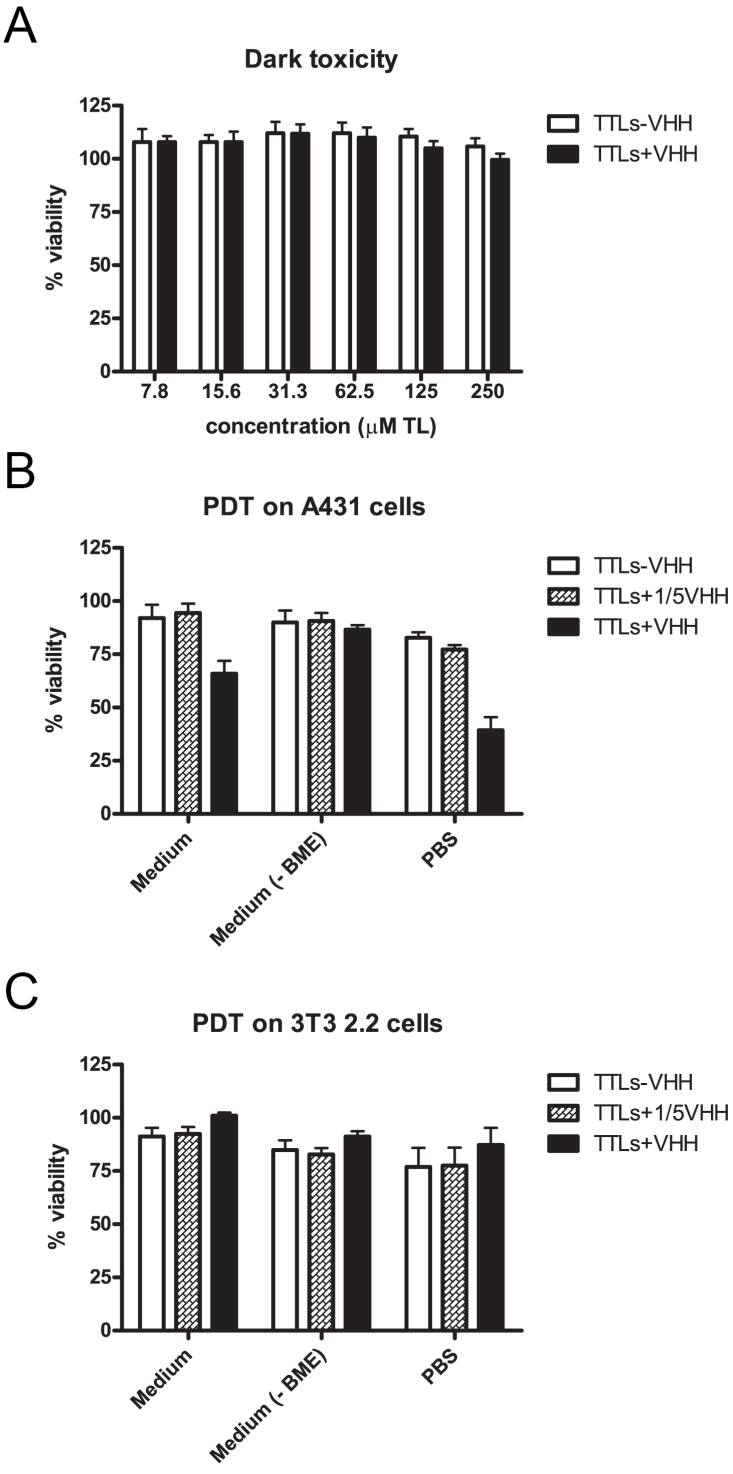
A
Dark toxicity
% viability
125
100
75
50
25
0
7.8
15.6
31.3
62.5
125
250
concentration (μM TL)
TTLs-VHH
TTLs+VHH
B
PDT on A431 cells
% viability
125
100
75
50
25
0
Medium
Medium (- BME)
PBS
TTLs-VHH
TTLs+1/5VHH
TTLs+VHH
C
PDT on 3T3 2.2 cells
% viability
125
100
75
50
25
0
Medium
Medium (- BME)
PBS
TTLs-VHH
TTLs+1/5VHH
TTLs+VHH

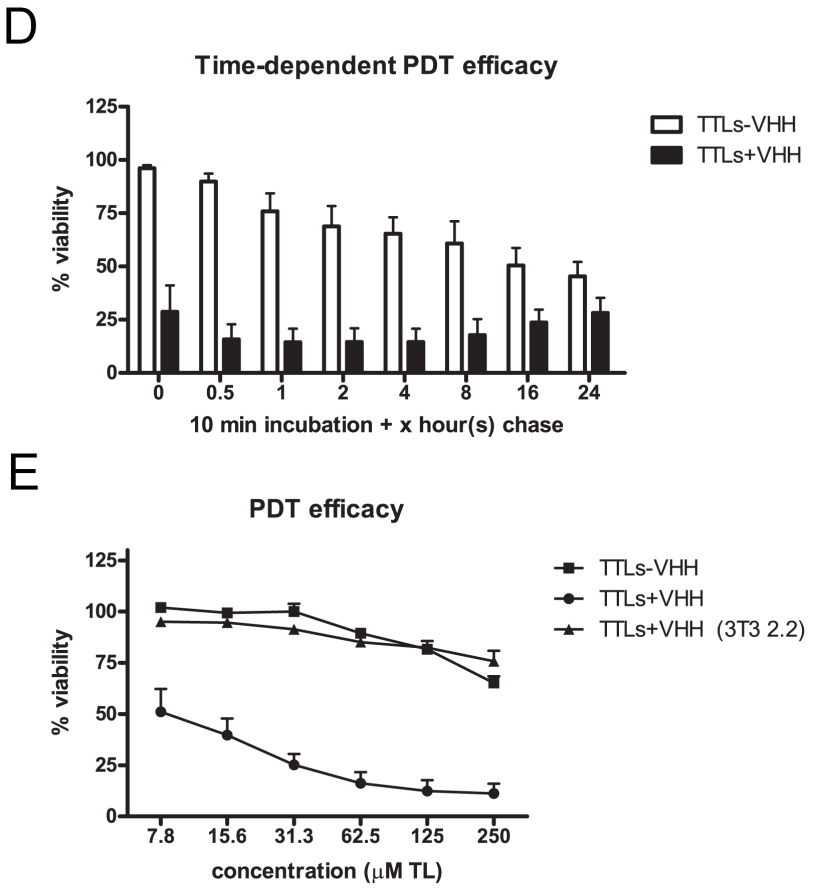

Figure 5. *In vitro* PDT efficacy of non-targeted liposomes (TTLs-VHH) as well as TTLs (TTLs+1/5VHH and TTLs+VHH). (A) The dark toxicity was determined in A431 cells for the TTLs-VHH and TTLs+VHH liposomes. Cells were incubated for 10 min with a serial dilution of liposomes, followed by refreshing the medium without PDT. The PDT efficacy of the three liposomal formulations was evaluated under standards conditions (10 min incubation with 125 μM total lipids (TL), cells resuspended in phenol red-lacking but otherwise fully supplemented DMEM, and PDT with a light dose of 10 J/cm^2), under standards conditions with liposomes without 2-mercaptoethanol (BME)-quenched maleimide groups, or under standard conditions with cells in PBS while applying PDT for A431 cells (B) and 3T3 2.2 cells (C). (D) In order to determine the effect of liposomal uptake and the intracellular distribution of ZnPC on PDT efficacy, PDT was applied at different time points. A431 cells were incubated under standard conditions, followed by a chase in the dark for 0 – 24 hrs, after which all samples were treated with PDT at the same time. (E) The concentration-dependent effect of TTLs-VHH and TTLs+VHH liposomes on A431 cells was determined under the optimized PDT conditions (standard + chase for 2 hrs). As additional control, the PDT efficacy of TTLs+VHH liposomes was also evaluated for the EGFR-null 3T3 2.2 cell line. Data from two experiments are presented as mean ± SEM (n=6).

Longer incubation times (e.g., 30 min) were required to fully eradicate A431 cells, but consequently also affected the specificity of the TTLs (Fig S1).

5. Conclusion

In conclusion, PEGylated ZnPC-encapsulating TTLs containing anti-EGFR nanobodies (EGa1) were developed to facilitate active targeting towards EGFR overexpressing cancers. The beneficial binding and uptake of these actively targeted liposomes by EGFR-overexpressing A431 cells was confirmed by fluorescence spectroscopy and confocal microscopy, whereby the uptake of nanobody-lacking liposomes or the uptake of TTLs by 3T3 2.2 cells was inferior. The TTLs demonstrated increased PDT efficacy *in vitro* compared with their non-targeted counterparts. These results request the validation and characterization of actively targeted TTLs for PDT treatment *in vivo*.

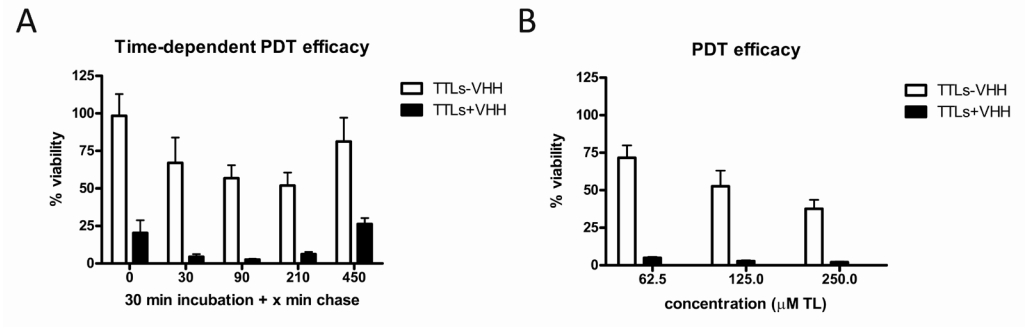

Figure S1. *In vitro* PDT efficacy of non-targeted liposomes (TTLs-VHH) and targeted liposomes (TTLs+VHH) without 2-mercaptoethanol (BME)-quenched maleimide groups. (A) A431 cells were incubated for 30 min with 125 μM total lipids (TL), followed by a chase in the dark for 0 – 450 min, after which all samples were treated with PDT at the same time. (B) The concentration-dependent effect of TTLs-VHH and TTLs+VHH liposomes on A431 cells was determined. Cells were incubated for 30 min with 62.5, 125 or 250 μM total lipids (TL), followed by a chase in the dark for 90 min and PDT treatment. Data from two experiments are presented as mean ± SEM (n=6).

Acknowledgements

This work was funded by the Focus & Massa project of the Utrecht University, the Netherlands.

References

1. Szeimies, R.-M., Morton, C. A., Sidoroff, A. & Braathen, L. R. Photodynamic therapy for non-melanoma skin cancer. *Acta Derm. Venereol.* **85,** 483–90 (2005).
2. Qumseya, B. J., David, W. & Wolfsen, H. C. Photodynamic Therapy for Barrett's Esophagus and Esophageal Carcinoma. *Clin. Endosc.* **46,** 30–7 (2013).
3. Moghissi, K. & Dixon, K. Update on the current indications, practice and results of photodynamic therapy (PDT) in early central lung cancer (ECLC). *Photodiagnosis Photodyn. Ther.* **5,** 10–8 (2008).
4. Pinthus, J. H., Bogaards, A., Weersink, R., Wilson, B. C. & Trachtenberg, J. Photodynamic therapy for urological malignancies: past to current approaches. *J. Urol.* **175,** 1201–7 (2006).
5. Wildeman, M. A. M., Nyst, H. J., Karakullukcu, B. & Tan, B. I. Photodynamic therapy in the therapy for recurrent/persistent nasopharyngeal cancer. *Head Neck Oncol.* **1,** 40 (2009).
6. Khan, S. A., Thomas, H. C., Davidson, B. R. & Taylor-Robinson, S. D. Cholangiocarcinoma. *Lancet* **366,** 1303–14 (2005).
7. Lee, T. Y., Cheon, Y. K. & Shim, C. S. Current status of photodynamic therapy for bile duct cancer. *Clin. Endosc.* **46,** 38–44 (2013).
8. Sun, Z. Q. [Photodynamic therapy of nasopharyngeal carcinoma by argon or dye laser--an analysis of 137 cases]. *Zhonghua Zhong Liu Za Zhi* **14,** 290–2 (1992).
9. Brown, S. B., Brown, E. A. & Walker, I. The present and future role of photodynamic therapy in cancer treatment. *Lancet Oncol.* **5,** 497–508 (2004).
10. Wilson, B. C. Photodynamic therapy for cancer: principles. *Can. J. Gastroenterol.* **16,** 393–6 (2002).
11. Castano, A. P., Mroz, P. & Hamblin, M. R. Photodynamic therapy and anti-tumour immunity. *Nat. Rev. Cancer* **6,** 535–45 (2006).
12. Agostinis, P. *et al.* Photodynamic therapy of cancer: an update. *CA. Cancer J. Clin.* **61,** 250–81
13. Moor, A. C. Signaling pathways in cell death and survival after photodynamic therapy. *J. Photochem. Photobiol. B.* **57,** 1–13 (2000).
14. Yoon, I., Li, J. Z. & Shim, Y. K. Advance in photosensitizers and light delivery for photodynamic therapy. *Clin. Endosc.* **46,** 7–23 (2013).
15. Thurston, G. *et al.* Cationic liposomes target angiogenic endothelial cells in tumors and chronic inflammation in mice. *J. Clin. Invest.* **101,** 1401–13 (1998).
16. Broekgaarden, M., de Kroon, A. I. P. M., Gulik, T. M. van & Heger, M. Development and in vitro proof-of-concept of interstitially targeted zinc- phthalocyanine liposomes for photodynamic therapy. *Curr. Med. Chem.* **21,** 377–91 (2013).
17. Jori, G. Factors controlling the selectivity and efficiency of tumour damage in photodynamic therapy. *Lasers Med. Sci.* **5,** 115–120 (1990).
18. Roovers, R. C. *et al.* Efficient inhibition of EGFR signaling and of tumour growth by antagonistic anti-EFGR Nanobodies. *Cancer Immunol. Immunother.* **56,** 303–317 (2007).
19. Oliveira, S. *et al.* Downregulation of EGFR by a novel multivalent nanobody-liposome platform. *J. Control. Release* **145,** 165–75 (2010).
20. Hamers-Casterman, C. *et al.* Naturally occurring antibodies devoid of light chains. *Nature* **363,** 446–8 (1993).
21. Muyldermans, S. Nanobodies: natural single-domain antibodies. *Annu. Rev. Biochem.* **82,** 775–97 (2013).
22. Harmsen, M. M. & De Haard, H. J. Properties, production, and applications of camelid single-domain antibody fragments. *Appl. Microbiol. Biotechnol.* **77,** 13–22 (2007).
23. Rouser, G., Fleischer, S. & Yamamoto, A. Two dimensional thin layer chromatographic separation of polar lipids and determination of phospholipids by phosphorus analysis of spots. *Lipids* **5,** 494–496 (1970).
24. Ge, X. *et al.* Self-cleavable stimulus responsive tags for protein purification without chromatography. *J. Am. Chem. Soc.* **127,** 11228–9 (2005).
25. Derycke, A. S. L. & de Witte, P. A. M. Liposomes for photodynamic therapy. *Adv. Drug Deliv. Rev.* **56,** 17–30 (2004).
26. Fang, J., Nakamura, H. & Maeda, H. The EPR effect: Unique features of tumor blood vessels for drug delivery, factors involved, and limitations and augmentation of the effect. *Adv. Drug Deliv. Rev.* **63,** 136–51 (2011).

27. Rello-Varona, S., Stockert, J. C., Cañete, M., Acedo, P. & Villanueva, A. Mitotic catastrophe induced in HeLa cells by photodynamic treatment with Zn(II)-phthalocyanine. *Int. J. Oncol.* **32,** 1189–96 (2008).
28. Rodal, G. H., Rodal, S. K., Moan, J. & Berg, K. Liposome-bound Zn (II)-phthalocyanine. Mechanisms for cellular uptake and photosensitization. *J. Photochem. Photobiol. B.* **45,** 150–9 (1998).
29. Fabris, C. *et al.* Photosensitization with zinc (II) phthalocyanine as a switch in the decision between apoptosis and necrosis. *Cancer Res.* **61,** 7495–500 (2001).

Chapter 6

Incorporation of unnatural amino acids in nanobodies

Remko van Vught, Erik Oude Blenke, Enrico Mastrobattista, Nathaniel Martin, Rob Roovers, Paul van Bergen en Henegouwen, Roland Pieters, Eefjan Breukink

Abstract

Unnatural amino acids (UAA) with a diverse set of chemical, physical and biological properties have been site-specifically incorporated into proteins to study their biological function. In addition, proteins have been produced with UAAs to improve existing or introduce new properties. Recently, UAAs were employed to produce therapeutic antibodies in a homogeneous manner by using bioorthogonal 'click reactions'. In order to further explore this potential, unnatural amino acids were site-specifically incorporated into nanobodies, the variable domains derived from heavy chain only antibodies from camelids. The fusion to maltose-binding protein and optimization of induction conditions resulted in efficient production of nanobodies bearing UAAs. Copper-catalyzed azide alkyne cycloaddition (CuAAC) and strain-promoted alkyne-azide cycloaddition (SPAAC) were employed to site-specifically label nanobodies with biomolecules and to demonstrate their functionality. As proof-of-concept, nanobody-biotin-streptavidin conjugates were generated and evaluated for their ability to inhibit tumor cell proliferation.

1. Introduction

Amino acids are the building blocks of proteins and their order in the polypeptide chain determines protein structure and function. Extended diversity in the protein landscape is however introduced after protein synthesis by post translational modifications (PTMs)[1]. In order to study the effects of amino acid modifications and their role in protein function as well as in protein-protein interactions, researchers are forced to closely mimic the protein of interest. Over the years, a wide set of methods were developed to produce proteins with desired modifications[2]. One of the first methods involves the replacement of a canonical amino acid by an unnatural analog[3]. By depletion of one amino acid in the culture medium, a close structural analogue can be accepted by the biological machinery. Although this method was originally demonstrated for replacement of phenylalanine and methionine by analogs[3], the introduction of selenomethionine or ^{15}N labeled amino acids for protein structure determination is now-a-days more common[4–6].

The substitution of one amino acid at multiple sites throughout the protein and limited structural freedom for amino acid modifications (to be accepted by the biological machinery) are profound limitations of this method[7]. Methods based on the established knowledge were developed to overcome this limitations by the introduction of unnatural amino acids (UAA) at defined sites in the protein without affecting the canonical amino acids[8–11]. This incorporation is based on an orthogonal tRNA/aminoacyl-tRNA synthethase pair to facilitate the incorporation of the UAA at a specific codon. The TAG (amber) codon is the least used stop codon and is therefore commonly employed but in addition some 4/5 base codons have also been described[12,13]. Evolution of the tRNA/aminoacyl-tRNA synthethase pair under strong selection pressure resulted in the recognition of predominantly only the designed UAA and none of the canonical amino acids[14]. Until today, over 70 UAAs have been site-specifically incorporated into proteins using this method[15]. Although employment of the amber codon affects the protein yield (from 10 % to 75 % of wild-type protein expression), UAA are generally incorporated with high fidelity (>95 %) and therefore comprise a useful toolbox for many applications including protein structural and functional studies[16].

The incorporation of UAA into antibodies has also been described. One of the applications comprises the introduction of UAA in CDRs to extent the diversity of amino acids and their functional groups for epitope recognition. Phage display screening against GP120 for instance with sulfotyrosine as 21st amino acid, identified multiple clones bearing the UAA[17]. Expressed as Fab, the importance of sulfotyrosine was demonstrated by a 15-fold higher affinity compared with the fab expressing a tyrosine instead[17]. Another application is the introduction of a functional group at a defined site for bioorthogonal chemistry[2]. Although the labeling of monoclonal antibodies (mAbs) with biomolecules can be employed via random conjugation strategies, this often results in the loss of antigen recognition and/or introduces heterogeneity[2].

Recently, trastuzumab (mAbs against HER2) was expressed with the unnatural amino acid p-acetylphenylalanine (pAcF) and modified with an auristatin analog[18]. This antibody drug conjugate (ADC) demonstrated a high degree of homogeneity, similar pharmacokinetics and potency *in vivo*. In another study, Fabs with an UAA were demonstrated to yield an anti-HER2/anti-CD3 bispecific antibody to target CD3 positive cells (T lymphocytes) to cancer cells[19]. The same Fabs were also employed for the structural formation of homo/heterodimers as well as homotetramers by peptide nucleic acids of defined sequences[20].

Although UAA have been incorporated into several antibody fragments, this is mainly limited to Fabs and has not included nanobodies. These smaller antibody fragments are derived from heavy chain only antibodies from camelids and as a consequence harbor unique properties including enhanced stability, solubility, extended CDR3 loop and straightforward selection via phage display[21–23]. Nanobodies have, because of their small size, a short half-life *in vivo* and are therefore especially suitable for diagnostic applications[24–27]. Alternatively, they can be conjugated to various scaffolds to increase the circulation time in blood[28–32].

In this study the incorporation of unnatural amino acids into nanobodies was evaluated. From all the previously described UAAs, *p*-azidophenylalanine (pAzF) was chosen as a model amino acid since its conjugation to biomolecules via Staudinger ligation and [3+2] cycloaddition has been well established[8]. Several constructs were generated for the production of the antagonistic EGa1 nanobody and were evaluated for their expression yields. The most suitable construct was subsequently optimized and analyzed for the incorporation of pAzF. As a proof-of-concept of this method, expressed azide functionalized EGa1 (EGa1-N_3) was conjugated to biomolecules via strain-promoted alkyne-azide cycloaddition (SPAAC).

6

2. Materials and Methods.

2.1 Chemical and reagents.

DNAse, lysozyme, l-arabinose, imidazole, ampicillin, tris(2-carboxyethyl)phosphine (TCEP), tris[(1-benzyl-1H-1,2,3-triazol-4-yl)methyl]amine (TBTA), sodium ascorbate (SA), bovine serum albumin (BSA), accutase, formalin, streptavidin, coomassie brilliant blue r, dithiothreitol and sodium choride (NaCl) were from Sigma-Aldrich (St. Louis, MO, USA). Tetracycline was obtained from OPG Farma (BUVA, Uitgeest, the Netherlands). Factor Xa was obtained from New England Biolabs (P8010S, Ipswich, MA, USA). DBCO-PEG_4-DBCO, DBCO-NHS (CLK-A134) and sulfo-DBCO-biotin were obtained from Jena Bioscience (Jena, Germany). N_3-IRDye 800CW was from LI-COR Biosciences (Lincoln, NE, USA). Isopropyl β-D-1-thiogalactopyranoside (IPTG), supersignal west pico chemiluminescent substrate (ECL), restriction enzymes and Ni-NTA beads were from Thermo Fisher Scientific (Waltham, MA, USA). Sterile PBS was from Lonza (Basel, Switzerland). Chloramphenicol was from Duchefa biochemie (Haarlem, the Netherlands). Bugbuster and

copper sulfate ($CuSO_4$) were from Merck KGaA (Darmstadt, Germany). Lipids 1,2-dioleoyl-*sn*-glycero-3-phosphocholine (DOPC), 1,2-dioleoyl-*sn*-glycero-3-phosphoethanolamine (DOPE), L-α-Phosphatidylethanolamine-N-(lissamine rhodamine B sulfonyl) (Rho-PE) and cholesterol (chol) were from Avanti Polar Lipids (Alabaster, AL, USA).

2.2 Plasmid generation

The antagonistic anti-EGFR nanobody EGa1 (Roovers et al.[33]) was employed as a model nanobody for the incorporation of unnatural amino acids. In all constructs, the nanobody was followed by a small spacer, TAG codon and (Flag +) HIS_6-tag. The first construct (1; pClick4) was generated by replacing the promotor and chloramphenicol resistance gene of plasmid pACYC184 (Thermo Fisher Scientific) by a promoter and a multiple cloning site of plasmid pMEK221 (tetracycline resistance gene, p15A origin of replication and placZ promoter). The multiple cloning site was previously modified (with a duplex of ggcccagccggccatggcccaggtgcagctgcaggagtcataatgagggacccaggtcaccgtctcctcagcggccg cataggactacaaagacgacgacgacaaaggggccgcacatcaccatcatcaccatggggccgcataatgagaattc) and allows straightforward insertion of nanobody genes using 5' SfiI or NcoI, and 3' NotI sites. The second construct (2; pTXB-pClick4), was based on a modified pTXB1 construct described in chapter 4 and was digested with NotI and MunI to allow insertion of the TAG codon, HIS_6-tag and TAA stop codons by a duplex of primers (gcggccgcataggccgcacatcaccatcatcaccatggggccgcataataacaattg). In contrast to pClick4, this construct contains an ampicillin resistance gene, pMB1 origin of replication from pBR322 and T7 promoter. The third construct (3; pMal-C2-pClick4) was based on pMal-C2X construct. The nanobody, TAG codon, HIS_6-tag was amplified from the pTXB-pClick4 construct using ggtggtgaattcgcggcccagccggccatg and ggtggtaagcttctcgagttattatgcggccccatggtgatg as forward and reverse primers, respectively. The amplified product was digested with EcoRI and XhoI and ligated into pMal-C2X. In contrast to the previous constructs, this construct contains an ampicillin resistance gene, pBR322 origin of replication, T7 promoter and MBP fusion protein (which can be cleaved by factor Xa). Constructs were verified by sequencing (Macrogen Europe).

2.3 Nanobody expression

E. coli DH10Bac cells were transformed with pClick4 and pEvol-pAzF (for tRNA/tRNA synthethase; kind gift from Peter G. Schultz, The Scripps Research Institute, La Jolla, CA, USA), and selected using 12.5 mg/mL tetracycline and 34 mg/mL chloramphenicol. E. coli BLR(DE3) cells were transformed with pTXB-pClick4 or pMal-C2-pClick4 and pEvol-pAzF, and selected using 100 mg/mL ampicillin and 34 mg/mL chloramphenicol. Unless mentioned otherwise, expression of the tRNA/tRNA synthethase was induced at OD_{600} = 0.3 by addition of 0.1 % l-arabinose (m/v) and 1 mM pAzF (kindly provided by Nathaniel Martin), from a freshly prepared stock of 250 mM pAzF in 0.5 M NaOH. After 15 min, the expression of the nanobody was also induced (OD_{600} +/- 0.5) by the addition of 1 mM IPTG for 3-4 hrs at 37 °C or 16 hrs at 25 °C.

For analysis, 100 µL of each culture was collected by centrifugation at 19 000 xg for 5 min and resuspended in 15 µL 2x Laemmli sample buffer supplied with reducing agent (DTT). Samples were boiled for 5 min at 99 °C, separated on 15 % SDS-PAGE gel and blotted onto nitrocellulose membrane. After blocking with 5 % skim milk, membranes were incubated with monoclonal anti-polyHistidine–Peroxidase antibody (A7058, Sigma-Aldrich) in PBS and the expressed nanobody was detected by ECL. For the optimization experiments the signals were analyzed and quantified by ImageJ 1.4.7. In case of coomassie stained SDS-PAGE gels, proteins were separated by SDS-PAGE, coomassie stained and detected using ODYSSEY CLx (Li-COR Biosciences).

2.4 Nanobody purification

The harvested cultures were lysed in 1:50 bugbuster supplemented with lysozyme and DNAse and incubated for 15 min at room temperature (RT). The pellet was collected by centrifugation at 19 000xg at 4 °C for 30 min and washed twice with bugbuster to isolate inclusion bodies. The supernatant was incubated with in PBS equilibrated Ni-NTA beads (1 mL beads per liter culture) for 1 hr at 4 °C. The beads were washed three times with PBS after which the protein was eluted in 250 mM imidazole in PBS. The eluted protein was dialyzed against PBS and incubated with factor Xa (supplemented with 2 mM CaCl) overnight at 37° C. The nanobody was concentrated and further purified using an in PBS equilibrated Superdex 75 10/300 GL column (GE Healthcare Europe GmbH, Munich, Germany). The purified protein was stored at 4 °C until further use.

2.5 Copper-catalyzed azide alkyne cycloaddition (CuAAC)

Cu(I) catalyzed click reactions between EGa1-N_3 and tetramethylrhodamine (TAMRA) Alkyne dye (Life technologies, Thermo Fisher Scientific) were performed in a 1:100 (mol/mol) ratio in presence of 400 mM phosphate buffer pH 8.0, 0.4 mM TBTA and 1 mM $CuSO_4$. The reaction was initiated by reduction of Cu(II) to Cu(I) by the addition of ~6 mg copper wire, 2 mM TCEP, 5 or 10 mM sodium ascorbate. The Cu(I) catalyzed click reactions were also performed in 1x Laemmli sample buffer without reducing agent to denature the protein and provide more access to the pAzF.

Cu(I) catalyzed click reactions between EGa1-CCH (alkyne) and N_3-Alexa 488 (Life technologies) were performed in a 1:100 (mol/mol) ratio in presence of 100 mM phosphate buffer pH 8.0 and 1 mM $CuSO_4$, with and without 0.4 mM TBTA. The reaction was initiated by the addition 2 mM sodium ascorbate and stopped by addition of 2.3 mM choline-alkyne (kind gift from Per Haberkant, EMBL, Heidelberg, Germany).

All reactions were incubated for 4 hrs at 37 °C, were subsequently separated onto SDS-PAGE gels and visualized by a Typhoon 9400 fluorescence imager (Amersham Biosciences, GE Healthcare Europe GmbH).

2.6 Strain-promoted alkyne-azide cycloaddition (SPAAC)

Prior to SPAAC, DBCO-GPLGLAGGEALEALS was prepared in situ. Briefly, a mixture of 50 mM DBCO-NHS, 250 mM NH_2-GPLGLAGGEALEALS-OH and 50 mM phosphate buffer pH 8.0 in DMSO/H_2O in a ratio of 9:1 (v/v) was incubated for 4 hrs at RT, analyzed by TLC and stored at -20 °C until further use.

SPAAC between EGa1-N_3 and DBCO-GPLGLAGGEALEALS or DBCO-PEG_4-DBCO was performed in a 1:10 (mol/mol) ratio in PBS and incubated for 16 hrs at RT. The EGa1-DBCO-PEG_4-DBCO conjugate was subsequently incubated with N_3-IRDye800 CW in a 1:2 DBCO-PEG_4-DBCO to N_3-IRDye800 CW ratio (mol/mol) and incubated for 24 hrs at RT. To demonstrate the specificity of SPAAC, the reactions were also performed without DBCO-GPLGLAGGEALEALS/N_3-IRDye800 CW as well as in presence of DBCO-GPLGLAGGEALEALS/N_3-IRDye800 CW and a 120-fold or 45-fold excess of sodium azide compared with DBCO-GPLGLAGGEALEALS or N_3-IRDye800 CW, respectively. Protein samples were separated by SDS-PAGE, coomassie stained and/or detected using the ODYSSEY CLx scanner (Li-COR Biosciences).

2.7 Preparation of liposomes.

Liposomes were prepared according to the lipid-film technique. Briefly, a mixture of DOPC/DOPE/chol in the molar ratios of 50:25:25 was supplemented with 0.2 % Rho-PE. For the liposomes bearing the cyclooctyne lipid (kindly provided by Nathaniel Martin), 1 % of cyclooctyne lipid was added at the expense of DOPC. After removal of the organic solvents by a N_2 stream followed by drying under vacuum, the lipid film was hydrated in HBS and liposomes were sized by extrusion through 100 nm filters (GE Healthcare). The nanobody EGa1 bearing an azido group was incubated with liposomes in a 1:10 ratio (mol/mol) over the weekend at 4 °C. The non-coupled nanobodies were removed by three times ultracentrifugation at 277 072xg for 55 min and resuspended in 200 µL HBS. The total lipid concentration was determined according the rouser assay[34] and liposomes were stored in the dark at 4°C until further use.

2.8 Cell culture

The human breast adenocarcinomal cell line MDA-MB-468 was cultured in Dulbecco's modified Eagle's medium (DMEM, Gibco, Life Technologies, Thermo Fisher Scientific) supplemented with 10 % fetal bovine serum (FBS, Thermo Fisher Scientific) (v/v). The human epidermoid carcinoma cell line A431 (CRL-1555) was cultured in DMEM supplemented with 8 % FBS (v/v), antibiotics (100 U/mL penicillin, 100 µg/mL streptomycin), and 2 mM L-glutamine (PAA, Cölbe, Germany). Cells were kept under standard culture conditions (at 37 °C in a humidified atmosphere containing 95 % O_2 and 5 % CO_2) and were consistently free of mycoplasma (MycoAlert Mycoplasma Detection Kit, Lonza).

2.9 FACS

MDA-MB-468 cells were incubated with accutase and divided over a roundbottom 96-wells plate (40.000 cells per well). Serial dilutions of liposomes were incubated with cells for 1 hr at 4 °C in the dark. The non-bound liposomes were removed by centrifugation at 300xg and washing twice with 200 µL 0.3 % BSA (m/v) in PBS. After the third centrifugation step, cells were resuspended in 150 µL PBS and fixed with 50 µL 10% formalin solution (neutral buffered, Sigma-Aldrich). FACS analysis was performed the next day on a FACSCanto HTS (BD Biosciences, Franklin Lakes, NJ, USA) and mean fluorescent intensities were analyzed and plotted using GraphPad Prism 5.02 software.

2.10 Nanobody multimerization

EGa1-N_3 was incubated with sulfo-DBCO-biotin in PBS in a ratio of 1:20 (mol/mol) for 16 hrs at RT followed by purification using an in PBS equilibrated Superdex 75 10/300 GL column. Streptavidin was subsequently incubated with the purified EGa1-biotin (streptavidin to nanobody ratios employed were 1:1, 1:2, 1:4, 1:10 and 1:40 (mol/mol)) for 30 min at RT. All protein samples were separated by SDS-PAGE, coomassie stained and detected using ODYSSEY CLx (Li-COR Biosciences).

Samples of EGa1-biotin, EGa1-biotin-streptavidin conjugate (in a streptavidin to nanobody ratio of 1:10, mol/mol) and biotin-streptavidin (in a streptavidin to biotin ratio of 1:100, mol/mol) were analyzed by SEC using an ÄKTA Prime, in PBS equilibrated Superdex 75 10/300 GL column and detector at 280 nm.

2.11 Nanobody multimerization

A431 cells were seeded in 96-wells plates (Greiner Bio-One, Alphen a/d Rijn, the Netherlands) at a density of 2.000 cells/well and cultured for 24 hrs. Next, cells were incubated for 48 hrs with a serial dilution of EGa1-biotin, EGa1-biotin-streptavidin conjugate and biotin-streptavidin in DMEM (8 % FBS) at 37 °C. To compensate for the four nanobodies per EGa1-biotin-streptavidin conjugate, the actual concentration of EGa1-biotin was 4x higher than indicated. After 48 hrs, all samples were washed twice with DMEM and incubated 2-3 hrs with phenol red-lacking but otherwise fully supplemented DMEM containing 1:10 (v/v) Alamar Blue (Life Technologies Europe BV, the Netherlands) to determine the cell viability. The fluorescence was measured with a FluoStar Optima fluorescence plate reader (BMG Labtech GmbH, Ortenberg, Germany). The cell viability was expressed as a percentage of dead cells relative to untreated cells after background subtraction and data were plotted using GraphPad Prism 5.02 software.

3. Results and discussion

3.1 Incorporation of unnatural amino acids: optimizing expression systems

An optimized expression system based on the evolved Methanocaldococcus jannaschii aminoacyl-tRNA synthetase(s) (aaRS)/suppressor tRNA pairs was recently reported (pEVOL) and was employed in this study[35]. In addition, existing plasmids for nanobody expression were modified with a TAG codon in between the nanobody gene and HIS_6-tag to introduce pAzF at the C-terminus. Because of this genetic order, premature termination by the TAG codon resulted in nanobodies without pAzF and HIS_6-tag, and were not purified by immobilized metal ion affinity chromatography (IMAC). An overview of the incorporation of pAzF and the employed expression constructs is presented in scheme 1. Expression constructs harbor the general genetic consensus of a nanobody gene (VHH), followed by TAG codon and HIS_6-tag of which 1) was induced by the Lac promotor (17.1 kDa), 2) was induced by the T7 promotor (16.0 kDa) and 3) was a maltose-binding protein (MBP) fusion protein induced by the T7 promotor (59.6 kDa, after factor Xa treatment 17.2 kDa). Although MBP fusion proteins provide high expression and prevent aggregation, additional processing after purification is required to remove the MBP domain[36].

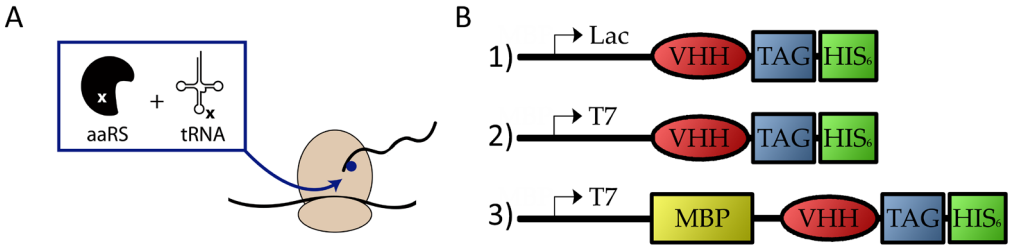

Scheme 1. Schematic representation of the incorporation of unnatural amino acids (UUAs). (A) During protein expression a TAG stop codon was suppressed by an orthologous tRNA/aminoacyl-tRNA synthethase pair (pEVOL) and incorporated the UAA of interest. (B) Several constructs were evaluated for the expression of the EGa1 nanobody with C-terminal pAzF and a His_6-tag. Upon suppression of the TAG codon and incorporation of the UAA, the nanobody was produced with a His_6-tag and was purified using immobilized metal ion affinity chromatography (IMAC). The relative expression yields were determined for the different constructs: 1) Lac promotor (17.1 kDa), 2) T7 promotor (strong inducer, 16.0 kDa), 3) Maltose-binding protein (MBP) fusion protein with a T7 promotor (59.6 kDa, after factor Xa treatment 17.2 kDa).

The incorporation of pAzF into EGa1 and its expression was evaluated by SDS-PAGE gel and western blot (Fig. 1). Cell lysates of induced cultures were separated by SDS-PAGE to analyze the relative expression yields (Fig. 1a). Small size differences between the truncated EGa1 (termination at TAG codon) and full length EGa1 (suppression of the TAG codon) prevented the separation of the two populations. Based on the estimated size of EGa1 and MBP-EGa1 (see Scheme 1), overexpression of only the MBP-EGa1 fusion protein was identified

at approximately 60 kDa. The expression by constructs 1 and 2 were not distinguishable from endogenous proteins and thus required western blot for detection using the HIS_6-tag (Fig. 1b). As expected, the T7 promotor induces EGa1 expression more strongly compared with the weaker Lac promotor. High production of the MBP-EGa1 fusion protein however saturated the western blot and was in agreement with the overexpression detected by SDS-PAGE gel. Since the HIS_6-tag was only present in full length proteins, the incorporation of pAzF into EGa1 was the most efficient for the MBP-EGa1 construct. To assess whether the detected proteins were functional and not aggregated, cultures were lysed with bugbuster to isolate inclusion bodies (Fig. 1c) and to concentrate the supernatant by IMAC (Fig. 1d). The MBP-EGa1 fusion protein was clearly visualized after concentration by IMAC and to a minor extent in inclusion bodies. Despite the previous identification of EGa1 by western blot, applications for constructs 1 and 2 were limited due to the low induction and/or expression in inclusion bodies and thus were not further analyzed.

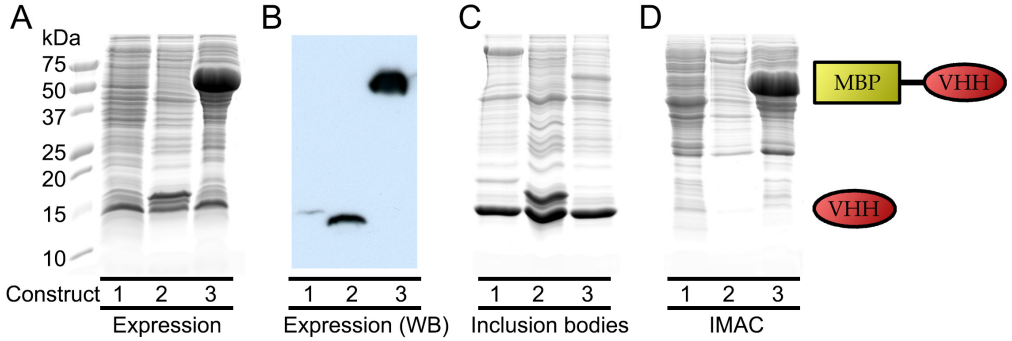

Figure 1. Incorporation of pAzF through nonsense suppression of the TAG codon into the EGa1 nanobody. (A) Relative expression of EGa1 by the three constructs (presented in scheme 1) was analyzed using SDS-PAGE. Towards this end, cultures were induced under standard conditions (1 mM ITPG, 0.1% l-arabinose, 1 mM pAzF), after which only the MBP-EGa1 fusion protein was identified after separation by SDS-PAGE. Differentiation between the truncated EGa1 (termination at TAG codon) and full length EGa1 (suppression of the TAG codon and incorporation of pAzF) was not possible due to the limited size difference. (B) Expression of full length EGa1 with pAzF was detected by western blot using an anti-HIS_6 monoclonal antibody. (C) Inclusion bodies of the induced cultures were isolated by lysing and washing the pellets with bugbuster and separated on SDS-PAGE gel. (D) Induced cultures were lysed with bugbuster, after which EGa1 nanobodies bearing pAzF and HIS_6-tag were concentrated from the supernatant using IMAC and subsequently separated on SDS-PAGE gel.

3.2 Expression and purification of MBP-EGa1 fusion protein

The fusion protein requires additional processing by factor Xa to obtain the final protein (EGa1-N_3). The expression, purification and cleavage by factor Xa were analyzed in more detail (Scheme 2).

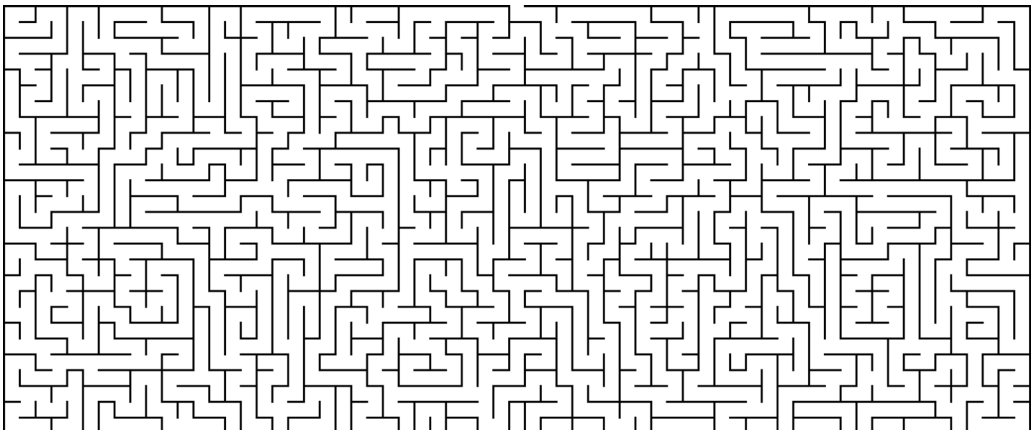

Scheme 2. Schematic representation of the production and purification of EGa1 from the MBP-EGa1 fusion protein. (A) The full length MBP-EGa1 fusion protein was only produced in presence of UAA and tRNA/aminoacyl-tRNA synthethase pair, while else the TAG codon serves as stop codon resulting in truncated MBP-EGa1 without pAzF and HIS_6-tag. (B) The MBP-EGa1 fusion protein was first purified by IMAC, followed by factor Xa cleavage and isolation of EGa1-N_3 by size-exclusion chromatography (SEC).

Expression of the MBP-EGa1 fusion protein requires induction by IPTG, expression of the tRNA/aminoacyl-tRNA synthethase pair (constitutively induced and under control of l-arabinose) and the UAA[35]. The contribution of each component was analyzed by western blot (Fig. 2a-c). Constitutive induction of the tRNA/aminoacyl-tRNA synthethase pair was sufficient for expression of the MBP-EGa1 fusion protein. High amounts of l-arabinose (0.1 - 0.5 %) strongly enhanced the protein production, but did not result in incorporation of canonical amino acids (data not shown). Moreover, the protein expression was greatly affected by the concentration of ITPG. Addition of IPTG was required for protein expression and maximal production was achieved at 1 mM IPTG. Interestingly, addition of more IPTG (in this case 5 mM) was counterproductive and reduced the protein production to 19.3 % compared with the standard conditions. The production of MBP-EGa1 fusion protein was also dependent on the concentration of pAzF. Although most protein was produced at the highest concentration, the most optimal condition (based on protein expression vs mM UAA) was at 1 mM pAzF. More importantly, production of the full length protein in the absence of pAzF was only 3.4 %. The incorporation of pAzF therefore occurs with high fidelity >96 % and was in agreement with previously reported studies[16].

In order to obtain the final EGa1-N_3, the fusion protein was first purified from the cell lysate by IMAC, after which the protein was cleaved by factor Xa (Fig. 2d). Based on separation by SDS-PAGE gel, the overnight incubation with factor Xa was not sufficient to fully process the fusion protein and prevented isolation of EGa1-N_3 by a second IMAC purification. Instead, the EGa1-N_3 (17.2 kDa) was separated from the MBP-EGa1 fusion protein (59.6 kDa) and cleaved

MBP (42.5 kDa) by size-exclusion chromatography (SEC, Fig. 2e). The purified EGa1-N_3 nanobody was obtained in 0.5 – 1.0 mg / liter culture.

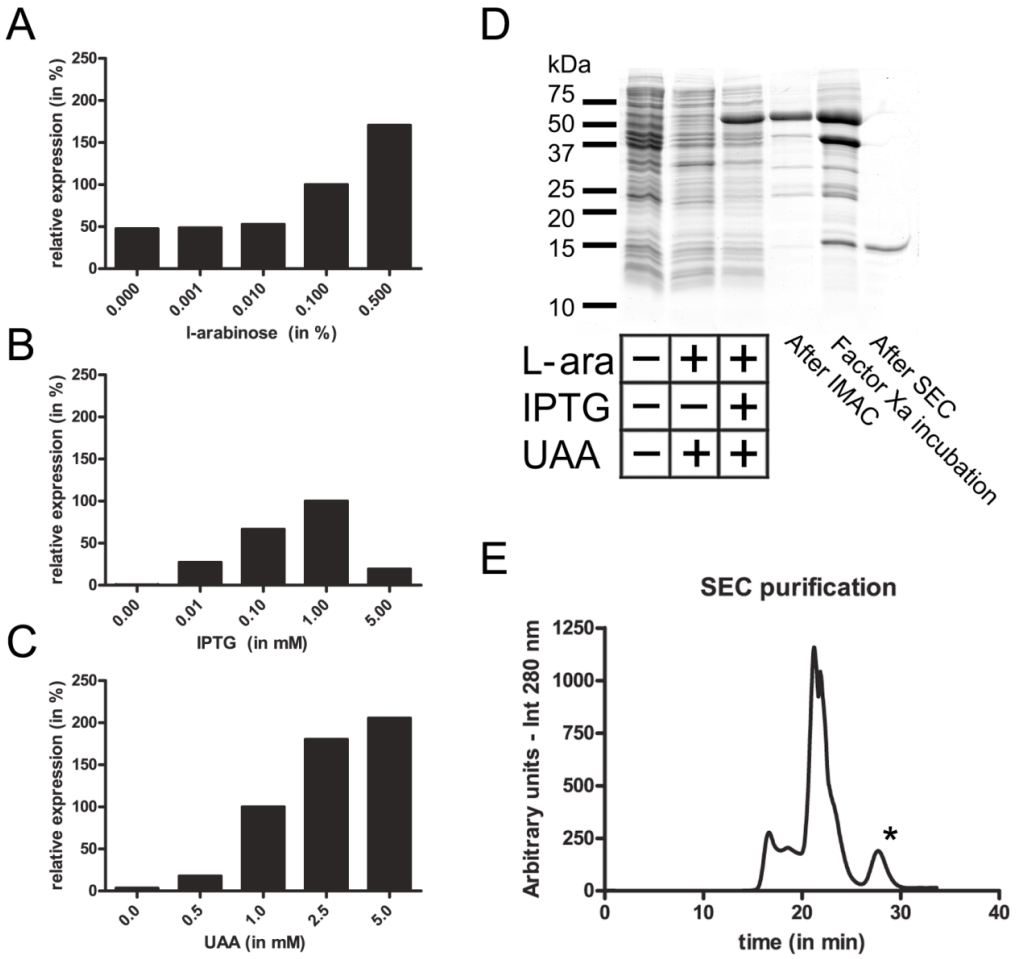

Figure 2. Incorporation of pAzF into the MBP-EGa1 fusion protein was analyzed. The contribution of l-arabinose (A), IPTG (B) and pAzF (C) were evaluated in order to obtain optimal induction conditions. The expression of fusion protein was induced under standard conditions (0.1 % l-arabinose (m/v), 1 mM IPTG and 1 mM pAzF) and set to 100 %. Expression was induced for 4 hrs and optimized separately for the different components, while the others remained constant at the standard conditions. Cell lysates were separated using a reducing 15 % SDS-PAGE gel, blotted onto nitrocellulose membranes and the MBP-EGa1 fusion protein was detected by an anti-HIS_6 monoclonal antibody. (D) The optimized conditions were employed to produce MBP-EGa1 fusion protein. Isolation of EGa1-N_3 from the MBP-EGa1 fusion protein (purification by IMAC, followed by overnight incubated at RT with factor Xa and isolation using a PBS equilibrated Superdex 75 10/300 GL column) was analyzed by non-reducing 15 % SDS-PAGE gel (E). The corresponding SEC profile during purification of EGa1-N_3(*) using an ÄKTA Prime, Superdex 75 10/300 GL column and detector at 280 nm.

3.3 Nanobody labeling via click chemistry

In order to demonstrate the incorporation of pAzF in EGa1-N_3, copper-catalyzed azide alkyne cycloaddition (CuAAC) with a TAMRA-Alkyne dye was employed (Fig. 3a). The click reaction was initiated by addition of the reducing agents (TCEP, Cu-wire or sodium ascorbate) and analyzed by separation on SDS-PAGE gel. Based on the fluorescent signal at approximately 15 kDa, 5 % sodium ascorbate yielded the highest EGa1 labeling, while addition of Laemmli buffer without reducing agent (to denaturate the protein) completely abolished the reaction under all conditions.

Alternatively, *p*-propargyloxyphenylalanine (pPrF) was incorporated into EGa1 (EGa1-CCH) to perform the CuAAC with N_3-Alexa 488 (Fig. 3b). Lower expression levels of EGa1-CCH

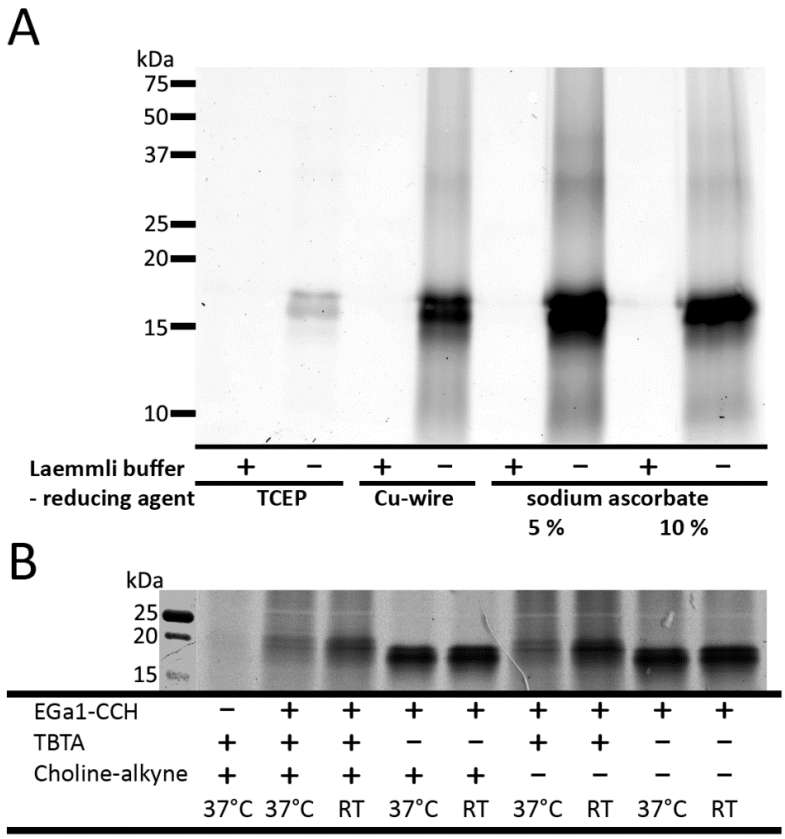

Figure 3. Evaluation of copper-catalyzed azide alkyne cycloaddition (CuAAC) for nanobody labeling. (A) The conjugation of TAMRA-Alkyne to EGa1-N_3 was performed in 400 mM phosphate buffer pH 8.0, 0.4 mM TBTA and 1 mM $CuSO_4$, initiated by addition of 2 mM TCEP, ~6 mg copper wire, 5 or 10 mM sodium ascorbate and incubated for 4 hrs at 37 °C. Click reactions were also performed in 1x Laemmli sample buffer without reducing agent to denature the protein and provide more access to the azido group. (B) The conjugation of N_3-Alexa 488 to EGa1-CHH was performed in 100 mM phosphate buffer pH 8.0 and 1 mM $CuSO_4$, with and without 0.4 mM TBTA. The reaction was initiated by the addition 2 mM sodium ascorbate, incubated for 4 hrs at 37 °C and stopped by addition of choline-alkyne. The protein samples were separated onto SDS-PAGE gels and visualized by a Typhoon 9400 fluorescence imager.

compared with EGa1-N_3 were generally achieved and was in agreement with previous reported observations[35]. Click reactions without TBTA were more efficient than reactions in the presence of the Cu(I) stabilizing ligand. Interestingly, higher conversion was observed in reactions at RT compared with CuAAC at 37 °C, while no fluorescent signal was detected in the absence of nanobody. Excess of choline-alkyne was added to stop the click reaction to EGa1-CCH but this also reduced smearing on SDS-PAGE gel.

Despite the conjugation of fluorescent dyes to EGa1, protein precipitation and/or aggregation was consistently observed after initiation of both click reactions and resulted in a smear on SDS-PAGE gel. Although additives including aminoguanidine have been described to function as scavenger to prevent these side reactions[37], copper-free click reaction via strain-promoted alkyne-azide cycloaddition (SPAAC) has also been reported[38]. In contrast to CuAAC, SPAAC requires no reducing agent and Cu(I), is compatible with biological systems and was therefore evaluated as alternative for EGa1-N_3 labeling.

SPAAC modification of EGa1-N_3 with DBCO-GPLGLAGGEALEALS was analyzed using protein migration on non-reducing SDS-PAGE gel (Fig. 4a). The unmodified EGa1-N_3 which has a molecular weight of 17.2 kDa, migrated at approximately 16 kDa. Conjugation of EGa1-N_3 to DBCO-GPLGLAGGEALEALS resulted in a shift towards higher molecular weight (approx. 18 kDa) and corresponds to the attachment of one peptide (1.9 kDa). In contrast, no shift on SDS-PAGE gel was observed when the click reaction was performed with an excess of sodium azide to compete with the protein[39]. EGa1-N_3 was furthermore labeled with IRDye 800CW, by first conjugation to DBCO-PEG_4-DBCO followed by conjugation to N_3-IRDye 800CW (Fig. 4b). In this case, a shift and strong fluorescent signal were detected. Addition of sodium azide again prohibited the click reaction, thereby indicating the selectivity of the click reaction. Based on protein shift on SDS-PAG gel, 70.7 % of EGa1-N_3 was modified with the peptide.

In addition to this, liposomes were decorated with EGa1-N_3 to analyze the functionality of the nanobody after SPAAC. Towards this end, rhodamine-labeled liposomes equipped with a cyclooctyne functionalized lipid were labeled with EGa1-N_3 after which the non-bound nanobodies were removed. Binding of the targeted-liposomes to MDA-MB-468 cells was subsequently analyzed by fluorescence-activated cell sorting (FACS, Fig. 4c). A concentration-dependent fluorescent signal was observed for the targeted-liposomes, indicating binding to the EGFR positive cells. In contrast, rhodamine-labeled liposomes bearing the cyclooctyne functionalized lipid but lacking EGa1-N_3 displayed no fluorescent signal and were thus not bound to MDA-MB-468 cells. These results demonstrated the functionality of EGa1-N_3 as well as the biocompatibility of the cyclooctyne, since no interaction with cells was observed.

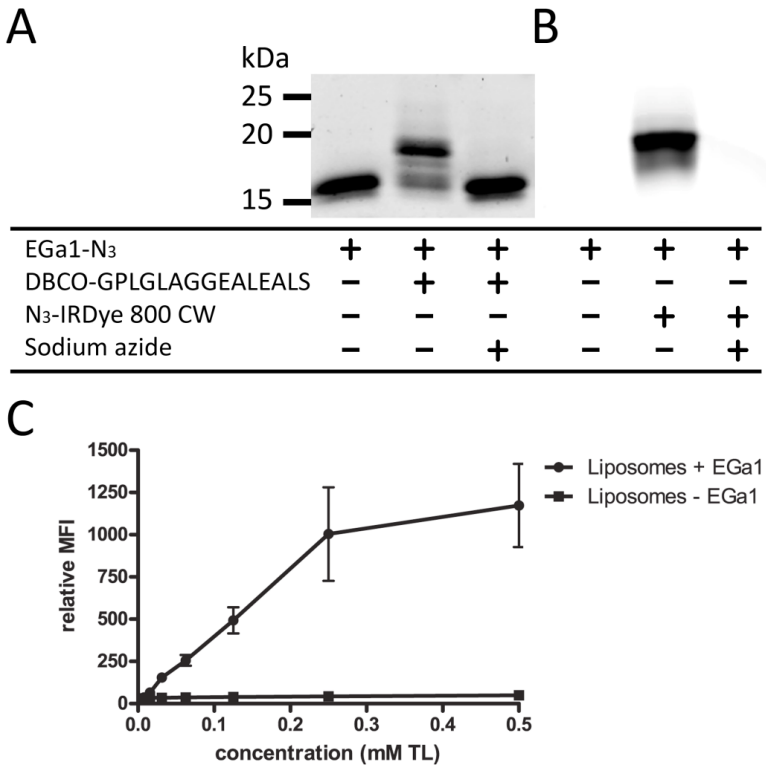

Figure 4. Labeling of EGa1-N_3 with biomolecules via strain-promoted alkyne-azide cycloaddition (SPAAC). (A) The coupling of EGa1-N_3 to the DBCO-GPLGLAGGEALEALS peptide was analyzed by non-reducing SDS-PAGE gel. EGa1-N_3 was incubated with 10 equivalents of the peptide for 16 hrs at RT in the absence or presence of sodium azide. (B) EGa1-N_3 was also labeled with IRDye 800 CW. Towards this end, EGa1-N_3 was first incubated with 10 equivalents DBCO-PEG_4-DBCO (mol/mol) for 16 hrs at RT, followed by addition of N_3-IRDye 800 CW (in a 1:2 ratio of DBCO-PEG_4-DBCO to N_3-IRDye 800 CW, mol/mol) in the absence or presence of sodium azide and incubated for 24 hrs at RT. The protein samples were analyzed by reducing SDS-PAGE gel followed by detection using the Odyssey (LI-COR Biosciences). (C) Rhodamine-labeled liposomes bearing the cyclooctyne functionalized lipid were decorated with EGa1-N_3 by incubation over weekend for 64h at RT. The functionality of EGa1-N_3 after SPAAC conjugation to the liposomal surface was assayed by incubation with MDA-MB-468 cells followed by FACS analysis. Data from two experiments are presented as mean ± SEM (n=6).

3.4 Nanobody multimerization through biotin-streptavidin conjugates

Multimerization of ligands and antibody (fragments) has been widely adopted to improve avidity and subsequently increase binding affinities. One of the natural scaffolds which is ideally suitable for this multimerization is streptavidin and binds four biotin molecules with high affinity (Kd < 10^{-14} mol/L). Towards this end, EGa1-N_3 was modified with sulfo-DBCO-biotin followed by binding to streptavidin (Fig. 5). To assess this multimerization, streptavidin

was incubated with increasing concentrations of EGa1-biotin and analyzed by non-reducing SDS-PAGE gel (Fig. 5a). The band corresponding to streptavidin without EGa1-biotin was completely gone at a streptavidin to nanobody ratio of 1:10 (lane 4). Interestingly, addition of more EGa1-biotin (lane 5, 1:40) did not change the migration of the EGa1-biotin-streptavidin conjugates and thus the 1:10 ratio was sufficient for full conversion.

Since more than the theoretical ratio of 1:4 (lane 3) was required for a complete shift on gel, EGa1-biotin was incubated with increasing concentrations of streptavidin to analyze the sulfo-DBCO-biotin modification (Fig. 5b). The disappearance of the EGa1-biotin by interaction with streptavidin was maximal at a ratio of 1:1 (lane 4) while slightly stronger signals were detected at ratios of 1:4 (lane 2) and 1:2 (lane 3). Based on densitometric analysis of the protein signals, the modification of EGa1-N_3 with sulfo-DBCO-biotin was 74.8%. Although this value was comparable to modification by DBCO-GPLGLAGGEALEALS, the incorporation of pAzF was, at a level of <96 %, much higher and the conversion might therefore be improved by longer reaction times and protection from (UV-) light (e.g. during ÄKTA purification).

The formation of EGa1-biotin-streptavidin conjugates was also analyzed by SEC (Fig. 5c). Separation of EGa1-biotin and streptavidin incubated with biotin (biotin-streptavidin) were shown in black and red, respectively. The EGa1-biotin-streptavidin conjugates (after incubation at a streptavidin to nanobody ratio of 1:10) were presented in blue and demonstrated a peak shift towards shorter retention time and thus larger size compared with biotin-streptavidin. In addition, an increase in absorption at 280 nm was observed and can be attributed to the combined absorption of the nanobody and streptavidin. The multimerization of EGa1 using streptavidin as scaffold was therefore straightforward and was purified by SEC.

The EGa1-biotin-streptavidin complex was subsequently evaluated for its ability to inhibit cell proliferation. Towards this end, A431 cells overexpressing EGFR were incubated for 48 hrs with the EGa1-biotin-streptavidin conjugate, EGa1-biotin or streptavidin, after which the relative cell viability was assayed using Alamar Blue (Fig. 5d). To compensate for the four nanobodies per EGa1-biotin-streptavidin conjugate, the actual concentration of EGa1-biotin was 4x higher than presented in the graph. The EGa1-biotin-streptavidin complex inhibited cell proliferation for 22 % while no inhibition was observed after treatment with EGa1-biotin or streptavidin. Interestingly, this maximal inhibition was already achieved at a concentration of 3 nM. In contrast, EGa1 decorated liposomes were previously demonstrated to effectively downregulate EGFR and inhibit cell proliferation in 14C cells in a dose-dependent manner[29]. Whether the limited inhibition of A431 cells by the EGa1-biotin-streptavidin conjugate is the result of differences between cell lines (e.g. higher EGFR expression compared with 14C cells) or fewer nanobodies per particle (4 versus 30) remains unclear.

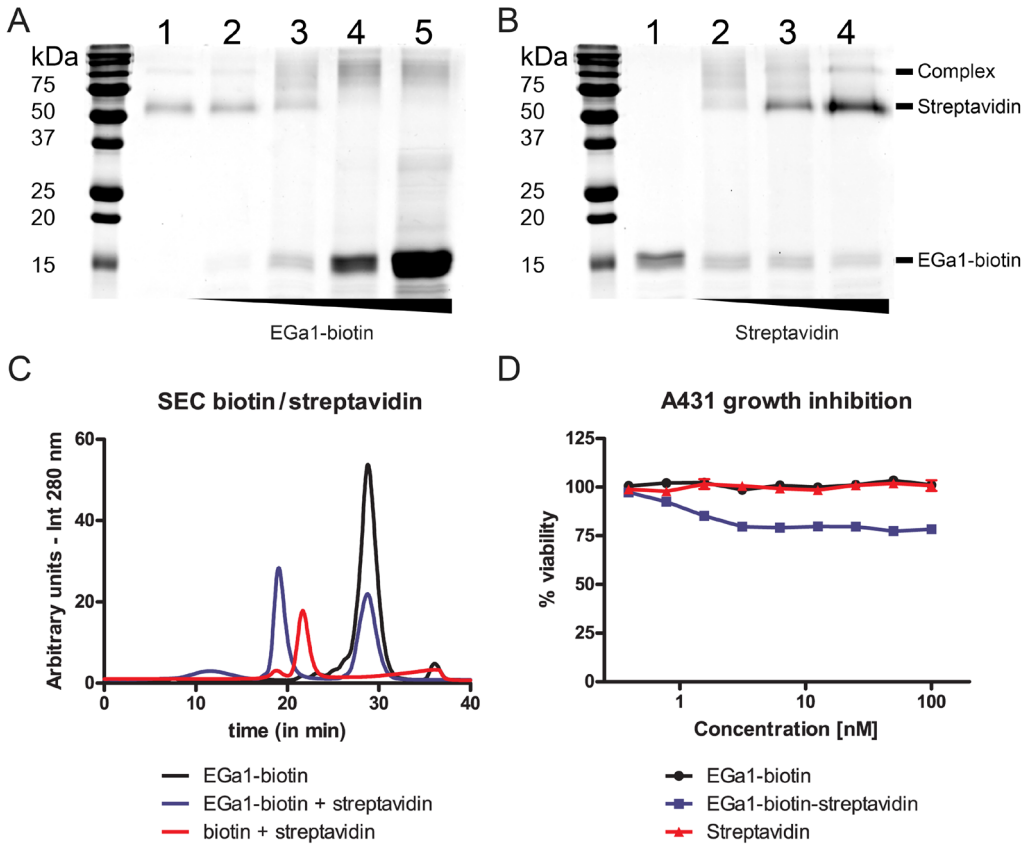

Figure 5. Nanobody multimerization through biotin-streptavidin conjugates. EGa1-N_3 was incubated with 20 equivalents of sulfo-DBCO-biotin for 16 hrs at RT, after which EGa1-biotin was purified by SEC. (A) Incubation of streptavidin with increasing concentrations of EGa1-biotin for 30 min at RT were separated by non-reducing SDS-PAGE gel and detected using the Odyssey (noise reduction from Image Studio 3.1 was applied to improve visualization). Streptavidin to EGa1-biotin ratios employed were 1:1, 1:4, 1:10 and 1:40 (mol/mol) for lanes 2 to 5 respectively while lane 1 contained only streptavidin. (B) In a similar experiment, the incubation of EGa1-biotin with increasing concentrations of streptavidin for 30 min at RT was analyzed. Streptavidin to EGa1-biotin ratios employed were 1:4, 1:2, and 1:1 (mol/mol) for lanes 2 to 4 respectively while lane 1 contained only EGa1-biotin. (C) SEC analysis of EGa1-biotin (black), biotin-streptavidin (red) and EGa1-biotin-streptavidin (blue) using an ÄKTA Prime, Superdex 75 10/300 GL column and detector at 280 nm. Note: comparable molar quantities were only injected for biotin-streptavidin and EGa1-biotin-streptavidin. (D) Growth inhibition of A431 cells by streptavidin (red), SEC purified EGa1-biotin (black) and EGa1-biotin-streptavidin (blue). Cells were incubated for 48 hrs after which the cell viability was assayed using Alamar Blue. To compensate for the four nanobodies per EGa1-biotin-streptavidin conjugate, the actual concentration of EGa1-biotin was 4x higher. Data from two experiments are presented as mean ± SEM (n=4).

5. Conclusion

In conclusion, several constructs were evaluated for the incorporation of unnatural amino acids in nanobodies. Of these, the MBP-EGa1 fusion protein was expressed at high levels, which was further optimized for the incorporation of pAzF. SEC purified EGa1-N_3 was conjugated to fluorophores and a peptide to demonstrate the reactivity of the azide group. In addition, liposomes decorated on the surface with EGa1-N_3 were bound to MDA-MB-468 cells, indicating the functionality of the EGa1-N_3 nanobody. Multimerization of the EGa1 nanobody was demonstrated by formation of nanobody-biotin-streptavidin conjugates and demonstrates the potential of site-specific functionalization of nanobodies. Moreover, this study reports for the first time the incorporation of unnatural amino acids in nanobodies and opens up new possibilities for their therapeutic applications.

Acknowledgements

This work was funded by the Focus & Massa project of the Utrecht University, the Netherlands.

References

1. Walsh, C. T., Garneau-Tsodikova, S. & Gatto, G. J. Protein Posttranslational Modifications: The Chemistry of Proteome Diversifications. *Angew. Chemie Int. Ed.* **44,** 7342–7372 (2005).
2. Van Vught, R., Pieters, R. J. & Breukink, E. Site-specific functionalization of proteins and their applications to therapeutic antibodies. *Comput. Struct. Biotechnol. J.* **9,** e201402001 (2014).
3. COHEN, G. N. & MUNIER, R. [Incorporation of structural analogues of amino acids in bacterial proteins]. *Biochim. Biophys. Acta* **21,** 592–3 (1956).
4. Hendrickson, W. A., Horton, J. R. & LeMaster, D. M. Selenomethionyl proteins produced for analysis by multiwavelength anomalous diffraction (MAD): a vehicle for direct determination of three-dimensional structure. *EMBO J.* **9,** 1665–1672 (1990).
5. Yang, W., Hendrickson, W. A., Crouch, R. J. & Satow, Y. Structure of ribonuclease H phased at 2 A resolution by MAD analysis of the selenomethionyl protein. *Science* **249,** 1398–1405 (1990).
6. McIntosh, L. P. & Dahlquist, F. W. Biosynthetic incorporation of nitrogen-15 and carbon-13 for assignment and interpretation of nuclear magnetic resonance spectra of proteins. *Q. Rev. Biophys.* **23,** 1–38 (1990).
7. Van Hest, J. C. & Tirrell, D. A. Efficient introduction of alkene functionality into proteins in vivo. *FEBS Lett.* **428,** 68–70 (1998).
8. Lang, K. & Chin, J. W. Cellular incorporation of unnatural amino acids and bioorthogonal labeling of proteins. *Chem. Rev.* **114,** 4764–806 (2014).
9. Chin, J. W. Expanding and reprogramming the genetic code of cells and animals. *Annu. Rev. Biochem.* **83,** 379–408 (2014).
10. Bain, J. D., Diala, E. S., Glabe, C. G., Dix, T. A. & Chamberlin, A. R. Biosynthetic site-specific incorporation of a non-natural amino acid into a polypeptide. *J. Am. Chem. Soc.* **111,** 8013–8014 (1989).
11. Noren, C. J., Anthony-Cahill, S. J., Griffith, M. C. & Schultz, P. G. A general method for site-specific incorporation of unnatural amino acids into proteins. *Science* **244,** 182–8 (1989).
12. Hohsaka, T., Ashizuka, Y., Taira, H., Murakami, H. & Sisido, M. Incorporation of nonnatural amino acids into proteins by using various four-base codons in an Escherichia coli in vitro translation system. *Biochemistry* **40,** 11060–4 (2001).
13. Hohsaka, T., Ashizuka, Y., Murakami, H. & Sisido, M. Five-base codons for incorporation of nonnatural amino acids into proteins. *Nucleic Acids Res.* **29,** 3646–51 (2001).
14. Wang, L. & Schultz, P. G. A general approach for the generation of orthogonal tRNAs. *Chem. Biol.* **8,** 883–90 (2001).
15. Liu, C. C. & Schultz, P. G. Adding New Chemistries to the Genetic Code. *Annu. Rev. Biochem.* **79,** 413–444 (2010).
16. Wang, L., Xie, J. & Schultz, P. G. Expanding the genetic code. *Annu. Rev. Biophys. Biomol. Struct.* **35,** 225–249 (2006).
17. Liu, C. C. *et al.* Protein evolution with an expanded genetic code. *Proc. Natl. Acad. Sci. U. S. A.* **105,** 17688–93 (2008).
18. Axup, J. Y. *et al.* Synthesis of site-specific antibody-drug conjugates using unnatural amino acids. *Proc. Natl. Acad. Sci.* **109,** 16101–16106 (2012).
19. Kim, C. H. *et al.* Synthesis of bispecific antibodies using genetically encoded unnatural amino acids. *J. Am. Chem. Soc.* **134,** 9918–9921 (2012).
20. Kazane, S. A. *et al.* Self-assembled antibody multimers through peptide nucleic acid conjugation. *J. Am. Chem. Soc.* **135,** 340–346 (2013).
21. Muyldermans, S. Nanobodies: natural single-domain antibodies. *Annu. Rev. Biochem.* **82,** 775–97 (2013).
22. Hamers-Casterman, C. *et al.* Naturally occurring antibodies devoid of light chains. *Nature* **363,** 446–8 (1993).
23. Muyldermans, S., Atarhouch, T., Saldanha, J., Barbosa, J. A. & Hamers, R. Sequence and structure of VH domain from naturally occurring camel heavy chain immunoglobulins lacking light chains. *Protein Eng.* **7,** 1129–35 (1994).
24. Huang, L., Muyldermans, S. & Saerens, D. Nanobodies®: proficient tools in diagnostics. *Expert Rev. Mol. Diagn.* **10,** 777–85 (2010).

25. Devoogdt, N. *et al.* Molecular imaging using Nanobodies: a case study. *Methods Mol. Biol.* **911,** 559–67 (2012).
26. Oliveira, S. *et al.* Rapid visualization of human tumor xenografts through optical imaging with a near-infrared fluorescent anti-epidermal growth factor receptor nanobody. *Mol. Imaging* **11,** 33–46 (2012).
27. Kijanka, M. *et al.* Rapid optical imaging of human breast tumour xenografts using anti-HER2 VHHs site-directly conjugated to IRDye 800CW for image-guided surgery. *Eur. J. Nucl. Med. Mol. Imaging* **40,** 1718–1729 (2013).
28. Debets, M. F. *et al.* Nanobody-functionalized polymersomes for tumor-vessel targeting. *Macromol. Biosci.* **13,** 938–45 (2013).
29. Oliveira, S. *et al.* Downregulation of EGFR by a novel multivalent nanobody-liposome platform. *J. Control. Release* **145,** 165–75 (2010).
30. Van der Meel, R. *et al.* Inhibition of tumor growth by targeted anti-EGFR/IGF-1R nanobullets depends on efficient blocking of cell survival pathways. *Mol. Pharm.* **10,** 3717–27 (2013).
31. Altintas, I. *et al.* Nanobody-albumin nanoparticles (NANAPs) for the delivery of a multikinase inhibitor 17864 to EGFR overexpressing tumor cells. *J. Control. Release* **165,** 110–8 (2013).
32. Talelli, M. *et al.* Nanobody-shell functionalized thermosensitive core-crosslinked polymeric micelles for active drug targeting. *J. Control. Release* **151,** 183–92 (2011).
33. Roovers, R. C. *et al.* Efficient inhibition of EGFR signaling and of tumour growth by antagonistic anti-EFGR Nanobodies. *Cancer Immunol. Immunother.* **56,** 303–317 (2007).
34. Rouser, G., Fleischer, S. & Yamamoto, A. Two dimensional thin layer chromatographic separation of polar lipids and determination of phospholipids by phosphorus analysis of spots. *Lipids* **5,** 494–496 (1970).
35. Young, T. S., Ahmad, I., Yin, J. A. & Schultz, P. G. An enhanced system for unnatural amino acid mutagenesis in E. coli. *J. Mol. Biol.* **395,** 361–74 (2010).
36. Kapust, R. B. & Waugh, D. S. Escherichia coli maltose-binding protein is uncommonly effective at promoting the solubility of polypeptides to which it is fused. *Protein Sci.* **8,** 1668–74 (1999).
37. Hong, V., Presolski, S. I., Ma, C. & Finn, M. G. Analysis and optimization of copper-catalyzed azide-alkyne cycloaddition for bioconjugation. *Angew. Chem. Int. Ed. Engl.* **48,** 9879–83 (2009).
38. Baskin, J. M. *et al.* Copper-free click chemistry for dynamic in vivo imaging. *Proc. Natl. Acad. Sci. U. S. A.* **104,** 16793–7 (2007).
39. Wang, L., Dai, C., Chen, W., Wang, S. L. & Wang, B. Facile derivatization of azide ions using click chemistry for their sensitive detection with LC-MS. *Chem. Commun. (Camb).* **47,** 10377–10379 (2011).

Chapter 7

Selective targeting of EGFRvIII-positive glioblastomas by a nanobody-based immunotoxin

Remko van Vught, Nik Sol, Rachid el Khoulati, Tonny Lagerweij, Rob Roovers, Eefjan Breukink, Roland Pieters, Tom Wurdinger, Paul van Bergen en Henegouwen

Abstract

Glioblastoma multiforme (GBM) is the most common primary brain tumor and associated with poor prognosis. Besides overexpression of the epidermal growth factor receptor (EGFR), also a truncated variant, EGFRvIII, is often found in GBM. The constitutively active EGFRvIII is tumor specific and therefore an ideal target for antibody therapy. Monoclonal antibody therapies are currently under evaluation (e.g. mAb806) however, these often lack efficient tumor penetration. In an attempt to overcome this limitation, we explored the genetic fusion of a nanobody with exotoxin A of *Pseudomonas aeruginosa* (PE38). Nanobodies, the variable domains of heavy chain only antibodies from camelids, have emerged as potent targeting modalities that can be selected via phage display. We identified one EGFRvIII specific nanobody with 11-fold specificity over wild-type EGFR. The nanobody was further characterized for agonistic and/or downregulating properties after which it was fused to PE38, expressed in *Escherichia coli* and purified from inclusion bodies followed by on-column refolding. *In vitro* validation showed efficient and EGFRvIII specific cell death after immunotoxin treatment. Co-culture experiments furthermore demonstrated the efficacy and selectivity of this immunotoxin.

1. Introduction

One of the most common and aggressive form of brain cancer is glioblastoma multiforme (GBM)[1]. As a result of the high tumorigenicity and the difficult treatment, the one-year life expectancy for newly diagnosed patients is only 18%[2]. GBM is often characterized by the amplification and overexpression of the epidermal growth factor receptor (EGFR) gene[3,4]. Next to this, a genetic rearrangement into the truncated EGFRvIII is commonly found in EGFR-positive glioblastomas[4]. EGFRvIII is the result of an in-frame deletion of 801 base pairs spanning exons 2-7 and therefore it misses a part of the extracellular domains I and II[5]. Despite the loss of ligand binding capacity, EGFRvIII is constitutively phosphorylated, and known to activate several downstream signaling pathways[6–9]. The poor patient prognosis of EGFRvIII-positive glioblastomas and unique genetic rearrangement, which only occurs in tumors, makes EGFRvIII a potential therapeutic target for the treatment of GBM[10].

Treatment of brain diseases is complicated by the inability of drugs to cross the blood-brain barrier[11]. In addition, brain tissue regenerates only minimally and is therefore more susceptible to drug toxicity. Existing anti-EGFR therapies have been evaluated for GBM treatment[12–14]. The molecular difference of EGFRvIII, however, renders ligand blocking monoclonal antibodies and EGFR tyrosine kinase inhibitors ineffective[2]. These disappointing results of conventional anti-EGFR therapies let to the development of new approaches. An EGFRvIII specific monoclonal antibody (mAb806) was raised by vaccination of mice with EGFRVIII positive (and EGFR negative) fibroblasts[15]. Interestingly, mAb806 is able to pass the blood-brain barrier and localizes to *in situ* GBM in patients[16]. In addition, the EGFRvIII specific antibody showed less toxicity and is being evaluated as antibody-drug conjugate (ABT-414)[17]. Another approach is the vaccination of patients with Rindopepiglycine, a peptide mimicking the gene rearrangement of EGFRvIII[18]. This vaccination in combination with chemo-radiation is now in phase 3 clinical study[19].

Despite these recent advances, the urge for good alternatives for the treatment of EGFRvIII-positive glioblastomas still exists. Anti-cancer treatments are increasingly based on monoclonal antibody therapy. Yet, one of their problems is the limited tumor penetration as a result of their size. Application of antibody fragments could improve this therapy without affecting the specificity. Promising antibody fragments for therapeutic application are derived from camelids[20]. These antibodies are indicated as nanobodies (or VHHs), lack their light chain and as a result, epitope binding is completely orchestrated by the CDR domains of the variable region[20,21]. The small VHHs (15 kDa) can be selected by phage display, are highly stable and easily produced[22]. Genetic fusion to an effector domain would allow the efficient delivery of a toxic payload, also known as immunotoxins [23,24].

One of the best described effector domains is PE38, a truncation of the exotoxin A of *Pseudomonas aeruginosa* [23]. PE38 inhibits elongation factor-2 by ADP ribosylation resulting in inactivation of protein synthesis and induction of apoptosis after receptor-mediated endocytosis,

but it is devoid of a targeting domain[25]. Antibody targeting of PE38 has been employed for the treatment of several human cancers[23]. Of these, the anti-CD22 immunotoxin (Moxetumomab pasudotox) is currently in phase III clinical trials[26]. Recently, also an anti-VEGFR2 nanobody-PE38 fusion was created and demonstrated the *in vitro* inhibition of VEGFR2-positve cells[27]. Despite these promising results, the evaluation *in vivo* has not been published yet.

Here we present the *in vitro* validation of a novel PE38 based immunotoxin targeting EGFRvIII. Llamas were immunized with a stably expressing EGFRvIII human astrocytoma U373 cell line (U373-vIII). Subsequent library production and phage display selections yielded specific anti-EGFRvIII VHHs, of which one (34E5) has an 11-fold higher affinity for EGFRvIII than for wild-type EGFR. Characterization of 34E5 indicates no agonistic and downregulation features for both EGFRvIII and wild-type EGFR. *In vitro* evaluation of the 34E5-PE38 immunotoxin demonstrated a dose-dependent toxicity on EGFRvIII-positive cell lines. These data indicate 34E5-PE38 as a promising immunotoxin for the treatment of EGFRvIII positive brain cancer.

2. Materials and Methods.

2.1 Chemicals and reagents

DNAse, lysozyme, imidazole, kanamycin, coomassie brilliant blue r and sodium choride (NaCl) were from Sigma-Aldrich (St. Louis, MO, USA). Isopropyl β-D-1-thiogalactopyranoside (IPTG), fetal bovine serum (FBS) and o-phenylenediamine (OPD) were from Thermo Fisher Scientific (Waltham, MA, USA). Sterile PBS was from Lonza (Basel, Switzerland). Triethylamine HiPerSolv CHROMANORM (triethylamine) was from VWR International (Radnor, PA, USA). Bugbuster, urea and 2-mercaptoethanol (BME) were from Merck KGaA (Darmstadt, Germany).

2.2 Cell lines

The EGFR negative mouse fibroblast cell line NIH 3T3 2.2 (abbreviated 3T3 2.2) was obtained from ATCC (LGC Standards, Germany). The HER14 stably express EGFR and are derived from NIH 3T3 2.2. Stable transfection of the NIH 3T3 2.2 and U373 cell lines with EGFRvIII resulted in 3T3-vIII and U373-vIII, respectively. The U251 and U251-vIII cell lines were a kind gift from Tom Wurdinger (VU University Medical Center, Amsterdam, The Netherlands) All cell lines were cultured in Dulbecco's Modified Eagle's Medium (DMEM; Gibco, Invitrogen, United Kingdom) supplemented with 8 % FBS (v/v) and antibiotics to a final concentration 100 U/mL penicillin, 100 µg/mL streptomycin, and 2 mM L-glutamine (PAA, Germany). The cell lines were cultured at 37 °C in a humidified atmosphere containing 5 % CO_2 and were consistently found to be free of mycoplasma (MycoAlert Mycoplasma Detection Kit, Lonza Benelux BV, Breda, the Netherlands).

2.3 Immunization of llamas and construction of VHH libraries

Llamas were immunized by 7 times subcutaneously administration of U373 cells stably expressing EGFRvIII (U373-vIII) (~10^8 cells). Sera was collected before and after immunization and evaluated for the binding to purified EGFRvIII ectodomain in enzyme-linked immunosorbent assays (ELISA). Four days after he last immunization, peripheral blood lymphocytes (PBLs) were collected from blood and purified by density gradient centrifugation on Ficoll-Paque™ PLUS gradients (GE Healthcare). The total RNA extracted from these cells was transcribed into cDNA (RT-PCR, Life Technologies) and used for the generation of immune libraries as previously described[28].

2.4 Phage display selection and production of anti-EGFRvIII VHH fragments

The EGFRvIII ectodomain was fused with an antibody Fc fragment, produced in HEK cells (U-Protein Express, Utrecht, the Netherlands) and captured onto maxisorp plates via IgG binding to the Fc domain. The library was incubated for 2 hrs, washed twice with 0.05 % Tween-20 (v/v) in PBS and bound phages were eluted using: 1. 100 mM triethylamine; 2. a peptide encoding the transition between domain 1 and 2 (sequence: LEEKKGNYVVTDHGSK) (Isogen Life Sciences, De Meern, the Netherlands); 3. the EGFRvIII specific L8A4 monoclonal antibody. After this first round of selection, a second round was performed on U373 cells expressing the vIII mutant of EGFR, with counter-selection using Her14 cells expressing wt EGFR and specific elution using the above-mentioned peptide. After two rounds of selection, clones were tested for their binding to EGFR-VIII ectodomain in ELISA and whole cell ELISA using Her14 cells and U373-EGFRvIII cells. Eluted VHH genes were transferred to a modified expression vector pET28a, and protein expression was induced in BL21(DE3) bacteria growing the log phase by addition of 0.1 mM IPTG for 4 hrs at 37 °C. All VHHs were collected from the periplasmic fraction and purified using PBS equilibrated talon beads (Clontech Laboratories, Mountain View, CA, USA). The beads were washed three times with 50 column volumes PBS, prior to protein elution by 250 mM imidazole in PBS. VHHs were dialyzed overnight against PBS and stored at -20 °C until further use.

2.5 Characterization of VHHs

Binding assays were performed to determine the Kd of the VHHs for EGFR and EGFRvIII as previously described[29]. MaxiSorp plates (Nunc, Penfield, NY, USA) plates were coated overnight at 4 °C with the ecto-domain of EGFR or EGFRvIII (1 µg/well in PBS). The next day, unbound ecto-domain was removed by washing with PBS followed by blocking with 4 % milk powder in PBS for 1 h at room temperature (RT). Serial dilutions of the VHHs in PBS were shaken for 2 hrs at RT. Plates were washed with PBS, after which the bound VHH was detected with rabbit anti-VHH serum (1:500) and goat anti-rabbit PO (1:5000, Jackson ImmunoResearch, Newmarket, United Kingdom). The conversion of OPD was stopped by addition of 3 M H_2SO_4 and detected by Bio-Rad Ultramark Microplate Imaging System (Bio-Rad Laboratories, Hercules, CA, USA). Data

points of the binding assays were background corrected and plotted in GraphPad Prism 5.02 software to estimate the Kd and Bmax using the one-site binding function.

The phosphorylation assays were performed as previously described[28]. Briefly, ~10^5 cells were seeded and serum-starved overnight in DMEM containing 0.1 % (v/v) FBS. Cells were incubated for 15 min with 500 nM VHH or 8 nM EGF and subsequently washed twice with ice-cold PBS. For the downregulation assays, ~10^5 cells were seeded and incubated for 72 hrs with 500 nM VHH. Lysates were collected by dissolving the cells in laemmli buffer, size-separated on SDS-PAGE and blotted onto PVDF membrane (Bio-Rad). The phosphorylated EGF receptor was detected by a monoclonal anti-EGFR phospho-tyrosine 1068 antibody (Cell Signaling Technology, Danvers, MA, USA). The total EGFR was detected with anti-EGFR (C74B9, Cell Signaling Technology). Tubulin and phosphorylated MAPK were respectively detected by anti-Tubulin (DM1A, Merck Millipore) and anti-phospho-p44/42 MAPK (Erk1/2) (Thr202/Tyr204) (Cell Signaling Technology). IRdye 680 nm and IRdye 800 nm secondairy antibodies (LI-COR Biosciences, Lincoln, NE, USA) were use to detect the primary antibodies using an Odyssey Infrared Imager (LI-COR Biosciences). The downregulation by VHHs was performed in duplo, quantified and plotted in histograms as percentage of EGFR expression of untreated cells.

2.6 Production of VHH-PE38 immunotoxins

The immunotoxins are the direct fusion of the VHHs to PE38. The PE38 gene was a kind gift from Khalid Shah (Massachusetts General Hospital, Harvard Medical School, Boston, MA, USA) and was amplified using 5' end HindIII CATGATAAGCTTATGGGCGGCAGCCTGGC (forward primer) and 3' end NotI CATGATGCGGCCGCCTTCAGGTCCTCGCGCGGC (reverse primer). The VHHs were amplified using 5' end SfiI GTTCCATTCTATGCGGCCCAGCCGGCC (forward primer) and 3' end HindIII TCTTCTGAGATGAGTTTTTGTTCTGCAAGCTTTGAGGA (reverse primer). The amplified PE38 gene and VHH's were cloned into the modified expression vector pET28a using a 3 point ligation (sites: SfiI and NotI), in between the pelB leader sequence and his6-tag. Expression cultures in LB medium were supplemented with 2 % glucose and grown overnight (~16 hrs) till the stationary phase. Prior to induction, the medium was refreshed by pelleting down the cells at 10 000xg for 10 min at 4 °C followed by resuspension in fresh LB. Protein expression was induced by addition of 0.5 mM ITPG for 3 hrs at 37 °C. To isolate inclusion bodies, cells were lysed in 1:50 bugbuster supplemented with lysozyme and DNAse and incubated for 15 min at RT. The pellet was collected by centrifugation at 19 000xg at 4 °C and this step was repeated twice with only Bugbuster. Inclusion bodies were stored up to one month at -20°C before refolding. Pellets were resuspended in 1:100 refolding buffer (20 mM phosphate buffer pH = 8.0, 500 mM NaCl, 8 M urea, 1 mM BME) of their original culture volume, incubated for 1 h at RT and centrifugated at 19 000xg at 4°C to remove the insoluble debris. The immunotoxins were loaded onto a HP HisTrap column (GE Healthcare, Little Chalfont, Buckinghamshire, United Kingdom) and refolded using

a linear gradient of 8 M to 0 M urea over 8 hrs. The protein was eluted in 250 mM Imidazole in PBS, concentrated and loaded onto a Superdex 200 10/300 GL column (GE Healthcare). The purified protein was stored at 4°C until further use.

2.7 Cell proliferation assay

For the proliferation assay, 1000 cells per well were seeded in a 96-wells plate (Microwell, Nunc). The next day, serial dilution of the immunotoxins were added and incubated for 1.5 hrs at 37 °C. After the incubation, cells were washed once with DMEM and incubated for 3 days at 37 °C. The cell proliferation was assayed with the Alamar Blue reagent according to the manufacturer's protocol (Life Technologies, Thermo Fisher Scientific). Briefly, the medium was replaced with phenol red-lacking but otherwise fully supplemented DMEM with 1:10 (v/v) Alamar Blue and incubated for 3 hrs. The fluorescent signal was measured with a FluoStar Optima fluorescent plate reader (BMG Labtech GmbH, Ortenberg, Germany). Cell viability was background corrected by assaying in empty wells, calculated in percentage (%) relative to untreated cells and plotted using the GraphPad Prism 5.02 software.

2.8 Co-culture experiments

A 1:1 mixture consisting of Hela and U251 or U251-vIII cells (150.000 cells per well per cell line) was seeded in 6-well plates. The next day, co-cultures were incubated with the immunotoxins for 2 hrs at 37 °C, washed once with DMEM and incubated with DMEM for 3 days at 37 °C. The growth inhibition was visualized by a reduction in fluorescent signal after 3 days using an EVOS cell imaging system (Life Technologies).

3. Results

3.1 Stable cell lines and selections

Cell lines derived from glioblastoma's are known to lose EGFRvIII expression when cultured *in vitro*[30]. In order to raise specific nanobodies, the cell lines U373 (EGFR positive) and 3T3 2.2 (EGFR negative) were stably transfected with EGFRvIII. Western blot analysis demonstrated the expression of both wild-type (wt) and truncated EGFR in U373-vIII, while only wt EGFR and EGFRvIII were detected for HER14 and 3T3-vIII, respectively (Fig. 1a). The expression of truncated EGFR was furthermore confirmed by the specific anti-EGFRvIII antibody L8A4 (Fig. 1a). After several immunizations with the U373-vIII cell line, sera of immunized animals were tested for the induction of a humoral immune response by whole cell ELISA (data not shown).

Phage display selection was employed to select for EGFRvIII specific VHH's. Phages from the immune library were bound to purified EGFRvIII ectodomain and eluted with either 100mM triethylamine, a competitive peptide (LEEKKGNYVVTDH) or the EGFRvIII specific L8A4

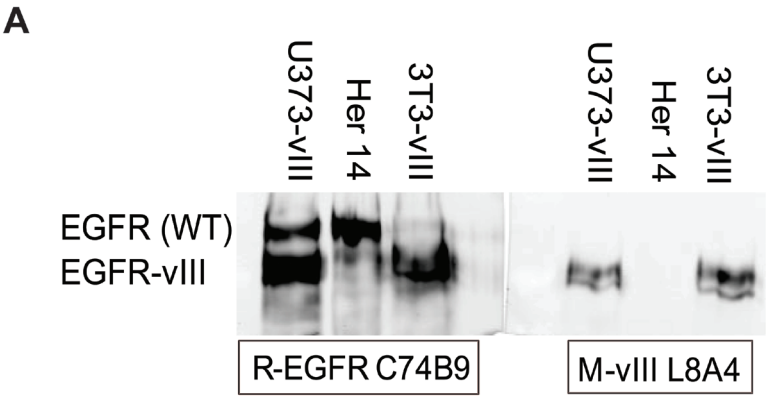

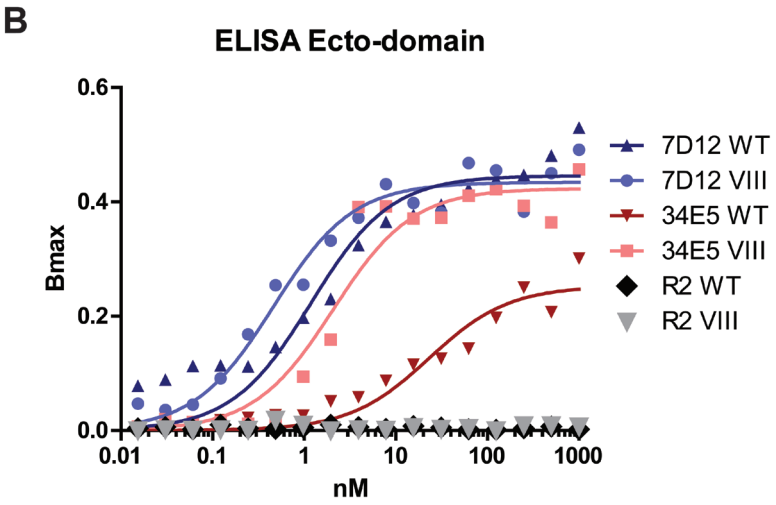

C

	EGFRvIII	wt EGFR
7D12	0.46 nM	1.19 nM
34E5	2.08 nM	23.14 nM
R2	NA	NA

Figure 1. Characterization of the stable cell lines and nanobodies. (A) Wild-type EGFR and EGFRvIII expression levels in the U373-vIII, Her 14 and 3T3-vIII cell lines. Bindingstudy of nanobodies 7D12, 34E5 and R2 towards the ecto-domains of wt EGFR and EGFRvIII (B) and their calculated affinities (C).

monoclonal antibody. In the next step, phages were bound to U373-vIII cells, counter-selected using wt U373 and specifically eluted using the above-mentioned peptide. Obtained clones were evaluated for their binding to EGFR and EGFRvIII, and resulted in the selection of one EGFRvIII

specific VHH with best binding properties (34E5).

The affinity of 34E5 against EGFR and EGFRvIII was determined in a binding study (Fig. 1b & 1c). As controls, R2 recognizing copper-containing azo-dye RR6[29] and 7D12 recognizing extracellular domain III of EGFR[28] were employed. Similar affinities against EGFR and EGFRvIII were observed for the positive control 7D12. This was expected since both ectodomains have the intact extracellular domain III. In contrast, affinities of 23.14 nM and 2.08 nM were observed for 34E5 against EGFR and EGFRvIII, respectively. The difference in affinity demonstrates an 11-fold specificity of 34E5 towards EGFRvIII. R2 displayed no affinity for EGFR.

3.2 Characterization of anti-EGFRvIII VHHs

The anti-EGFRvIII VHHs were further analyzed for their agonistic and downregulating properties. Phosphorylation of EGFR activates downstream signaling and proliferation pathways and is thus undesired. As a positive control, the above listed cell lines were stimulated with EGF. The natural ligand activates wt EGFR and the downstream MAPK pathway in the Her14 and U373-vIII cell lines (Fig. 2a). EGFRvIII is constitutively active explaining the high MAPkinase activity in the 3T3-vIII cell line[31]. Only a minor fraction of EGFRvIII was additionally activated in U373-vIII cells upon EGF stimulation, especially when comparing the actual expression levels of both receptors (Fig. 1a). Addition of the nanobodies 7D12 and 34E5 did not activate wt EGFR nor EGFRvIII or downstream signaling.

Another typical result of receptor activation is receptor internalization and degradation in lysosomes, a process indicated as receptor downregulation. In agreement with the absence of receptor activation, the monovalent nanobodies 7D12 and 34E5 have a minor effect on downregulation of wt EGFR or EGFRvIII (Fig. 2b). Quantification of the EGFR signals identified only 12 % and 15 % downregulation of EGFRvIII by 34E5 for 3T3-vIII and U373-vIII, respectively (Fig 2c).

3.3 Production of nanobody-based immunotoxins

After characterization of 7D12 and 34E5, we genetically fused the nanobodies to truncated Pseudomonas exotoxin A (PE38). The expression and refolding of PE38 based immunotoxins has previously been established[32]. The nanobody-based immunotoxins were expressed in inclusion bodies, purified after solubilization in 8 M urea using IMAC and on-column refolded. Subsequent separation by size exclusion chromatography (SEC) and detection with UV-215 nm resulted in multiple peaks (Fig. 3a) that were analyzed by SDS-PAGE (Fig. 3b). The largest population (fraction 1) predominantly consisted of soluble aggregates and was eluted at the void volume of the column. The active immunotoxin was recovered in fraction 3 and contained only minor contaminations. In addition, these impurities were found to be consistent for all produced immunotoxins (Fig. 3c).

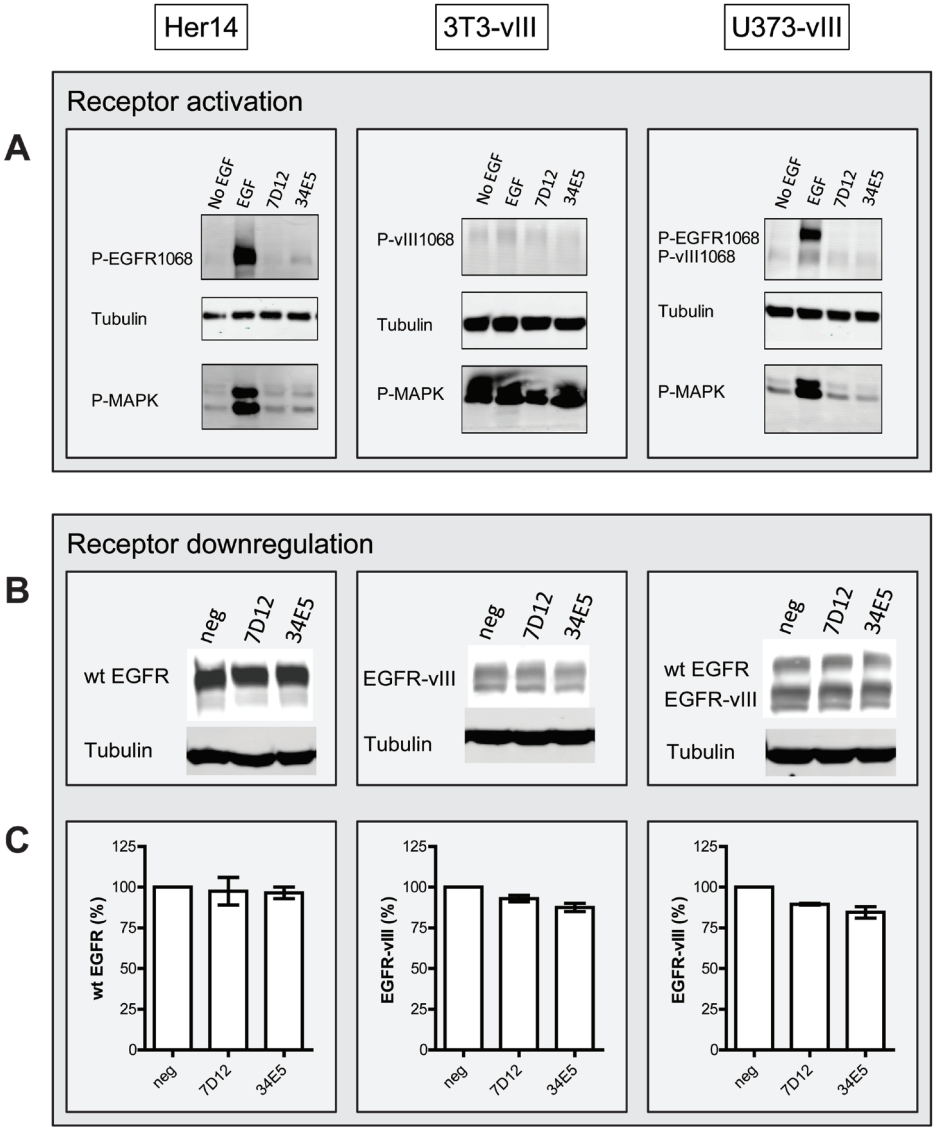

Figure 2. Characterization of nanobodies 7D12 and 34E5 for their agonistic and downregulating properties. Her14, 3T3-vIII and U373-vIII cells were serum starved overnight and exposed to 8 nM EGF or 500 nM nanobody for 15 min (A) or exposed to 8 nM EGF or 500 nM nanobody for 72 hrs (B). Phosphorylated EGFR and MAPK, EGFR/EGFRvIII, and α-tubulin were detected by western blotting. (C) Quantification of the total EGFR/EGFRvIII expression levels. Data from two experiments are presented as mean ± SEM (n=2).

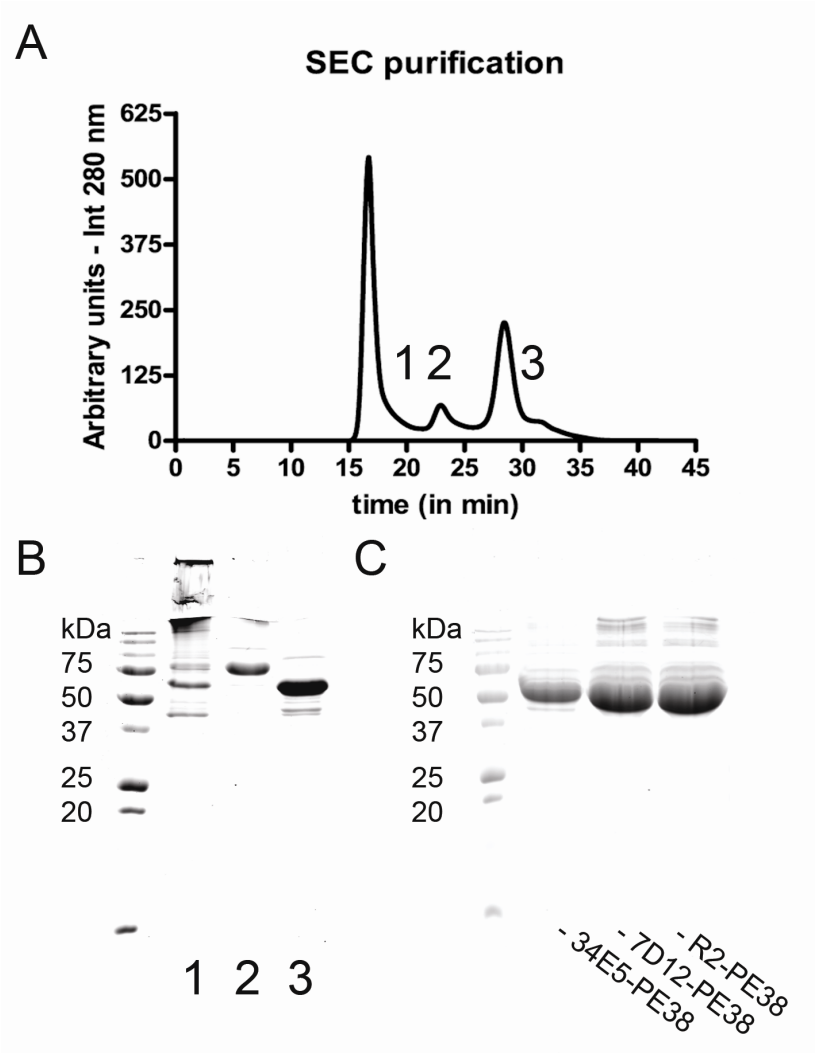

Figure 3. The production of nanobody-based immunotoxins. (A) On-column refolding of the immutoxins resulted in three major populations based on separation by Superdex 200, and absorbtion at 280 nm (blue) and conductivity (red) by ÄKTAprime. (B) Samples were boiled in non-reducing llaemli buffer and analyzed by SDS-PAGE gel. (C) Comparison of the different nanobody-based immunotoxin after on-column refolding and purification by Superdex 200.

3.4 In vitro toxicity

A panel of EGFRvIII positive and negative tumor cell lines were employed to determine whether the nanobody-based immunotoxins could effectively inhibit tumor cell proliferation. In this assay, the cells were exposed to the immunotoxins for 1.5 hrs and after 3 days the relative growth was quantified by the cell viability reagent Alamar Blue (Fig 4). The non-specific R2-PE38 fusion served as negative control and demonstrated no toxicity for all cell lines. In

contrast, dose-dependent reduction of cell growth was observed for 7D12-PE38 and 34E5-PE38 in all cell lines except for the EGFR negative cells (3T3 2.2). In the cell lines lacking EGFRvIII, U251-wt and Her14, the nanobody-based immunotoxins demonstrated limited efficacy. At the highest concentration tested (500 nM), 34E5-PE38 was most effective for U251-wt cells (75 % growth reduction), while the maximal inhibition by 7D12-PE38 treatment was obtained for Her14 cells (46 % growth reduction). Inhibition by the immunotoxins was however far more effective in EGFRvIII positive cell lines. The maximal reduction by 7D12-PE38 ranged from 68 % for U251-vIII cells to 83 % for 3T3-vIII cells while nearly complete inhibition of cell proliferation was observed in all EGFRvIII positive cells for 34E5-PE38 at the highest concentration tested (500 nM).

To further validate the specificity of the immunotoxins, co-culture experiments were performed (Fig 5). The previous established EGFRvIII positive and negative U251 cell lines were transfected with mCherry (red). As control, HeLa cells (low EGFR expression) were transfected with GFP (green). The specificity of immunotoxins towards EGFRvIII (or high EGFR expressing cells) was visualized by mixing the two cell lines. Both co-cultures, HeLa cells with either EGFRvIII positive or negative U251 cells, showed comparable mCherry signal for the R2- and 7D12-based immunotoxins. For the 34E5-PE38 immunotoxin, the mCherry signal was strongly reduced in the U251-vIII co-culture and to a lesser extent in the U251-wt co-culture. The GFP signal however remained comparable for all immunotoxins and the negative control, and is the result of the lower EGFR expressing level in HeLa cells. Therefore, the co-culture results were in agreement with the growth inhibition experiments and demonstrated the selectivity of 34E5-PE38 based on EGFR expression level.

4. Discussion

The success of antibody therapy depends on multiple factors including the expression level and genetic status of oncogenes. The latter is of importance since activating mutations in downstream signaling pathways can reduce the efficacy of receptor targeting mAbs (e.g. mutations in KRAS result in poor response to anti-EGFR mAbs) [33,34]. Another relevant factor is tumor penetration of mAbs into (solid) tumors, restricting the therapy to the outside layer of the tumor, which can be overcome by the use of a smaller antibody fragment[35].

Here, we developed a nanobody-based immunotoxin for the treatment of EGFRvIII overexpressing gliobastoma's. In contrast to the previously developed mAb806 (~150 kDa), the immunotoxin is composed of one nanobody and the toxic protein PE38 with a total molecular weight of 53 kDa, which is about the size of a Fab' fragment. Previously, Fab' fragments were demonstrated to rapidly distribute throughout the tumor, which was not the case for a complete IgG[35]. In order to efficiently target the immunotoxin to EGFRvIII expressing glioblastoma's selections were employed to screen for EGFRvIII specific nanobodies. Two rounds

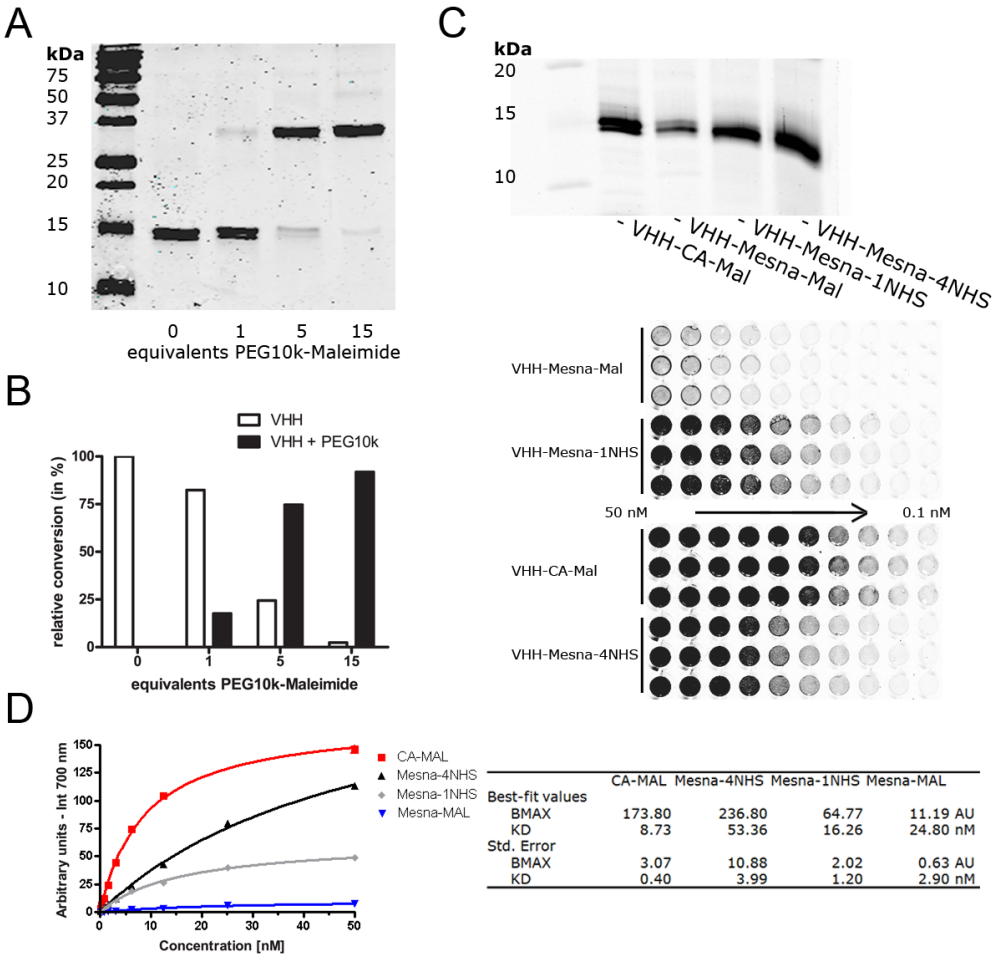

	CA-MAL	Mesna-4NHS	Mesna-1NHS	Mesna-MAL
Best-fit values				
BMAX	173.80	236.80	64.77	11.19 AU
KD	8.73	53.36	16.26	24.80 nM
Std. Error				
BMAX	3.07	10.88	2.02	0.63 AU
KD	0.40	3.99	1.20	2.90 nM

Figure 4. Evaluation of the nanobody-based immunotoxins on 3T3 2.2, 3T3-vIII, U251-wt, U251-vIII, Her14 and U373-vIII cells. Cells were incubated 1.5 hrs with the immunotoxin, after which the medium was refreshed. Total growth inhibtion was evaluated 3 days later by the Alamar Blue cell viability reagent. Data from two experiments are presented as mean ± SEM (n=6).

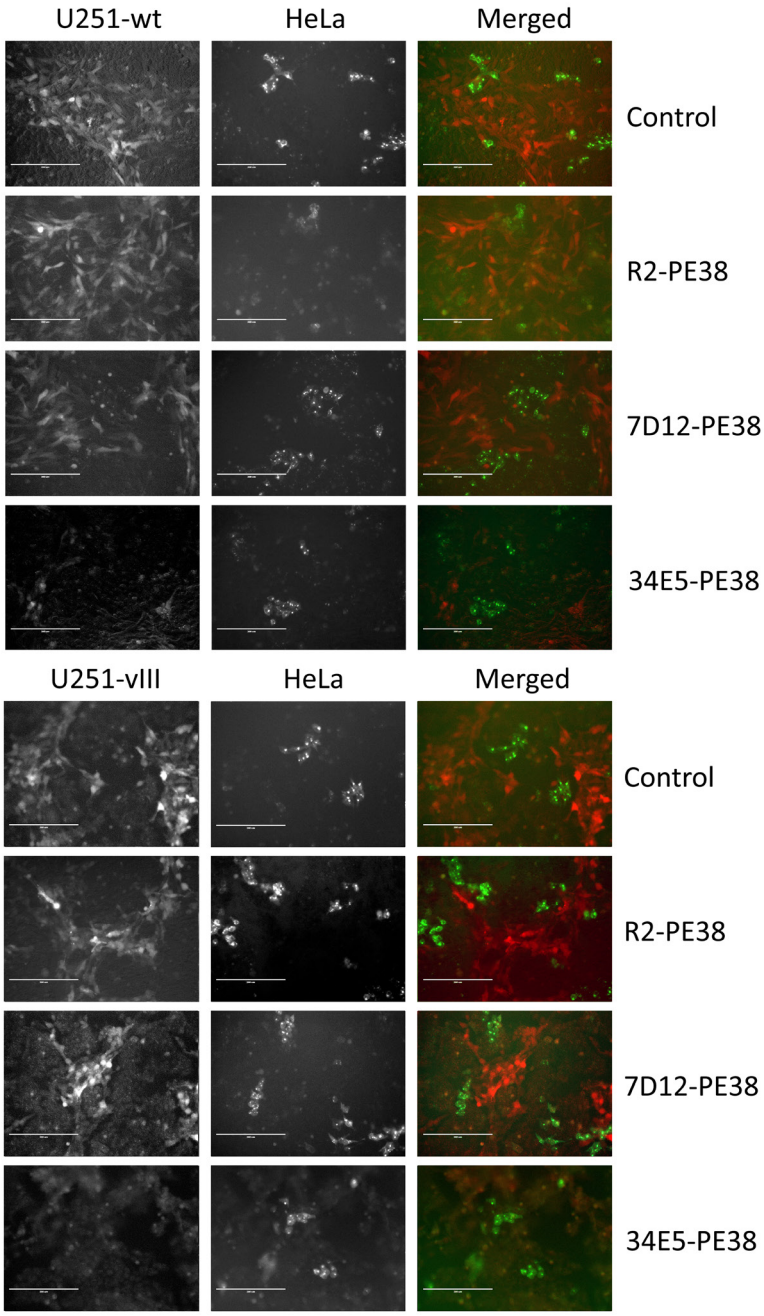

Figure 5. Evaluation of the specificity of nanobody-based immunotoxins on co-cultures with EGFRvIII positive and negative U251 cell lines (mCherry in red) and HeLa cells (low EGFR expression level; GFP in green). A 1:1 mixture of the cell lines were cultured and after one day treated with the immunotoxin for 2 hrs, after which the cells were washed and supplied with fresh DMEM. The growth inhibtion was visualized after 3 days using an EVOS cell imaging system.

of selection resulted in the non-agonistic 34E5 nanobody. 34E5 binds EGFRvIII in the low molecular range (2.08 nM) and showed an 11x fold selectivity over wt EGFR. The immunotoxins were expressed in inclusion bodies and on-column refolded as previously described[32]. Effective and selective inhibition of EGFRvIII positive cell lines was evident after treatment with 34E5-PE38. The specificity was further confirmed in co-cultures where Hela cells not expressing EGFRvIII remained unaffected.

The immunotoxin 34E5-PE38 also demonstrated higher potency for the EGFRvIII negative cell lines compared with 7D12-PE38. This is unexpected because 7D12 binds both wt EGFR and EGFRvIII in the low molecular range (1.19 nM and 0.46 nM, respectively) while 34E5 harbors only a high affinity for EGFRvIII (2.08 nM) and a lower affinity for wt EGFR (23.14 nM). The limited toxicity is probably the result of a reduced affinity of 7D12 when genetically fused to PE38 and/or its inability to be refolded. Interestingly, EGFRvIII positive cell lines responded better towards 7D12-PE38 treatment and can be explained by the higher EGFR expression level (wt EGFR + EGFRvIII). A direct fusion of 7D12 and 34E5, generating the biparatopic immunotoxin 7D12-34E5-PE38, was less toxic on EGFRvIII positive cell lines than the monovalent 34E5-PE38 (Fig S1). This was unexpected given the increased uptake of biparatopic nanobodies against wt EGFR[36]. The issues of 7D12 are therefore not confined to its own domain, but in case of the biparatopic immunotoxin also affects binding properties of 34E5 and/or affects the immunotoxin as whole.

The *in vitro* efficacy of 34E5-PE38 has been demonstrated for several EGFRvIII positive cell lines. In order to successfully translate these results to the *in vivo* situation, several important factors should be considered. Firstly, previous studies have investigated PE38-based immunotoxins and revealed non-specific liver toxicity[37,38]. This toxicity was demonstrated to be dependent on the isoelectric point (pI) of the immunotoxin and could be 3-fold reduced when lowering the pI from 10.21 to 6.82[37]. In a follow up study the pI's were lowered to 4.8 – 5.2, which even further reduced the toxicity[38]. The theoretical pI's of nanobody-based immunotoxins however, are naturally low, between 5.43 – 5.75 and may not require optimization of the pI.

Secondly, the appearance of neutralizing antibodies towards the immunotoxin has been described[39]. Immunogenic epitopes on PE38 were recently identified and mutated to improve multiple treatment cycles[40]. Currently however, immune responses are suppressed to limit these side effects. This is not necessarily beneficial since the efficacy of PE38 was demonstrated to not solely depend on the cytotoxicity but also on the stimulation of an immune response against the tumor[41]. Long term anti-tumor immunity was observed towards tumor cells with and without the targeted receptor, and was essential for the efficacy of PE38-based treatments.

Thirdly, the delivery of immunotoxins to GBM tumors is complicated by the blood-brain barrier (BBB)[11]. In patients with GBM, disruption of the BBB has been reported but varies among patients and is therefore an unreliable factor for GBM treatment[42,43]. One interesting approach is

the transport of antibody (fragments) across the BBB via receptor-mediated transcytosis but this is hampered by its low efficiency [44]. Instead, we envision the local production of immunotoxins via stem cell therapy. The production of therapeutic proteins in the brain circumvents the BBB and has therefore drawn much attention for treatment of brain cancer as well as neurological diseases. Previously, we demonstrated the expression of EGFR-specific nanobodies by therapeutic stem cells and showed *in vitro* and *in vivo* inhibition of GBM growth [45]. The established expression by stem cells can be employed for the evaluation of nanobody-based immunotoxins for GBM treatment. Despite the remaining challenges such as regulating immune responses, expression levels and life time of stem cells, stem cell therapy offers tremendous clinical applications for brain diseases as well as chronic indications.

5. Conclusion

In conclusion, we selected and characterized the EGFRvIII specific nanobody 34E5. An EGFRvIII specific immunotoxin was generated by the genetic fusion of the non-agonistic 34E5 to PE38. This immunotoxin demonstrated near complete *in vitro* inhibition of all EGFRvIII positive cell lines. In contrast, only moderate toxicity was observed towards cells lines expressing wt EGFR. Evaluation *in vivo* with stem cell therapy is required to truly demonstrate the clinical efficacy and implications for GBM treatment.

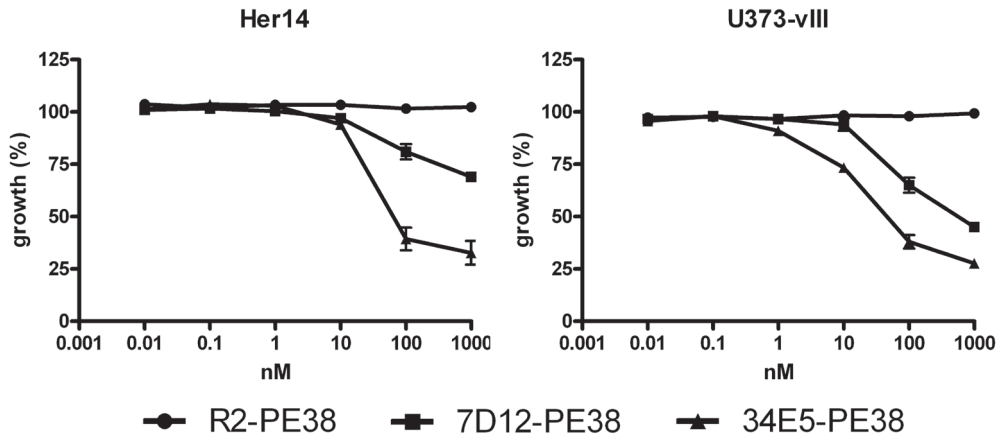

Figure S1. Evaluation of the nanobody-based immunotoxins on Her14 and U373-vIII cells. Cells were incubated 1.5 hrs with the immunotoxin, after which the medium was refreshed. Total growth inhibtion was evaluated 3 days later by the Alamar Blue cell viability reagent. Data are presented as mean ± SEM (n=3).

Acknowledgements

This work was funded by the Focus & Massa project of the Utrecht University, the Netherlands.

References

1. Holland, E. C. Glioblastoma multiforme: the terminator. *Proc. Natl. Acad. Sci. U. S. A.* **97,** 6242–4 (2000).
2. Gan, H. K., Cvrljevic, A. N. & Johns, T. G. The epidermal growth factor receptor variant III (EGFRvIII): where wild things are altered. *FEBS J.* **280,** 5350–70 (2013).
3. Hatanpaa, K. J., Burma, S., Zhao, D. & Habib, A. A. Epidermal growth factor receptor in glioma: signal transduction, neuropathology, imaging, and radioresistance. *Neoplasia* **12,** 675–84 (2010).
4. Heimberger, A. B., Suki, D., Yang, D., Shi, W. & Aldape, K. The natural history of EGFR and EGFRvIII in glioblastoma patients. *J. Transl. Med.* **3,** 38 (2005).
5. Voldborg, B. R., Damstrup, L., Spang-Thomsen, M. & Poulsen, H. S. Epidermal growth factor receptor (EGFR) and EGFR mutations, function and possible role in clinical trials. *Ann. Oncol.* **8,** 1197–206 (1997).
6. Cavenee, W. K. Genetics and new approaches to cancer therapy. *Carcinogenesis* **23,** 683–6 (2002).
7. Li, B. *et al.* Mutant epidermal growth factor receptor displays increased signaling through the phosphatidylinositol-3 kinase/AKT pathway and promotes radioresistance in cells of astrocytic origin. *Oncogene* **23,** 4594–602 (2004).
8. Prigent, S. A. *et al.* Enhanced tumorigenic behavior of glioblastoma cells expressing a truncated epidermal growth factor receptor is mediated through the Ras-Shc-Grb2 pathway. *J. Biol. Chem.* **271,** 25639–45 (1996).
9. Huang, P. H. *et al.* Quantitative analysis of EGFRvIII cellular signaling networks reveals a combinatorial therapeutic strategy for glioblastoma. *Proc. Natl. Acad. Sci. U. S. A.* **104,** 12867–72 (2007).
10. Kuan, C. T., Wikstrand, C. J. & Bigner, D. D. EGF mutant receptor vIII as a molecular target in cancer therapy. *Endocr. Relat. Cancer* **8,** 83–96 (2001).
11. Patel, M. M., Goyal, B. R., Bhadada, S. V, Bhatt, J. S. & Amin, A. F. Getting into the brain: approaches to enhance brain drug delivery. *CNS Drugs* **23,** 35–58 (2009).
12. Heimberger, A. B. *et al.* Brain tumors in mice are susceptible to blockade of epidermal growth factor receptor (EGFR) with the oral, specific, EGFR-tyrosine kinase inhibitor ZD1839 (iressa). *Clin. Cancer Res.* **8,** 3496–502 (2002).
13. Learn, C. A. *et al.* Resistance to tyrosine kinase inhibition by mutant epidermal growth factor receptor variant III contributes to the neoplastic phenotype of glioblastoma multiforme. *Clin. Cancer Res.* **10,** 3216–24 (2004).
14. Johns, T. G. *et al.* The efficacy of epidermal growth factor receptor-specific antibodies against glioma xenografts is influenced by receptor levels, activation status, and heterodimerization. *Clin. Cancer Res.* **13,** 1911–25 (2007).
15. Jungbluth, A. A. *et al.* A monoclonal antibody recognizing human cancers with amplification/overexpression of the human epidermal growth factor receptor. *Proc. Natl. Acad. Sci. U. S. A.* **100,** 639–44 (2003).
16. Scott, A. M. *et al.* A phase I clinical trial with monoclonal antibody ch806 targeting transitional state and mutant epidermal growth factor receptors. *Proc. Natl. Acad. Sci. U. S. A.* **104,** 4071–6 (2007).
17. Newman, D. J. & Cragg, G. M. Marine-sourced anti-cancer and cancer pain control agents in clinical and late preclinical development. *Mar. Drugs* **12,** 255–78 (2014).
18. Sampson, J. H. *et al.* Immunologic escape after prolonged progression-free survival with epidermal growth factor receptor variant III peptide vaccination in patients with newly diagnosed glioblastoma. *J. Clin. Oncol.* **28,** 4722–9 (2010).
19. Babu, R. & Adamson, D. C. Rindopepimut: an evidence-based review of its therapeutic potential in the treatment of EGFRvIII-positive glioblastoma. *Core Evid.* **7,** 93–103 (2012).
20. Hamers-Casterman, C. *et al.* Naturally occurring antibodies devoid of light chains. *Nature* **363,** 446–8 (1993).
21. Muyldermans, S. Nanobodies: natural single-domain antibodies. *Annu. Rev. Biochem.* **82,** 775–97 (2013).
22. Harmsen, M. M. & De Haard, H. J. Properties, production, and applications of camelid single-domain antibody fragments. *Appl. Microbiol. Biotechnol.* **77,** 13–22 (2007).

23. Pastan, I., Hassan, R., Fitzgerald, D. J. & Kreitman, R. J. Immunotoxin therapy of cancer. *Nat. Rev. Cancer* **6,** 559–65 (2006).
24. Pastan, I., Hassan, R., FitzGerald, D. J. & Kreitman, R. J. Immunotoxin treatment of cancer. *Annu. Rev. Med.* **58,** 221–37 (2007).
25. Zdanovsky, A. G., Chiron, M., Pastan, I. & FitzGerald, D. J. Mechanism of action of Pseudomonas exotoxin. Identification of a rate-limiting step. *J. Biol. Chem.* **268,** 21791–9 (1993).
26. Kreitman, R. J. Hairy cell leukemia-new genes, new targets. *Curr. Hematol. Malig. Rep.* **8,** 184–95 (2013).
27. Behdani, M. *et al.* Development of VEGFR2-specific Nanobody Pseudomonas exotoxin A conjugated to provide efficient inhibition of tumor cell growth. *N. Biotechnol.* **30,** 205–9 (2013).
28. Roovers, R. C. *et al.* Efficient inhibition of EGFR signaling and of tumour growth by antagonistic anti-EFGR Nanobodies. *Cancer Immunol. Immunother.* **56,** 303–317 (2007).
29. Oliveira, S. *et al.* Rapid visualization of human tumor xenografts through optical imaging with a near-infrared fluorescent anti-epidermal growth factor receptor nanobody. *Mol. Imaging* **11,** 33–46 (2012).
30. Bigner, S. H. *et al.* Characterization of the epidermal growth factor receptor in human glioma cell lines and xenografts. *Cancer Res.* **50,** 8017–22 (1990).
31. Sugawa, N., Ekstrand, A. J., James, C. D. & Collins, V. P. Identical splicing of aberrant epidermal growth factor receptor transcripts from amplified rearranged genes in human glioblastomas. *Proc. Natl. Acad. Sci. U. S. A.* **87,** 8602–6 (1990).
32. Wang, H. *et al.* Expression, purification, and characterization of an immunotoxin containing a humanized anti-CD25 single-chain fragment variable antibody fused to a modified truncated Pseudomonas exotoxin A. *Protein Expr. Purif.* **58,** 140–7 (2008).
33. Amado, R. G. *et al.* Wild-type KRAS is required for panitumumab efficacy in patients with metastatic colorectal cancer. *J. Clin. Oncol.* **26,** 1626–34 (2008).
34. Pantaleo, M. A. *et al.* Molecular imaging of EGFR: it's time to go beyond receptor expression. *J. Nucl. Med.* **50,** 1195–6; author reply 1196, 1197 (2009).
35. Yokota, T., Milenic, D. E., Whitlow, M. & Schlom, J. Rapid tumor penetration of a single-chain Fv and comparison with other immunoglobulin forms. *Cancer Res.* **52,** 3402–3408 (1992).
36. Heukers, R. *et al.* Endocytosis of EGFR requires its kinase activity and N-terminal transmembrane dimerization motif. *J. Cell Sci.* **126,** 4900–12 (2013).
37. Onda, M., Kreitman, R. J., Vasmatzis, G., Lee, B. & Pastan, I. Reduction of the nonspecific animal toxicity of anti-Tac(Fv)-PE38 by mutations in the framework regions of the Fv which lower the isoelectric point. *J. Immunol.* **163,** 6072–7 (1999).
38. Onda, M. *et al.* Lowering the isoelectric point of the Fv portion of recombinant immunotoxins leads to decreased nonspecific animal toxicity without affecting antitumor activity. *Cancer Res.* **61,** 5070–7 (2001).
39. Kreitman, R. J. *et al.* Phase I trial of recombinant immunotoxin anti-Tac(Fv)-PE38 (LMB-2) in patients with hematologic malignancies. *J. Clin. Oncol.* **18,** 1622–36 (2000).
40. Mazor, R. *et al.* Recombinant immunotoxin for cancer treatment with low immunogenicity by identification and silencing of human T-cell epitopes. *Proc. Natl. Acad. Sci. U. S. A.* (2014). doi:10.1073/pnas.1405153111
41. Ochiai, H. *et al.* EGFRvIII-targeted immunotoxin induces antitumor immunity that is inhibited in the absence of CD4+ and CD8+ T cells. *Cancer Immunol. Immunother.* **57,** 115–21 (2008).
42. Nathanson, D. & Mischel, P. S. Charting the course across the blood-brain barrier. *J. Clin. Invest.* **121,** 31–33 (2011).
43. Schneider, S. W. *et al.* Glioblastoma cells release factors that disrupt blood-brain barrier features. *Acta Neuropathol.* **107,** 272–6 (2004).
44. Abulrob, A., Sprong, H., Van Bergen en Henegouwen, P. & Stanimirovic, D. The blood-brain barrier transmigrating single domain antibody: mechanisms of transport and antigenic epitopes in human brain endothelial cells. *J. Neurochem.* **95,** 1201–14 (2005).
45. Van de Water, J. A. J. M. *et al.* Therapeutic stem cells expressing variants of EGFR-specific nanobodies have antitumor effects. *Proc. Natl. Acad. Sci. U. S. A.* **109,** 16642–7 (2012).

Chapter 8

Summarizing discussion

The first indication of cancer was reported in Edwin Smith Papyrus (copied approximately 1600 years BC)[1,2]. Many years later, Hippocrates believed that cancer was the result of natural causes and described cancer in different tissues including breast, mouth, skin, and stomach[2]. Although surgical intervention was recommended by Celsus already in the 1st century, it remained until 1700 when Deshaies Gendron described cancer as the transformation and continuous growth of 'structures'[2,3]. Soon after, specific types of cancer were attributed to use of tobacco (1761) and as workers disease by the exposure to soot by chimney-sweeps (1775)[3,4]. As a consequence of the medical revolution in the 19th and 20th century, the life expectancy of people has increased tremendously and cancer is now considered as one of the common elderly diseases of today with 8.2 million deaths in 2012[5].

Despite our detailed knowledge about cancer, therapeutic intervention remains challenging due to its complex nature and the similarity of cancerous tissue to healthy tissue. Current improvements are found in the field of early detection/diagnosis and targeted therapies with fewer side effects. Overexpression of receptors and ligands can be effectively neutralized by monoclonal antibody therapies. Complete eradication of the tumor however is complicated by (the development of) resistant populations in the heterogeneous tissue and by suppression of the immune system[6]. This either requires a combination of treatment regimes targeting multiple targets or more effective immunotherapy such as antibody drug conjugates (ADC), which delivers potent cytotoxic drugs to the tumor. The limited diffusion and tumor penetration of monoclonal antibodies led to the development of antibody fragments including Fabs, scFv's and nanobodies[7]. The latter is of particular interest since nanobodies harbor favorable biochemical and physical properties, which were described in detail in **Chapter 3**.

Site-specific functionalization of nanobodies

Since their discovery, nanobodies have been employed for a variety of therapeutic, diagnostic and research-related purposes[8]. Of these, some applications require the functionalization with biomolecules. One important criterion is that these modifications should not affect the binding properties of nanobodies. The current standard, manipulation by random labeling of lysine residues, potentially affects the ability to recognize the antigen. In **Chapter 2**, approaches for the site-specific functionalization of proteins were described. Of these, the functionalization based on intein protein ligation (IPL) was previously reported for nanobodies[9,10]. Although these studies demonstrated the site-directed conjugation to liposomes/polymersomes as well as the dual functionalization of nanobodies, non-commercially available compounds were required and/or a maximal conversion of only 50 % was achieved. The latter not only results in loss of protein, but also complicates separation of non-reacted nanobodies upon conjugation to small biomolecules. The further development and optimization of this method was described in **Chapter 4**. Evaluation of several substrates identified cysteamine as ideal reagent for the

quantitative introduction of a c-terminal thiol group. Additional advances were made by replacement of the chitin binding domain by the HIS_6-tag and an elastin-like polypeptide (ELP). The tandem purification not only provides high purity but also enables intein splicing in solution at high concentrations and efficient removal of the intein domain by ELP precipitation. The new construct in combination with cysteamine was demonstrated for conjugation of nanobodies to PEG and IRDye800 CW as well as decoration onto liposomes.

Another approach, the site-specific incorporation of unnatural amino acids (UAA), was described in **Chapter 6.** An orthogonal synthetase/tRNA pair suppresses an artificial introduced TAG codon to incorporate the UAA at the site of interest. Over 70 UAAs have been incorporated into a variety of proteins and are commonly applied for bioorthogonal reactions, structural biology or posttranslational modifications[11]. Here, we incorporated the azide analog of phenylalanine (pAzF) into nanobodies to facilitate the modification with biomolecules. Although the incorporation of an UAA seems straightforward, several constructs were evaluated for their nanobody expression and incorporation of pAzF. Optimized conditions were employed to produce EGa1-N_3 after which the presence of the azide group was confirmed by copper-assisted and copper-free click reaction to biomolecules. The functional validation of nanobodies decorated on liposomes demonstrated their robustness and stability as a targeting modality. This was further exemplified by the multimerization of biotinylated nanobodies using streptavidin and the subsequent growth inhibition of A431 cells.

The above-mentioned methods for site-specific functionalization of nanobodies differ in several aspects. The intein-mediated functionalization for instance is restricted to either the N- or C-terminus of the protein, while UAAs can theoretically be incorporated at every site in the protein (except the first amino acid). Both approaches require different components. In case of inteins, the genetic fusion and the substrate are essential. The UAAs approach however requires introduction of the TAG codon in the gene of interest, the UAA and expression of a compatible synthetase/tRNA pair. Although introduction of the TAG codon reduces the protein yield, this was compensated by the high expression of the maltose-binding protein (MBP).

Proteins are generally purified by immobilized metal ion affinity chromatography (IMAC) and this is compatible for both methods. For the unnatural amino acids approach, a C-terminal purification tag is required to also separate the desired protein from the truncated analog (due to termination of expression at the TAG codon). Although an IMAC tag can be employed for purification of the intein fusion protein, the tag is not compatible during splicing as the reducing environment will reduce the immobilized metal. Most intein approaches therefore employ different purification tags such as a chitin binding domain which binds immobilized chitin instead. Since the purification via chitin beads was not efficient, HIS_6-tag purification was combined with reversible precipitation by an elastin-like polypeptide (ELP). The latter is fully

compatible with reducing environments. In addition, the intein and the purification tag(s) are removed by splicing of the intein domain. This not only prevents misbehavior of the protein but also reduces kidney retention in case of a HIS_6-tag[12]. A detailed comparison of the two methods for site-specific functionalization of nanobodies is given in table 1.

Table 1. Comparison of site-specific functionalizion of nanobodies via intein and unnatural amino acids approach.

	Intein	**Unnatural amino acids**
Label site	N- or C-terminus	Anywhere (except first AA)
Chemistry	Thiol/oxime ligation	Click chemistry
Cloning	Fusion protein (IMPACT™ Kit)	Introduction of TAG codon
Expression requirements	-	Plasmid bearing synthetase/tRNA pair UAA
Expression	Regular	Regular
Purification	IMAC/ELP (or chitin beads)	IMAC
Post-translational modification	Intein splicing and ligation purification	-
Final protein yield	0.5 - 1.0 mg/L	0.5 - 1.0 mg/L
Comments	Incomplete pelB leader processing was observed (and previously reported[8]). Removal by Enterokinase treatment.	Expressed as MBP fusion (requires Factor Xa cleavage), without MBP results in lower yields and expression in inclusion bodies.

The site-specific functionalization of nanobodies resulted in different chemistry strategies for conjugation of biomolecules. Thiol maleimide conjugation is based on the preferential labeling of thiols over amines with a >1000 fold specificity at pH 7.0[13]. Although this generally results in site-specific modification of proteins, the decoration of nanobodies on liposomes was also prone to random labeling due to the excess of maleimide groups. In contrast, the site-specific labeling of azide functionalized nanobodies is more bioorthogonal since azides readily react with ring-strained alkynes, even in complex biological samples. The introduction of an azide is however more complicated and thiol-yne additions have been described as a potential side reaction[14]. The preferred strategy for nanobody functionalization therefore strongly depends on its application.

Nanobody-based cancer therapy

Over the years, nanobodies have been employed for many therapeutic applications which were summarized in **Chapter 3**. Among these, nanobodies have been investigated as anti-cancer therapeutics since their small size allows efficient distribution through the body and rapid tumor penetration[15]. As a consequence of these features however, the *in vivo* efficacy of

naked nanobodies is limited to a temporary tumor growth inhibition. The therapeutic effect of nanobodies can therefore be improved by the attachment of effector molecules or by decorating drug carriers with nanobodies. In the latter case, the drugs are efficiently transported inside nanoparticles which, because of their size and shielding from environment, have a long blood circulation time. Besides the passive targeting of these particles by the EPR effect, nanobodies can facilitate active targeting and receptor-mediated internalization of cytotoxic drugs into cancer cells.

The decoration of liposomes with nanobodies was described in **Chapters 4 & 5**. In chapter 4, rhodamine-labeled liposomes demonstrated no toxicity or growth inhibition after prolonged incubation (48 hrs) on cell lines with and without the targeted antigen. In contrast, a concentration dependent and nanobody specific fluorescence signal was observed after prolonged incubation and demonstrates the beneficial effect of active targeting. More important for drug delivery, the internalization of nanobody-targeted liposomes, was also confirmed by confocal microscopy and these liposomes are therefore suitable as drug carriers against EGFR-overexpressing tumors.

In contrast to the situation *in vitro* however, drug delivery *in vivo* is more complex. Despite active targeting by antibody (fragments) or ligands, only a fraction of the injected nanoparticles (and drugs) end up at the tumor site. The other fraction ends up in other organs including the liver and spleen, resulting in side effects due to accumulation of the cytotoxic drug[16]. This toxicity can be prevented by the application of prodrugs which require activation by key components of the diseased tissue. An alternative approach is photodynamic therapy (PDT) where 'the drug', better known as a photosensitizer, requires illumination to generate singlet oxygen ($^1O_2$) to induce deleterious reactions. Current PDT treatment mainly employs water soluble photosensitizers with low tumor accumulation and are remarkably improved when applied in liposomal formulations. Antibody-targeted liposomal formulations have the potential to further improve PDT by specific tumor accumulation and internalization. Targeted delivery of Zinc Phthalocyanine (ZnPc) by the previously established nanobody-liposome platform was described in **Chapter 5**. ZnPc is a hydrophobic photosensitizer and therefore resides in the lipid bilayer of liposomes. Since photochemical reactions are more destructive when located inside the cell, the specific uptake of ZnPc was confirmed and visualized. Moreover, the delivery of the photosensitizer into cancer cells by receptor-mediated internalization efficiently induces cell death as the result of PDT treatment. These promising results pave the way to evaluation of targeted liposomes for PDT in animal models.

Another example of nanobody-based cancer therapy is the targeting of PE38 towards glioblastoma multiforme (GBM) and was described in **Chapter 7**. In contrast to PDT, the immunotoxin requires no activation and thus needs to be specifically targeted towards the tumor to minimize side

effects. The high similarity between cancer cells and healthy tissue often restricts medicines to be targeted based on expression status of receptors. In GBM however, not only the overexpression of EGFR can be targeted but also a tumor specific marker, EGFRvIII[17]. Immunization and selections resulted in the novel 34E5 anti-EGFRvIII nanobody, which was genetically fused to PE38. The selective growth inhibition of this immunotoxin was demonstrated for EGFRvIII positive cell lines. In addition, the specificity was furthermore visualized in co-cultures where HeLa cells lacking EGFRvIII were mixed with EGFRvIII expressing cancer cells derived from a malignant glioblastoma tumor (U251) and remained unaffected during treatment. Whether the 11-fold selectivity of 34E5 combined with the degree of overexpression of EGFR in tumors is truly sufficient for GBM treatment, needs to be established in animal models. Interestingly, previous reported studies revealed that the therapeutic effect of PE38 is not restricted to direct toxicity, but additionally induces an immune response against the tumor[18]. This acquired immune response aids in complete tumor regression as well as in protection against future challenges.

Outlook

The functionalization of nanobodies offers tremendous possibilities for existing and new (therapeutic) applications. In general research, scientists will most likely benefit from the expanding nanobody toolbox. Manipulation of nanobodies by site-specific conjugation, including its conjugation to biomolecules and the attachment to surfaces without affecting the binding interface, are expected to become more easy and straightforward.

In molecular imaging, the state of the art involves optical imaging using non-radioactive fluorescent tracers. Despite the advantages of near-infrared probes, one remaining challenge is the limited tissue penetration. As labeling efficiency of antibody fragments including nanobodies range between 50 - 80 %[19–21], this can be remarkably improved. The first step would be the generation of nanobodies which are 100 % labeled. The conjugation of multiple dyes on a scaffold would even further increase the signal. For the employment of multiple dyes, the possible quenching and non-specific interactions should be taken into account. Still, a higher number of labels per nanobody can improve the current detection limits up to 600 % (for 3 labels).

Alternatively, (dual) labeling by site-specific conjugation also opens up possibilities for combining diagnostics and therapy, also known as theranostics. One interesting application would be the combination of optical imaging and photodynamic therapy. During image-guided surgery, the surgeon is aided in the discrimination between healthy and tumor tissue. After resection, the remaining border tissue can be treated with PDT to eradicate remaining cancer cells. Currently, nanobodies have been separately investigated for either optical imaging[21,22] or photodynamic therapy[23]. The combination might improve the therapeutic outcome of patients and therefore needs to be evaluated.

References

1. Brorson, S. Management of fractures of the humerus in Ancient Egypt, Greece, and Rome: An historical review. *Clin. Orthop. Relat. Res.* **467,** 1907–1914 (2009).
2. Hajdu, S. I. A note from history: landmarks in history of cancer, part 1. *Cancer* **117,** 1097–102 (2011).
3. Hajdu, S. I. A note from history: landmarks in history of cancer, part 2. *Cancer* **117,** 2811–20 (2011).
4. Hajdu, S. I. A note from history: landmarks in history of cancer, part 3. *Cancer* **118,** 1155–68 (2012).
5. IARC., I. A. for R. on C. W. H. O. GLOBOCAN 2012: Estimated Cancer Incidence, Mortality and Prevalence Worldwide in 2012. *GLOBOCAN* (2012). at <http://globocan.iarc.fr/Pages/fact_sheets_cancer.aspx?>
6. Scott, A. M., Wolchok, J. D. & Old, L. J. Antibody therapy of cancer. *Nat. Rev. Cancer* **12,** 278–87 (2012).
7. Holliger, P. & Hudson, P. J. Engineered antibody fragments and the rise of single domains. *Nat. Biotechnol.* **23,** 1126–36 (2005).
8. Muyldermans, S. Nanobodies: natural single-domain antibodies. *Annu. Rev. Biochem.* **82,** 775–97 (2013).
9. Reulen, S. W. A., van Baal, I., Raats, J. M. H. & Merkx, M. Efficient, chemoselective synthesis of immunomicelles using single-domain antibodies with a C-terminal thioester. *BMC Biotechnol.* **9,** 66 (2009).
10. Debets, M. F. *et al.* Nanobody-functionalized polymersomes for tumor-vessel targeting. *Macromol. Biosci.* **13,** 938–45 (2013).
11. Chin, J. W. Expanding and reprogramming the genetic code of cells and animals. *Annu. Rev. Biochem.* **83,** 379–408 (2014).
12. D'Huyvetter, M. *et al.* Targeted radionuclide therapy with A 177Lu-labeled anti-HER2 nanobody. *Theranostics* **4,** 708–20 (2014).
13. Kratz, H. *et al.* Straightforward thiol-mediated protein labelling with DTPA: Synthesis of a highly active 111In-annexin A5-DTPA tracer. *EJNMMI Res.* **2,** 17 (2012).
14. Van Geel, R., Pruijn, G. J. M., van Delft, F. L. & Boelens, W. C. Preventing thiol-yne addition improves the specificity of strain-promoted azide-alkyne cycloaddition. *Bioconjug. Chem.* **23,** 392–8 (2012).
15. Oliveira, S., Heukers, R., Sornkom, J., Kok, R. J. & Van Bergen En Henegouwen, P. M. P. Targeting tumors with nanobodies for cancer imaging and therapy. *J. Control. Release* **172,** 607–617 (2013).
16. El-Ansary, A. & Al-Daihan, S. On the toxicity of therapeutically used nanoparticles: an overview. *J. Toxicol.* **2009,** 754810 (2009).
17. Kuan, C. T., Wikstrand, C. J. & Bigner, D. D. EGF mutant receptor vIII as a molecular target in cancer therapy. *Endocr. Relat. Cancer* **8,** 83–96 (2001).
18. Ochiai, H. *et al.* EGFRvIII-targeted immunotoxin induces antitumor immunity that is inhibited in the absence of CD4+ and CD8+ T cells. *Cancer Immunol. Immunother.* **57,** 115–21 (2008).
19. Mume, E. *et al.* Evaluation of ((4-hydroxyphenyl)ethyl)maleimide for site-specific radiobromination of anti-HER2 affibody. *Bioconjug. Chem.* **16,** 1547–1555 (2005).
20. Lee, S. B. *et al.* Affibody molecules for in vivo characterization of HER2-positive tumors by near-infrared imaging. *Clin. Cancer Res.* **14,** 3840–3849 (2008).
21. Kijanka, M. *et al.* Rapid optical imaging of human breast tumour xenografts using anti-HER2 VHHs site-directly conjugated to IRDye 800CW for image-guided surgery. *Eur. J. Nucl. Med. Mol. Imaging* **40,** 1718–1729 (2013).
22. Oliveira, S. *et al.* Rapid visualization of human tumor xenografts through optical imaging with a near-infrared fluorescent anti-epidermal growth factor receptor nanobody. *Mol. Imaging* **11,** 33–46 (2012).
23. Heukers, R., van Bergen En Henegouwen, P. M. P. & Oliveira, S. Nanobody-photosensitizer conjugates for targeted photodynamic therapy. *Nanomedicine* 1–11 (2014). doi:10.1016/j.nano.2013.12.007

Addendum

Nederlandse samenvatting

Kanker is de verzamelnaam voor ziektes die worden veroorzaakt door een ongecontroleerde celdeling. In 2012 werd naar schatting voor 14.1 miljoen mensen wereldwijd de diagnose kanker gesteld. Daarnaast was kanker de oorzaak van ongeveer 8.2 miljoen sterfgevallen. De afgelopen jaren is de medische kennis sterk verbeterd. Een fundamenteel probleem blijft echter dat kankercellen ontstaan vanuit gezonde cellen en daardoor lastig te onderscheiden zijn. Dit maakt vroegtijdige opsporing van tumoren, wat gunstig is voor de genezingskans, zeer lastig. Ook zijn behandelingen niet altijd effectief of zorgen voor nevenschade elders in het lichaam.

De behandeling van kanker hangt af van diverse factoren zoals het type tumor en het stadium waarin deze ontdekt is. Operatieve ingrepen worden voornamelijk ingezet voor de verwijdering van vaste tumoren. Radio- en chemotherapie wordt gebruikt voor de behandeling van kleinere tumoren of uitzaaiingen, en om restanten na operatie te behandelen. Om kankercellen van gezonde cellen te kunnen onderscheiden richt chemotherapie zich op snel delende cellen door te binden aan het DNA of de celdeling te verstoren. Desondanks zijn deze stoffen vaak ook schadelijk voor andere gezonde snel delende cellen zoals in het maag-darmstelsel, beenmerg en haar follikels. Chemotherapie gaat hierdoor vaak gepaard met diverse (ernstige) bijwerkingen.

Een nieuwe klasse van kankermedicijnen, de ‘doelgerichte therapieën’, beperken bijwerkingen door direct in te grijpen op een, voor de kanker cel, specifiek proces. Deze doelgerichte therapieën zijn op te delen in twee soorten: chemische remmers en antilichamen. Chemische remmers zijn kleine moleculen die de signalering verantwoordelijk voor celdeling blokkeren en zo tumorgroei remmen. Antilichamen daarentegen, zijn eiwitten en vele malen groter (+/- 300x). Naast het blokkeren van (groei)signalen kunnen antilichamen ook het immuunsysteem activeren. Een andere toepassing van antilichamen is het gericht loodsen van medicijnen naar de tumor. Antilichamen zijn zeer specifiek en komen van nature in de mens voor. Hierdoor is er nauwelijks sprake van schadelijke bijwerkingen en zijn ze uitermate geschikt voor de behandeling van kanker.

Antilichamen kunnen ook worden opgedeeld in kleinere fragmenten. Een antilichaam fragment herkent nog steeds een kankercel maar kan, doordat het een stuk kleiner is, sneller door het lichaam migreren en de tumor beter binnendringen. Een nadeel is echter een korter verblijf in het lichaam wat een verminderde therapeutische werking tot gevolg heeft. Dit is geen obstakel voor kankertherapie wanneer antilichaam fragmenten worden gecombineerd met zeer effectieve medicijnen. Daarnaast zijn ook diverse aanpassingen mogelijk om de aanwezigheid van antilichaam fragmenten in het lichaam weer te verlengen.

Een unieke klasse van antilichaam fragmenten zijn gebaseerd op antilichamen van lama’s. Deze hebben zeer gunstige eigenschappen en staan voornamelijk bekend als nanobodies. Een overzicht van de eigenschappen en therapeutische toepassingen van nanobodies is beschreven in **hoofdstuk 3**.

Nanobodies zijn sinds de ontdekking gebruikt voor diverse therapeutische, diagnostische en onderzoek gerelateerde toepassingen. Sommige van deze toepassingen vereisen dat nanobodies worden voorzien van additionele (bio)moleculen. Deze stoffen maken bijvoorbeeld het detecteren van de nanobodies mogelijk of versterken het therapeutische effect. Een voorwaarde is echter dat deze moleculen niet de werking van het nanobody verstoren (oftewel de herkenning van een kankercel). Hiervoor is het noodzakelijk dat de additionele (bio)moleculen op specifieke plaatsen aan de nanobody worden gekoppeld. Een overzicht van de methoden die dit kunnen bewerkstelligen is gegeven in **hoofdstuk 2**. Verder zijn in dit hoofdstuk ook de mogelijke therapeutische toepassing van deze methoden besproken.

Een van deze methoden, de 'intein protein ligation', is al eerder toegepast voor nanobodies. Hoewel deze studies de werking van de methode voor nanobodies hebben aangetoond was deze niet optimaal. Een van de problemen was dat niet alle nanobodies konden worden voorzien van een extra (bio)molecuul. In de praktijk zorgt dit ervoor dat deze nanobodies niet allemaal hetzelfde zijn en minder medicijnen kunnen loodsen naar de tumor. In **hoofdstuk 4** is deze methode verder ontwikkeld zodat deze problemen zijn verholpen. Hiervoor is deze methode op diverse punten aangepast (zuivering, reactiecondities en aanwezige componenten). In experimenten is aangetoond dat bijna alle nanobodies nu worden voorzien met een extra bio(molecuul) en dat deze nog steeds functioneel blijven.

Een andere methode is gebaseerd op het gebruik van niet-natuurlijke aminozuren en is beschreven in **hoofdstuk 6**. Aminozuren zijn de bouwstenen van eiwitten en door een niet-natuurlijke variant te gebruiken worden eiwitten uitgerust met nieuwe eigenschappen. In dit geval wordt een chemisch handvat geïntroduceerd in nanobodies. Dit is de eerste keer dat deze methode is ingezet voor dit type antilichamen. Net als de 'intein protein ligation' kunnen nanobodies worden uitgerust met bio(moleculen), maar dan via een andere koppelingsreactie. Een voordeel van deze methode is dat de nanobody op praktisch alle plaatsen in het eiwit kan worden voorzien van een nieuwe eigenschap, in plaats van alleen op het begin of eind in het geval van de inteine methode. Ook in dit hoofdstuk is aangetoond dat de nanobodies functioneel zijn en gebruikt kunnen worden voor diverse toepassingen. Verder biedt deze methode de mogelijkheid om nanobodies te groeperen zodat deze als groep sterker aan kankercellen binden.

Naast het ontwikkelen van methoden om nanobodies te voorzien van nieuwe eigenschappen, zijn ook twee potentiële medicijnen ontwikkeld. De eerste maakt gebruikt van de in **hoofdstuk 4** beschreven 'intein protein ligation' om nanobodies te koppelen aan vetbolletjes. Ter illustratie, een dergelijk vetbolletje is ongeveer 100 nanometer in diameter en 1000x kleiner dan een menselijk haar. Door (actieve) stoffen in vetbolletjes op te nemen worden deze geloodst door het lichaam en afgegeven bij de tumor. Een extra veiligheidsmarge is ingebouwd door stoffen te gebruiken die onder normale omstandigheden niet schadelijk zijn, maar actief worden door

bestraling met niet schadelijk licht. In **hoofdstuk 5** is aangetoond dat deze vetbolletjes met nanobodies zeer effectief kankercellen kunnen doden. Dit komt doordat deze vetbolletjes zich snel aan kankercellen vastgrijpen en vervolgens effectief worden opgenomen. De in de vetbolletjes opgenomen stof eindigt dus in de kankercel waarna de bestraling ervan celdood veroorzaakt. Andere cellen nemen minder vetbolletjes op en worden daardoor nauwelijks aangetast. De meerwaarde van nanobodies gekoppeld aan vetbolletjes voor photodynamische therapie is hiermee overtuigend aangetoond en moet verder worden onderzocht in diermodellen.

Een ander voorbeeld van een medicijn gebaseerd op nanobodies is de doelgerichte afgifte van toxines. In dit geval betreft het een bacteriële toxine (PE38) die zeer effectief de productie van eiwitten in een cel kan stilleggen, waardoor de cel dood gaat. Door de toxine te koppelen aan een nanobody kunnen tumoren specifiek worden behandeld. Een belangrijke vereiste is dat de nanobody zeer specifiek is voor kankercellen omdat anders ook gezonde cellen afsterven (hiervoor is immers geen bestraling met licht nodig). In **hoofdstuk 7** zijn de resultaten beschreven voor de behandeling van glioblastoma's, een zeer kwaadaardige hersentumor. Een deel van de glioblastoma's zijn te herkennen aan een eiwitafwijking (EGFRvIII) en daarom uitermate geschikt voor de behandeling met een toxine zoals PE38. Na selectie en bepaling van de eigenschappen van een nanobody tegen EGFRvIII is deze gefuseerd met de toxine. Het ontwikkelde medicijn (immunotoxine; nanobody + toxine) was instaat om kankercellen met de eiwitafwijking sterk te remmen. Ter controle zijn ook andere cellen behandeld. Deze cellen waren minder gevoelig voor de therapie door het ontbreken van de eiwitafwijking. Wanneer een ander nanobody werd gebruikt (niet specifiek voor deze cellen) was de therapeutische werking geheel verdwenen. Deze veelbelovende resultaten tonen aan dat de nanobody gerichte afgifte van een toxine zeer interessant is voor de behandeling van glioblastoma's. Verder onderzoek en ontwikkeling is noodzakelijk om de klinische effectiviteit aan te tonen.

Samengevat beschrijft dit proefschrift de resultaten en andere bevindingen van het gebruik van nanobodies als kankertherapie. Door de gunstige eigenschappen zijn er diverse mogelijkheden denkbaar waar deze speciaal uitgeruste nanobodies in de toekomst een bijdrage kunnen leveren aan de behandeling van kanker.

Addendum

Curriculum Vitae

Remko van Vught was born on February 28th 1986 in Tilburg, The Netherlands. After finishing secondary school at 2College Cobbenhagen in Tilburg, he studied Molecular Life Sciences at the Radboud University in Nijmegen. As part of the Master program, he performed an internship in the group of Pharmacology and Toxicology at the Radboud University under supervision of J.J.M.W. van den Heuvel and Dr. J.B. Koenderink. A second internship was performed at Pepscan Therapeutics in Lelystad under supervision of Dr. JW. Back, Prof. Dr. P. Timmerman and Prof. Dr. F.P.J.T. Rutjes. In 2009, Remko obtained his Master's degree *cum laude* and started his PhD project at the Membrane Biochemistry and Biophysics group under supervision of Dr. E.J. Breukink and Prof. Dr. R.J. Pieters. The results of this PhD project are described in this thesis.

Afterwards, he started as business development scientist at MIMETAS in Leiden where he works on predictive Organ-on-a-Chip cell culture models for better, more reliable and tailored medicines.

Addendum

List of publications

Van Vught R, Pieters RJ, Breukink E, Site-specific functionalization of proteins and their applications to therapeutic antibodies. *Comput. Struct. Biotechnol. J.* 2014 Feb 14; 9:e201402001

Back JW, Frisch C, Van Pee K, Boschert V, **van Vught R**, Puijk W, Mueller TD, Knappik A, Timmerman P., Protein Eng Des Sel. 2012 May;25(5):251-9.

Van Vught R, van Bergen En Henegouwen PM, Pieters RJ, Breukink E, Nanobodies and their therapeutic applications.
Manuscript in preparation

Van Vught R, Broekgaarden M, van Gulik TM, van Bergen En Henegouwen PM, Pieters RJ, Breukink E, Heger M, Epidermal growth factor receptor-targeted liposomes with zinc phthalocyanine for photodynamic therapy.
Manuscript in preparation

Van Vught R, Oude Blenke E, Mastrobattista E, Martin NI, Roovers RC, van Bergen En Henegouwen PM, Pieters RJ, Breukink E, Incorporation of unnatural amino acids in nanobodies.
Manuscript in preparation

Van Vught R, Sol N, el Khoulati R, Lagerweij T, Roovers RC, Breukink E, Pieters RJ, Wurdinger T, van Bergen En Henegouwen PM, Selective targeting of EGFRvIII-positive glioblastomas by a nanobody-based immunotoxin.
Manuscript in preparation

Addendum

Dankwoord

En zo zijn ~~4~~ 5 jaar voorbij gevlogen. Onderweg besef je dit niet, maar nu ik voor de eindstreep sta begint het langzaam door te dringen. Terugkijkend kan ik wel stellen dat ik in deze periode veel nieuwe mensen heb leren kennen, altijd met zin naar de Uithof ben gegaan en ontzettend veel heb geleerd. Dit is dan ook een uitgelezen moment om de mensen te bedanken die direct of indirect hebben bijgedragen aan deze fantastische tijd.

Allereerst mijn copromotor Eefjan Breukink. Als directe begeleider heb je me veel vrijheid gegeven om interessante ideeën uit te proberen en mij bijgestuurd waar nodig. Hierdoor voelde ik me als een vis in het water. Ik heb op diverse vlakken veel van je geleerd en ook in het lab kon ik op jouw hulp rekenen. Als 'ervaren Postdoc' had je een ruime collectie aan tools en altijd wel trucjes om praktische problemen op te lossen. Bedankt voor alles.

Verder wil ik mijn promotor Roland Pieters bedanken. Onze maandelijkse meetings waren de ideale gelegenheden om de voortgang te peilen en voor een goed gesprek. Jouw expertise en vakgroep waren op diverse momenten zeer waardevol. De afgelopen maanden kon ik altijd rekenen op zorgvuldige en kritische feedback op mijn proefschrift, bedankt hiervoor!

En ook mijn andere promotor Antoinette Killian. Hoewel je minder direct betrokken was bij mijn project stond de deur altijd open voor de nodige hulp en advies. Bedankt dat je de laatste maanden zo soepel hebt laten verlopen.

Daarnaast wil ik graag mijn leescommissie bestaande uit Paul van Bergen en Henegouwen, Maarten Egmond, Wim Hennink en Rob Liskamp van de Universiteit Utrecht, en Guus van Dongen van het VU Medisch Centrum bedanken voor het kritisch lezen van mijn proefschrift en de feedback die ik heb gekregen.

Promoveren is niet alleen pipetteren en op het eind een boekje typen, maar ook het lab delen met veel leuke collega's en studenten. Allereerst wil ik Eefjan's Angels bedanken: Tami, vanaf de eerste dag heb je me wegwijs gemaakt in ons lab. Zonder jouw hulp zou ik nog steeds verdwaald zijn =). Diana, ook jij was erg behulpzaam en wist altijd alles te vinden. Dat je nu in Barcelona zit betekent niet dat je onder onze weddenschap uitkomt…. Wanneer kom je langs in je heidi outfit? Paulien, niet te verwarren met Pauline, anders heb je een probleem. De afgelopen jaren was jij mijn kamergenootje en hebben we dus van alles meegemaakt. Bedankt voor alle fijne gesprekken, discussies en het negeren van de dumpert filmpjes. Inge, ook wel bekend als zonnestudio 't Veer en om gezelligheid zowel binnen als buiten het lab. Na alle verhalen ben ik toch wel erg benieuwd naar die Döner Kebab, wanneer gaan we stappen in Maassluis? Yao, ik heb nog nooit een chinees zo uitbundig zien juichen voor het Nederlands elftal. Bedankt voor alle choco pauzes, leuke avonden (ook buiten het lab ;)) en mijn opleiding tot sushi master. En ook de laatste Eefjan's Angels, Sabine en Lisette, hebben gezorgd voor veel gezelligheid door alle verhalen over Tinder en Azië, het disco uurtje, popduel en spelletjes (met poffertjes!).

En verder hebben we natuurlijk Joost. Naast dat wij bijna gelijktijdig zijn begonnen, ben

jij al jaren mijn squashmaatje en straks ook mijn paranimf. Bedankt voor de geweldige tijd en succes met de laatste loodjes. Stefan, jouw satirische humor brengt altijd leven in de brouwerij. Mocht je ooit genoeg krijgen van al dat smalpen, dan kun altijd een carrière als komiek of zanger overwegen.

In addition, I would like to thank the many other colleagues of our group (in random order) for the great atmosphere and chats at the coffee corner: Nick, Erica, Tania, Yvonne, Marlies, Ben, Nicole, Aline, Larissa, Saran, Steven, Toon, Patricia, Greg, Mike, Amrah, Tine, Xue, Gabi, Matthijs, Joost H., Maarten and the students. Jacques, thanks for the colorful experience (mainly orange), all your help and the good (old) times in and outside the lab. Jonas, for the discussions about food, language and 'vaguely' I recall something about berries =). Sam, four correkting my Inglish and annoying the lab with 'relaxing' classical music. Juan, the wisdom of your grandma significantly contributed to this thesis. My students Jessica, Anniek, Ivan, Cecilie, Niels and Wout (aka "the boys"), and Tom for their contribution to this thesis. I had a great time supervising you and wish you all the best with your (scientific) careers.

En niet te vergeten Martijn, Ruud, Joep en Mandy, bedankt voor het draaiende houden van het lab. Het zou vaker gezegd mogen worden, zonder jullie hulp zouden we nergens zijn. Minstens net zo belangrijk was overigens de organisatie van de VEvdWB (borrels). Hoewel ik vaak pas laat aansloot was het altijd fijn om de week luchtig en onder het genot van een biertje af te sluiten.

Daarnaast waren de afgelopen jaren ook Irene, Barbara, Cecile en Caroline onmisbaar. Caroline bedankt voor je interesse, hulp en voor het soepel laten verlopen van de administratieve hobbels rondom deze promotie.

En af en toe was er een invasie vanuit het AMC door Michal, Mans, Megan en Ruud als men lipo's kwam maken of zin had in een Rousertje. Bedankt voor de fijne samenwerking, discussies en suggesties rondom het TTL project. Michal, ook naast het TTL project kwam jouw kennis goed van pas en stond jouw aanwezigheid garant voor (verhitte) discussies gedurende alle tijdstippen/dagen van de week. Mans, wat begon met het begeleiden van studenten net voor de kerst is uitgelopen tot een mooi experimenteel hoofdstuk. Succes met de laatste loodjes en je nieuwe uitdaging in Boston!

Daarnaast wil ik graag de Medicinal Chemistry & Chemical Biology groep bedanken, met in het bijzonder Nathaniel, Cristina, Marcel, Nuria, Arwin, Peter, Jack en Marjon, voor de fijne samenwerkingen, leuke meetings en het beschikbaar stellen van diverse stofjes.

De buren (OCC) op de o zo groene 8^{e} verdieping van het Kruyt. Onze vele gezamenlijke borrels en activiteiten waren altijd een groot succes. Peter, jongen! Wat waren wij toch een geweldig team in organiseren van diverse activiteiten waar natuurlijk de leverworst en kaas nooit mochten ontbreken. Manueltje (and Sve), thanks for all the great parties, the Mexican vibe, bbq's and other great evenings! Jacco, bedankt voor jouw

nuchtere kijk op onderzoek. Na al die jaren op de uithof kan ik me haast niet voorstellen dat jij ooit nog zal vertrekken.

The nanobuddies Isil, Raimond and Roy of the Focus and Massa project. I was fortunate to be part of this great team and project that we started 5 years ago. Thanks for all the amazing evenings, discussions and for sharing your expertise. I really enjoyed our nanobeers and nanodinners, and hope that we can continue our tradition for many years to come!

The biopharmacy department and especially Robbert Jan, Raymond and Wim for their active involvement in the F&M project, great meetings and helpful suggestions. In addition, Erik and Enrico for their contribution to chapter 6.

Het altijd gezellige nanobody hoofdkwartier op de 5e. Ik kwam dan ook graag bij jullie celkweken ondanks onze lege kweekruimte op de 6e. Paul, de afgelopen jaren was je sterk betrokken bij mijn project. Bedankt voor je advies, leuke gesprekken en dat je mijn mentor was. Rob, bedankt voor de goede verhalen en tips & trucs bij het kloneren en squashen. Sabrina, your open-mindedness, advice, and feedback have been very helpful. Rachid, zonder jouw hulp was hoofdstuk 7 er niet geweest! Bram, bedankt voor de leuke gesprekken op de fiets en voor het project wat dankzij jou misschien nog een leuk staartje gaat krijgen. En ook de vele andere collega's die de afgelopen jaren op de 5e hebben rondgelopen wil ik graag bedanken: Sofia, Bas, Katarina, Chris, Andrea, Renée, Kim, Marta, Cilia, Jarno, Smiriti, Mireille, Aram, Mohammed, Edward, Lucy, Nika, Ava.

During these years I have also been involved in the organization of several activities for the Institute of Biomembrane together with Emma, Pauline, Oliver, Raimond, Marta and Susana. Thanks for this great time, experience and nice meetings at the Basket or Gutenberg.

Naast het werk is er de afgelopen jaren ook genoeg tijd geweest voor ontspanning en sport met familie en vrienden. Bedankt hiervoor! In het speciaal wil ik de (studie)vrienden uit Nijmegen bedanken voor hun betrokkenheid, interesse en natuurlijk voor de altijd gezellige verjaardagen, weekenden en bruiloften. Dat we dit maar lang mogen volhouden.
Daarnaast mijn squashmaatjes Hans, Joost en Joris. Mijn klimmaatjes Hans en Mark, ook wel beter bekend als de Pro's. En het bedrijfshockey team van Capgemini waar ik al enkele seizoenen als vaste invaller mee kan spelen. Bedankt voor de goede sfeer, leuke potten, 3e helft en teamuitjes.

En dan de schone familie van Cuijk, wat ben ik toch met mijn neus in de boter gevallen. Von, jouw kookkunsten doen niet onder voor die van een chef-kok. Het is dan ook een wonder dat ik nog geen 20 kilo ben aangekomen. Gerard, ik heb altijd genoten van onze mountainbike ritten (ook wel de balansdagen). Wanneer gaan we weer fietsen?

Mijn peetoom en peettante, René en Maria, Opa, Oma en Gerben. Ondanks dat de

afgelopen jaren in het teken stonden van het grote mensen leven, met alle drukte en hectiek, houden we goed contact. Zelfs direct email contact is tegenwoordig met Oud-Turnhout mogelijk! Bedankt voor jullie steun, interesse, gezellige verjaardagen en etentjes.

Casper, mijn 'kleine' broertje! We doen al jaren van alles samen en ik kan altijd op jou rekenen. Vooral het weekend in Göteborg, het waterskien en de sketch als pap en mam op de 25 jarige bruiloft waren in mijn ogen enkele hoogtepunten. Bedankt dat wij zo lekker kunnen kletsen en dat je mijn paranimf bent op deze bijzondere dag. Audrey, thanks for joining the family. We are especially happy with the cheese and chocolate from Switzerland =).

Pap en mam, bedankt voor jullie onvoorwaardelijke steun, vertrouwen en interesse. Dankzij jullie ben ik gekomen tot waar ik nu ben. Het is ongelofelijk fijn om een thuisfront te hebben waar de deur altijd openstaat. Ik heb genoten van onze vakantie op Cyprus, gaan we gauw nog een keer doen!

En ten slotte, mijn lieve Loes. Wat is het fijn om deze en andere ervaringen samen met jou te kunnen delen. Bedankt voor alles, ik hou van je! Daarnaast ben ik ongelofelijk trots dat ook jij bijna klaar bent. De afgelopen jaren met jou waren fantastisch, dat er nog vele mogen komen!

Remko

Ps. Voor de liefhebbers nog een doolhof op de volgende pagina, succes!